Technische Universität München

Klinik für Orthopädie und Sportorthopädie
der Technischen Universität München
(Direktor: Univ.-Prof. Dr. R. von Eisenhart-Rothe)

Effects of Cartilage Impact with and without Fracture on Chondrocyte Viability and the Release of Inflammatory Markers in Two in Vitro Models

Josef Stolberg-Stolberg

Vollständiger Abdruck der von der Fakultät für Medizin
der Technischen Universität München
zur Erlangung des akademischen Grades eines Doktors
der Medizin genehmigten Dissertation.

Vorsitzender: Univ.-Prof. Dr. E. J. Rummeny

Prüfer der Dissertation:

1. Priv.-Doz. R. H. H. Burgkart
2. Univ.-Prof. Dr. A. Imhoff
3. apl. Prof. Dr. A. K. Nüssler

Die Dissertation wurde am 08.01.2014 bei der Technischen Universität München eingereicht und durch die Fakultät für Medizin am 17.09.2014 angenommen.

Acknowledgement

There are many fabulous friends and colleagues who contributed to my work and made my research period in Durham to such an enjoyable time:

First of all I want to thank PD Dr. med. Rainer Burgkart. He supported me from the very beginning with my application, during all my time in the US with personal and project related advice and as thesis supervisor during the last steps of my thesis writing.

Furthermore, I thank Dr. Farshid Guilak for inviting me to his outstanding laboratory, for giving me so many great advices and opinions during the project development and for all the personal invitations.

Dr. Steven Olson was the head of our group. Thank you very much for always critically evaluating my data, for pushing me into the right direction whenever I was thinking around the problem and for showing me around the Duke ORs and clinic.

A million thanks go to Bridgette Furman who supported me on a daily basis. Thanks for hundreds of hours of always patiently discussing test results, explaining new methods and always being supportive in every possible way.

Louis DeFrate helped on all the mechanical problems we faced during our loading protocol development. I want to thank him especially for making mechanics understandable even for a medical student.

Thank you very much, Brien Diekman and Chia-Lung Wu for all you creative ideas during our lab meetings. Without you my project would look very poor today.

Special thanks go to the medical students KJ Hippensteel, Daniel Mangiapani and Craig Louer. They helped me with all the daily problems, explained many new methods to me and just became great friends during these seven months.

Dr. med. Hermann Albersdörfer gave me an always honest opinion and very valuable advice about career planning and orthopaedics from the very beginning of my graduate student time. Thank you very much.

Many thanks also go to my three Irish aunts Jennifer C. Matuschka, Jennifer Matuschka and Alice Fischer for doing the final proof-reading.

Finally, but most important I want to thank my parents Otto and Stefanie and my brothers Antonius, Ludwig and Johannes for making my research period possible and for keeping me in touch with home.

Table of Contents

Abbreviations

AAP ……	L-ascorbic acid 2-phosphate
AGG ……..	Aggrecanase
ATP ……	Adenosine Triphosphate
ADAMTS ……	A Disintegrin and Metalloproteinases with Thrombospondin Motifs
BMP ……	Bone Morphogenic Protein Family
BW ……	Body Weight
cAMP ……	Cyclic Adenosine Monophosphate
CD-Receptor ….	Cluster of Differentiation Receptor
CINOD ……..	COX-inhibiting Nitric Oxide Donor
cm ……	Centimeter
COMP ……	Cartilage Oligomeric Matrix Protein
CS ……	Chondroitin Sulfate
DAMP ……	Damage-Associated-Molecular-Pattern-Molecules
DC ……..	Dendritic Cell
DIC ……...	Differential Interference Contrast
DMB ……	1,9-Dimethylmethylene Blue
DMC ……..	Degenerative Morphological Changes
DMEM ……	Dulbecco's Modified Eagle Medium
dsDNA ……..	Double Stranded Deoxyribonucleic Acid
ECM……	Extracellular Matrix
EDA ……	Type III Repeat Extra Domain A
ER ……..	Endoplasmatic Reticulum
ERK ……	Extracellular-Signal-Regulated-Kinase
E-Selectin …….	Endothelial-Cell Selectin
FCD ……	Fixed Charge Density
FGF ……	Fibroblast-Growth-Factor
Fl Oz ……..	Fluid Ounce
ft ……	Foot
GAG ……..	Glycosaminoglycan
gal ……	Gallon
HA ……..	Hyaluronan
HMGB1 ……..	High Mobility Group Box 1 Protein
ICAM1 ……	Intercellular-Adhesion-Molecule 1
ICE ……	Il-1β Converting Enzyme
IGF-I ……..	Insulin-like-Growth Factor I
IKK-Complex ….	Inhibitor-of-NFκB- Kinase-Complex
Il-1 sR ……	Il-1 Soluble Receptor
In ……	Inch
INF-γ ……..	Interferon-Gamma
iNOS ……..	Inducible Nitric Oxide Synthase
IκB ……..	Inhibitor of NFκB
kg ……..	Kilogram
KS ……..	Keratan Sulfate
lb ……	Pound (lat. Libra)
LIF ……..	Leukemic Inhibitor Factor

LIF ……..	Leukemia Inhibitory Factor
l ……..	Liter
LPS ……..	Lipopolysaccharide
MMP ……..	Metalloproteinase
mRNA ……..	Messenger Ribonucleic Acid
MyD88 ……..	Myeloid-Differentiation-Primary-Response-Protein 88
NEMO ……..	NFκB-Essential-Modulator
NFκB ……..	Nuclear Factor Kappa-Light-Chain-Enhancer of Activated B Cells
NO ……..	Nitric Oxide
NOX ……..	Nitric Oxide Species
NOS ……..	Nitric Oxid Synthase
OA ……..	Osteoarthritis
PAMP ……..	Pathogen-Associated Molecular Patterns
pANCA ……..	Perinuclear-Anti-Neutrophil-Cytoplasmic-Antibody
PBS ……..	Phosphate Buffered Saline
PG ……..	Proteoglycan
Psi ……..	Pounds per square inch
PRR ……..	Pattern Recognition Receptors
PTA ……..	Post-Traumatic Arthritis
RA ……..	Rheumatoid Arthritis
RAGE ……..	Receptor for Advanced Glycation Endproducts
rER ……..	Rough Endoplasmatic Reticulum
RHD ……..	Rel Homology Domains
RNA ……..	Ribonucleic Acid
rNTP ……..	Ribonucleoside Triphosphate
ROI ……..	Reactive Oxygen Intermediate
SEAP ……..	Secreted Embryonic Alkaline Phosphate
SFM ……..	Serum Free Medium
sGC ……..	Soluble Cyclic Guanylate Cyclase
TACE ……..	TNF-α Converting Enzyme
TAK 1 ……..	Transforming-Growth-Factor-β-Activated Kinase 1
TBP ……..	TATA Box Binding Protein
TF ……..	Transcription Factor
TGF-β ……..	Transforming-Growth-Factor-β
TIMP ……..	Tissue Inhibitor of Metalloproteinases
TLR ……..	Toll-Like Receptor
TNF-sR ……..	TNF-soluble Receptor
TRAF-6 ……..	Tumor-Necrosisfactor-Receptor-Associated Factor 6
USD ……..	US Dollar
VCAM1 ……..	Vascular-Cell-Adhesion Molecule 1

Units

- 1 in = 2.54 cm
  1 cm = 0.3937 in

- 1 ft = 30.48 cm
  1 cm = 0.0328 ft

- 1 lb = 0.4535 kg
  1 kg = 2.2046 lb

- 1 fl oz = 29.57 ml
  1 ml = 0.0338 fl oz

- 1 gal = 3.79 l
  1 l = 0.2641 gal

Project Overview

Project overview for the TU annual book:

The development of post-traumatic arthritis involves chondrocyte death and inflammation of cartilage and surrounding tissues. Two *invitro* loading apparatus were designed to investigate the effect of trauma mechanism on chondrocyte viability and the release of Toll-like receptor (TLR) activating ligands. This study shows that low strain blunt impact ≤70% strain causes mainly apoptotic chondrocyte death whereas high strain blunt impact ≥80% strain and cartilage fracture lead to necrosis. Cartilage debris released from injured osteochondral cores is able to induce inflammation via TLR activation.

Zusammenfassung der Dissertation für das TU Jahrbuch:

Die Pathogenese der post-traumatischen Arthrose umfasst u.a. Chondrozytentod und Entzündung des Knorpels, sowie der umgebenden Gewebe. Zwei invitro Modelle wurden entwickelt, um den Effekt von unterschiedlichen Traumamechanismen auf Chondrozytenviabilität und die Freisetzung von Toll-like Rezeptor Liganden zu untersuchen. Stumpfe Traumata ≤70% Kompression verursachen hauptsächlich Chondrozyten Apoptose, wohingegen ≥80% Kompression zu Nekrose führt. Durch Trauma erzeugte Knorpelfragmente können Entzündung via TLR-Aktivierung hervorrufen.

Publications

According to Promotionsordnung §6 Abs. 6 own publications are listed:

1. Stolberg-Stolberg JA, Furman BD, Garrigues NW, Lee J, Pisetsky DS, Stearns NA, et al. Effects of cartilage impact with and without fracture on chondrocyte viability and the release of inflammatory markers. Journal of Orthopaedic Research. 2013 Aug;31(8):1283-92.

2. Kokosis G, Stolberg-Stolberg J, Eward WC, Richard MJ, Hollenbeck ST, Levinson H, et al. Femur reconstruction using combined autologous fibula transfer and humeral allograft. Chirurg. 2011 Dec;82(12):1120-3.

1 Introduction

1.1 Post-Traumatic Arthritis

Post- traumatic arthritis develops (PTA) most commonly after intra-articular fracture and accounts for 12% of all US Americans with symptomatic arthritis. In addition, it is most commonly found in young patients and is described as very debilitating and painful disease (Brown 2006 [40]). Several hypotheses about its pathophysiology have been made and partly been proven by *in vivo* and *in vitro* injury models (Fig. 1). The exact mechanisms and interactions that are involved in the onset and progression of PTA, however, are still largely unknown (Furman 2006 [74]).

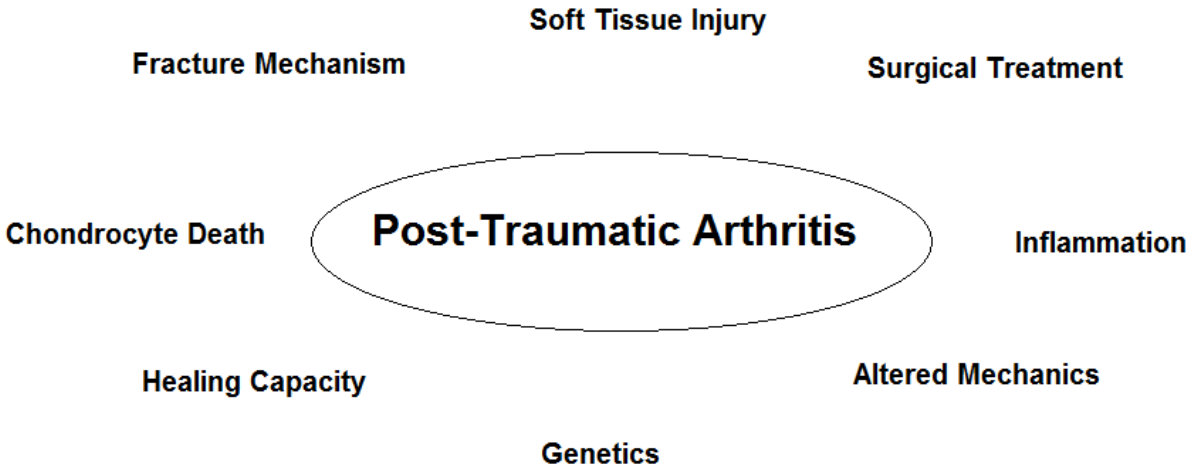

Fig. 1 The major components involved in the onset and progression of PTA (Furman 2006 [74]).

Arthritis is believed to be caused by an imbalance of cartilage homeostasis which consists of anabolic and catabolic reactions. Collagen and proteoglycan synthesis, for instance, have to be seen as a counter balance to degradative enzymes such as metalloproteinases and aggrecanase.

Cytokines such as TNF-α and Il-1, the inflammatory mediators NO and mechanic loading greatly influence chondrocyte's gene expression (Guilak 2003 [85], Mow 2005 [154]). It is important to state that the transcription factor NFκB is thought to play a major role for the intracellular signalling of TNF-α and Il-1 (Baeuerle 1998 [20], Renard 1999 [179]). Furthermore, extrinsic and intrinsic NO seems to have an equally important impact to chondrocyte's inflammatory response (Taskiran 1994

[211]). HMGB1 stands out as it acts as transcription factor and as damage-associated-molecular-pattern-molecule (DAMP). Toll-Like Receptors (TLR) are part of the innate immune system. Their endogenous ligands are a group of molecules that is typically released by sterile tissue damage. TLRs have been shown to be expressed by human chondrocytes (Bobacz 2007 [37]). HMGB1 and dsDNA are ligands to TLR-2 and 4 (Baxevanis 1995 [22]).

Necrotic and apoptotic cell death are the most relevant forms of chondrocyte loss. Apoptosis or programmed cell death might occur due to loading and exposure to an inflammatory environment. It is crucial, however, to distinguish apoptosis from necrosis because this programmed and energy dependent pathway might be a suitable point of medical intervention. Necrosis is associated with the release of cell content such as dsDNA and HMGB1 (Borrelli 2006 [39], Kuhn 2004 [120]).

For a long time supraphysiologic loading has been identified to cause degradative changes in the cartilage matrix and loss of chondrocyte viability. Stress levels, strain and strain rates have been extensively studied (Quinn 2000 [174], Repo 1977 [181], Warner 2004 [230]). Little research, however, has been done in the area of post-traumatic arthritis in order to better understand the link between inflammatory, mechanical and degradative changes after impact loading.

1.2 Motivation

Until now the treatment of intra-articular fractures includes open reduction and internal fixation of dislocated cartilage and bone fragments. Enhanced treatment options have not yet been successfully used on a large patient population as the understanding of the complex injury mechanisms, inflammatory and degradative changes is very limited (Furman 2006 [74]). Number, frequency and burden of disease of PTA, however, emphasize the need for further investigation and better understanding.

1.3 Aim

Specific Aim 1: In a first step we want to develop an *in vitro* loading apparatus that applies different amounts of strain to porcine osteochondral cores. We want to compare this to samples loaded by a fracture model. Samples loaded by these models will be characterized by total viability and amount of apoptotic cell death at days 0, 3 and 5.

Specific Aim 2: In a second step we want to characterize inflammatory and degradative changes in PTA. Early mediators such as NFκB, HMGB1 and double

strand DNA (dsDNA) and late stage indicators such as MMPs, aggrecanases, NO and PG (proteoglycan) release will be measured. The possibility of HMGB1 and dsDNA binding to TLR-2 and 4 will be elucidated.

1.4 Hypothesis

Strains bigger than 70% will induce a significant amount of chondrocyte death (Chahine 2007 [48]). Thus, with our loading apparatus we want to show decreasing viability with increasing strain beginning at 70%. Furthermore, we expect up-regulation of NFκB, MMPs, aggrecanases, PGs and NO after trauma (Anghelina 2008 [14], Backus 2010 [19]). Necrotic chondrocytes are expected to release HMGB1 and dsDNA which has to be proven to be a ligand to TLR-2 and 4 (Beg 2002 [25]).

1.5 Sources

All tests and experiments were done in the Orthopaedic Research Laboratory, Department of Orthopaedics of the Duke University Medical Center, Durham, North Carolina, USA. Farshid Guilak, Ph.D. and Steven Olson, MD. supervised the project development in Durham.

As two exceptions, TLR-studies were conducted in the laboratories of the Division of Surgery, Duke University Medical Center, Durham, North Carolina with the help of Jaewoo Lee, Ph.D., MS. PicoGreen assays were done in the laboratories of the department of medicine, Durham VA Hospital, Durham, North Carolina and the help of David Pisetsky, MD. Ph.D..
PD Dr. med. Rainer Burgkart contributed as thesis adviser and supervisor in Munich.

2 Background

2.1.1 Composition of Articular Cartilage

As previously stated, there are different types of joints covered with different cartilage. PTA most often occurs and is clinically most relevant in diarthrodial joints and hyaline/ articular cartilage. Hence, we will focus on this tissue:

2.1.1.1 Collagen in Articular Cartilage

The subunit of any type of collagen is a pro-collagen polypeptide (Fig. 2). It is coiled into left handed α-chain helixes. Three of these chains form a right handed coiled triple helix, also called tropo-collagen.

....-Glycin - X - Y - Glycin - X - Y - Glycin - X - Y - Glycin - X - Y - Glycin - X - Y - Glycin -...

Fig. 2 Gylcin is the only amino acid that is small enough to fit into the space at the central core of the triple helix. Thus we find it to be in every third space.

Procollagen (Fig. 3) is secreted from the cell. Enzymes remove loose ends and form tropocollagen. It is a chain of approximately 300nm and polymerizes into large fibrils. They are reported to have a diameter somewhere between 25 and 200nm. Covalent cross-linking grants collagen high tensile stiffness and strength.

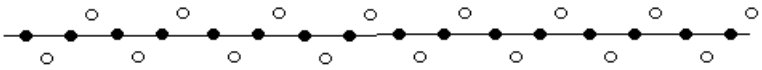

Fig. 3 Procollagen chain, • = glycin, o = other amino acid

Like in many other organs (Table 1), collagen has a definite arrangement in articular cartilage. The fibers are densely packed and orientated parallel to the surface in the superficial layer. Further down in the middle zone we find a wider knit homogeneous net of collagen. Moving towards the deep zone fibers align radially and form bundles which cross the tidemark and anchor in the calcified cartilage zone. It is striking that we find the highest density of collagen in the superficial layer. It is thought that this might lead to a more even distribution of pressure across the cartilage. However, another specific characteristic is the predominance of collagen II. Furthermore, we find small quantities of collagen V, VI, IX and XI. Anisotropy in the superficial layer is demonstrated by split lines which form in a concentric manner after piercing the articular surface with a small needle (Mow 2005 [154], Murray 2004 [157], Murray 2003 [158]).

Table 1: Major occurrences of collagen types.

Collagen Type	Tissue	Collagen Type	Tissue
I	Connective Tissue, Bone	**XI**	Together with Collagen II
II	Cartilage, Vitreous Humor	**XII**	Together with Collagen I
III	Extensible Connective Tissue (Skin, Lung, Vascular System)	**XIII**	Many Tissues
IV	Basement Membranes	**XIV**	Together with Collagen I
V	Together with Collagen I	**XV**	Many Tissues
VI	Connective Tissue	**XVI**	Many Tissues
VII	Anchoring Fibrils	**XVII**	Skin Hemidesmosome
VIII	Endothelium	**XVIII**	Many Tissues
IX	Together with Collagen II	**XIX**	Rhabdomyosarcoma
X	Hypertrophic Cartilage		

2.1.1.2 Proteoglycans in Articular Cartilage

There are many different types of proteoglycans in articular cartilage. The basic structure consists of one large protein-polysaccharide molecule with a protein core to which different glycosaminoglycans (GAGs) can attach. Some examples are biglycan, fibromodulin, lumican, perlecan and decorin. A specific role plays aggrecan (80- 90% of total PG) because it has a HA-binding domain which allows it to form bigger structures together with HA and also prevents it from escaping from the cartilage tissue (Fig. 4).

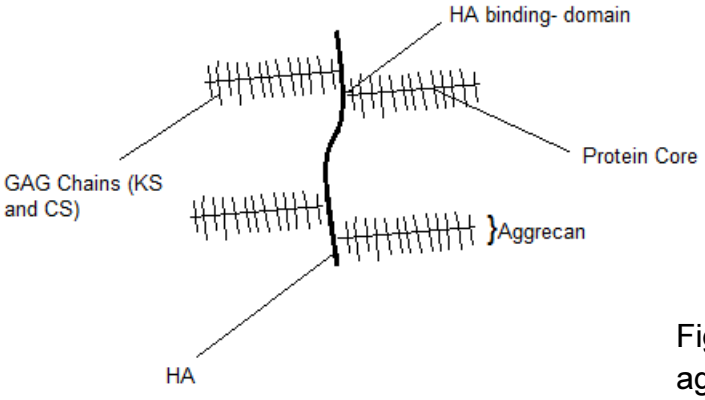

Fig. 4 Bottle-brush model of aggrecans attached to hyaluronan molecule.

Attached to the aggrecan protein core we typically find around 150 GAGs of chondroitin sulfate (CS) and keratan sulfate (KS). Each HA might be bound to up to several hundred aggrecan structures. The anionic property of the GAG side chains

due to negatively charged sulfate and carboxyl groups creates the Donnan osmotic pressure which hydrates the tissue. Furthermore, the repulsive forces in between the GAGs lead to an augmentation in volume within the collagen mesh. Both are parts of the swelling pressure which will be discussed in further detail later on. It must be noted, however, that the highest concentration of PGs and thus the highest swelling pressure is found in the middle zone (Mow 2005 [154], Murray 2004 [157], Murray 2003 [158]).

2.1.1.3 Water in Articular Cartilage

With 80% of cartilage's total weight, water might be the most important component. The highest concentration is found in the superficial layer and decreases going towards the osteochondral junction. As already stated, this water contains many cations such as Na^+, K^+ and Ca^{2+}. In addition, it is of particular importance because it supplies cartilage with nutrients and removes waste products. Fluid might also leave the extracellular matrix (ECM) and move into the joint space where it also functions as a lubricant (Margareta Nordin 2001 [141], Mow 2005 [154], Murray 2003 [158]).

2.1.2 General Embryology and Bone Formation

Looking at the early embryo, the skeletal system develops from the paraxial (thus somitomeres and somites) and lateral plate mesoderm and from the neural crest. The medial part of the somites is defined as the scleroderma. Around four weeks after fertilization this tissue differentiates into mesenchyme and will soon become fibroblasts, osteoblasts or chondroblasts. Now, it is important to distinguish between intramembranous and intracartilaginous ossification:

During the process of intramembranous bone formation the mesenchyme forms a membranous sheath. Within that sheath mesenchyme condenses and osteoblasts appear and form osteoid tissue. Bit by bit calcium phosphate precipitates and a solid bone is formed. At this stage most osteoblasts turn into osteocytes and a restructuration process as the beginning of a continuous remodelling of the bone starts.

Intracartilaginous ossification appears after a cartilaginous model was formed. In long bones this type of ossification typically occurs in the diaphysis first. In those ossification centers we find hypertrophy of the chondrocytes first before the matrix calcifies more and more and the cells die. We can find the same process at the outer core where perichondrium turns into periosteum. Simultaneously, hematopoietic cells are settling down in the core and form the bone marrow. The longitudinal growth can be found at both ends at the diaphysal-epiphysal junction. In those areas chondrocytes undergo mitosis and again the cells in the diaphysis hypertrophy and calcify, leaving trabeculae behind. Osteoblasts and Osteoclasts reorganize this

tissue into compact bone with Haversian and Volkmann Canals, Osteons and lamellae. During the first years after birth secondary ossification centers typically appear in the epiphyses. Vascular tissue invades those areas, we find hypertrophy of chondrocytes and calcification and ossification spreads all around. The cartilage remains at the outside. In a lot of bones secondary ossification terminates around the age of 20 years (Eroschenko 2005 [66], Gartner 2000 [76], Sadler 1995 [188], Sternberg 1997 [202]).

2.1.3 About the Histology of Cartilage

"The articulating cartilages are most happily contrived to all purposes of motion in those parts. By their uniform surface, they move upon one another with ease; by their soft, smooth and slippery surface, mutual abrasion is prevented; by their flexibility, the contiguous surfaces are constantly adapted to each other and the friction diffused equally over the whole; by their elasticity, the violence of any shock, which may happen in running, jumping, etc. is broken and gradually spent; which must have been extremely pernicious, if the hard surfaces of bones had been immediately contiguous" (William Hunter, 1743)

The functional unit of a joint consists of ligaments, synovium and cartilage. Following this definition there are three different types of joints: The diarthrodial joint which is a cavitated connection between two bones and generally is covered by hyaline (articular) cartilage. The amphiarthodial joint is characterized by intervertebral discs and the fibrous synarthrosis is a non-movable joint as we can see it in skull sutures. Apart from the hyaline cartilage we can also find fibrocartilage which is characterized by collagen I and is typically found in menisci and the annulus fibrosus of intervertebral discs. The third form of cartilage is elastic and can be encountered in the ligamentum flavum and the outer ear (Eroschenko 2005 [66], Gartner 2000 [76], Sadler 1995 [188], Sternberg 1997 [202]).

Looking at the cellular level, chondrocytes produce the needed factors for the matrix in order to obtain the right properties for each type of cartilage in each joint. Collagen is one of the most important factors produced. Their strong bundles of fibrils are giving cartilage its shape. In hyaline cartilage we typically find collagen II. Collagen generally has a horizontal orientation in the superficial layer (lamina splendens) and a vertical orientation in the deeper layer. It is also found to be closer packed at the surface whereas we find a wider knit mesh in the deeper zones. To fill out the spaces between the collagen fibers chondrocytes produce proteoglycans which are negatively charged macromolecules, the most important ones: aggrecan, dermatan sulfate, biglycan and decorin. Due to their size and charge they attract a large amount of water and let the cartilage swell up. Chondronectin is an adhesive glycoprotein that binds together the fibrils of collagen (Eroschenko 2005 [66], Gartner 2000 [76], Sadler 1995 [188], Sternberg 1997 [202]).

But we also find different shapes and expression patterns of chondrocytes within different layers of cartilage, each one sitting in its own lacunae: In the outmost layer they seem to be flat, in the intermediate zone they appear to follow the collagen mesh and form radial groups and in the zone next to the bone the matrix is calcified and cells appear nonviable. The calcified zone and the deep zone are divided by the tide mark. Chondrocytes themselves normally are surrounded by a matrix rich in proteoglycans and hyaluronic acid. That again is encapsulated by a mesh of collagen that protects the cells (Eroschenko 2005 [66], Gartner 2000 [76], Sadler 1995 [188], Sternberg 1997 [202]).

The synovial membrane forms the capsule of the joint and consists of two layers. The intimal layer is found to be smooth and moist and forms small villi. It is also in this layer where we find a high density of synoviocytes (type A for phagocytosis and type B for secretion of synovial fluid hyaluronate). Whereas in the subintimal layer, we typically find the connective tissue with fat cells, fibroblasts, histiocytes and mast cells. Thus the functions of the synovial membrane are secretion of synovial fluid, phagocytosis of waste material and regulation of movement of electrolytes, proteins and solutes from the capillaries into the synovial fluid (Eroschenko 2005 [66], Gartner 2000 [76], Sadler 1995 [188], Sternberg 1997 [202]).

2.1.4 General Changes in Arthritic Joints

Whichever diagnosis is made after inspection of an arthritic joint, there are some general aspects they all have in common: In an arthritic joint we clinically find joint instability, pain and disability of smooth joint movement. These symptoms may be caused by a variety of macroscopic and microscopic changes: Thus in many cases loss of bone, cartilage and tissue is visible with bare eyes. Other findings might be an addition of bone as in osteophytes or subchondral sclerosis or even a deformation of the joint as in Paget's disease.

Looking at the microscopic level (Table 2), we frequently observe fibrillation as collagen fibers brake and a velvet-like surface is found instead of a smooth and shiny one. At the same time water enters the tissue as it is not retained by the collagen mesh anymore and finally swelling and chondromalacia occurs. Ulceration describes the ablation of the cartilage sometimes down to the bone. The formation of vertical cracks into the cartilage is known as cracking. The appearance of ghost cells (dead chondrocytes) can also be found in damaged cartilage. It becomes obvious that due to little or non-vascularization, we will not find the same degree of repair as in other tissues. It is important, however, to note that there will always be an inflammatory response as the synovium and some vascularization is involved. Therefore, cartilage repair is taking place to some degree.

During the process of intrinsic repair chondrocytes divide and form little clumps of cells. Metachromasia gives evidence for proteoglycan synthesis under the light microscope. Despite of PG synthesis there is a net-loss of PGs (Bay-Jensen 2008 [23]). Extrinsic repair reaches the cartilage through the subchondral bone or from the joint margins. Thus, we can observe irregularities, doubling and invasion of blood vessels at the tide mark.

In extreme cases of osteoarthritis, cartilage is worn off as far as to the bone (eburnation). We find small regeneration knots appearing out of the subchondral bone. In some cases they re-cover parts of the surface. Under the microscope we find this cartilage to be fibrocartilage with a significantly higher proportion of collagen I as opposed to collagen II as in not injured articular cartilage. At the same time osteophytes are formed at the margins of the joint due to endochondral ossification. Integrative repair after intra-articular fracture, however, is very unlikely to be happening (Ahsan 1999 [7]).

Table 2: Collins-scale: Describing the different stages of degenerative morphological changes (DMC) (Muehleman 1997 [156]).

Grade	Description
Grade 0	no signs of DMC
Grade 1	early fibrillation, flaking, shallow pits or grooves and/or small blisters affecting the cartilage surface in the absence of changes in articular surface geometry
Grade 2	deep fibrillation and fissuring, flaking, pitting and/or blistering, early marginal hyperplasia and, possibly, small osteophytes
Grade 3	extensive fibrillation and fissuring, obvious osteophytes and 30% or less of the articular cartilage surface eroded down to the subchondral bone
Grade 4	Prominent osteophytes, lips or shelves at the articular margin, greater than 30% of the articular surface eroded down to the subchondral bone and gross geometric changes.

The synovium in an osteoarthritic joint can be hyperplastic with increased and hypertrophic villous folds. Inflammation can occur but never to the same degree as in rheumatoid arthritis (RA). Light infiltration of lymphocytes and mononuclear cells might be found. Loose bodies are the result of synovial metaplasia (Bullough 2004 [42], Vigorita 2008 [228]).

There seem to exist many similarities of PTA with OA. However, it is not clear to what extend etiology and progression of disease resemble. Thus, endpoint PTA appears to be very similar to OA but the mechanisms involved might be different.

2.2 Post-Traumatic Arthritis

2.2.1 About the Importance of Post-Traumatic Arthritis

Post-traumatic arthritis is a very frequent complication after fracture of weight bearing joints. However, only recent studies are starting to analyze its importance as an independent disease and thus surprisingly little literature was found. Nevertheless, it is possible to gain insight into its importance by looking at various aspects:

In order to get an impression about the impact of PTA a first approach might be achieved through follow-up studies made after joint reconstructive surgeries. One way to demonstrate this on the most important sites of PTA is to take the three load bearing joints of the hip, knee and ankle as an example:

Mata et al. (Matta 1996 [144]) reported a 24% rate of fair or poor outcomes after acetabular fracture reconstructive surgery of 255 patients in a follow up of six years. They state that proper anatomic reduction by the surgeon is the most important goal in order to prevent PTA. At the same time they say that PTA is the primary complication after this type of surgery. In a meta-analysis of 3670 patients this number was confirmed to be approx. 20% (Giannoudis 2005 [78]).

Looking at tibia plateau fractures, we can find the same pattern. In a long term follow-up of operative treatment of 109 patients and after a mean period of 14 years Rademakers et al. (Rademakers 2007 [175]) radiologically confirmed 31% of PTA in these patients although 64% of them showed no or hardly any clinical symptoms. A strong correlation between PTA and functional results was also stated.

Following this idea PTA also is the major complication after ankle surgery (Day 2001 [60]). Confirming this, Stufkens et al. (Stufkens 2010 [206]) consider the fracture reduction as one of the most important factors for excellent or good long term outcomes after ankle fractures.

In 2006 Brown et al. (Brown 2006 [40]) made an estimation on the prevalence and economic impact of PTA. Based on an extrapolation from patients of the University of Iowa Hospitals and Clinics, they calculated it to affect 5.6 million individuals in the United States. Furthermore, they encountered the percentage of PTA patients out of all patients with arthritis to be 12.04%.

From the economic point of view, 11.8 billion USD are lost through PTA per year of which 26% (3.1 billion USD) are spent for treatment and 74% (8.7 billion USD) are

lost due to indirect costs. Thus 3.1 billion USD account for 0.156% of the US health care costs.

Summing up, PTA has a high percentage of young patients as compared to osteoarthritis as a whole and it generally is described as a very painful and disabling condition. It is the number one complication after trauma of weight bearing joints and affects 5.6 million persons in the United States. In addition it causes 11.8 billion USD costs per year of which 3.1 billion USD account for direct treatment and therefore 0.156% of the total of the US health care costs.

2.2.2 An Overview on Post-Traumatic Arthritis

PTA develops in a very predictable manner after intra-articular fracture. Other joint injuries might also lead up to degenerative changes of the articular cartilage but are not as frequently observed (Swiontkowski 2000 [208]). An intra-articular fracture does not only comprise a disruption of the cartilage and underlying bone but often also includes a complex pattern of soft tissue and nerve injuries around the joint or might even affect the joint on a systemic level as frequently seen in poly-traumata.

The current treatment of an intra-articular fracture is open reduction and internal fixation. Although failure to do so in an adequate manner is associated with higher incidence of PTA (Wright 1994 [232]), there is a complicated mechanism to be discovered in this particular area of arthritis which includes far more complex interactions than those ones that can be explained by failure of anatomic reduction (Fig. 5). Despite all efforts made to restore the joint's original shape after fracture, clinical reduction of joint fragments always leads to an alteration of stress levels within the joint (Hak 1998 [87], Huberbetzer 1990 [102]). Areas of abnormal high stress are the result and this has been associated with joint degeneration (Guilak 1997 [84]). Decreased compressive stiffness, increased hydration and proteoglycan loss have been reported as consequence (Setton 1997 [195]). Recent studies also describe inflammatory processes associated with altered loading (Fermor 2002 [68]). Further research has to be done in order to elucidate this aspect of PTA.

As an avascular, aneural and alymphatic tissue, cartilage is characterized by little self-healing capacity. After intra-articular fracture chondrocytes typically react with an increase of biosynthesis and matrix degradative changes (Huiskes 2005 [103]). The osteochondral defect is filled with a fibrocartilageneous scar which is rich in collagen I. As disease progresses cartilage potentially fibrillates, clefts are formed and in end stage PTA the cartilage is worn down to the bone (Vigorita 2008 [226]).

Chondrocyte death is believed to play an important role for PTA. Necrosis is the type of cell death that occurs immediately after impact due to direct trauma. Apoptosis is

a tightly controlled way of cell death. There is sufficient literature that strongly suggests a correlation between chondrocyte death and cartilage degeneration. Which role direct impact and inflammation play on apoptosis still has to be elucidated (Borrelli 2006 [39], Hembree 2007 [97], Mistry 2004 [146]).

Inflammation after intra-articular fracture is thought to be part of the physiologic healing process but might as well lead to degenerative changes. Il-1 and TNF-α are able to lead to an up-regulation of inflammatory mediators such as nitric oxide, prostaglandins and cyclooxygenases (Abramson 1999 [2], Amin 1996 [11]). Il-6 and Il-8 have also been shown in increased concentrations after joint trauma (Irie 2003 [106]). Changes in gene expression are found as a result whereby biosynthesis of enzymes such as metalloproteinases is believed to encourage degradative changes (Pickvance 1993 [169]).

Although primary osteoarthritis differs in many aspects from PTA a variety of genetic studies have been done that might as well help to understand our subset of degradative changes. Genomic intervals have been associated for OA susceptibility, for instance, that code for Il-1 and the metalloproteinase ADAM12 (Loughlin 2005 [136]). Different studies have shown a 50% heritability of OA implying genes that code for insulin-like growth factor, transforming growth factor beta, aggrecan and collagens II, IX, and XI (Spector 2004 [200]). Additionally, there are many other genetic factors that only due to a secondary pathway lead to OA or PTA. Obesity, for example, is a known risk factor for OA (Bell 2005 [26]).

PTA is a very debilitating disease after intra-articular fracture which is commonly found in young patients. Altered mechanics, loss of chondrocyte viability, inflammatory responses and genetics are some areas which cause particular interest and might even yield some future treatment options. The exact mechanisms and how they interact with each other, however, are still largely unknown and need further research.

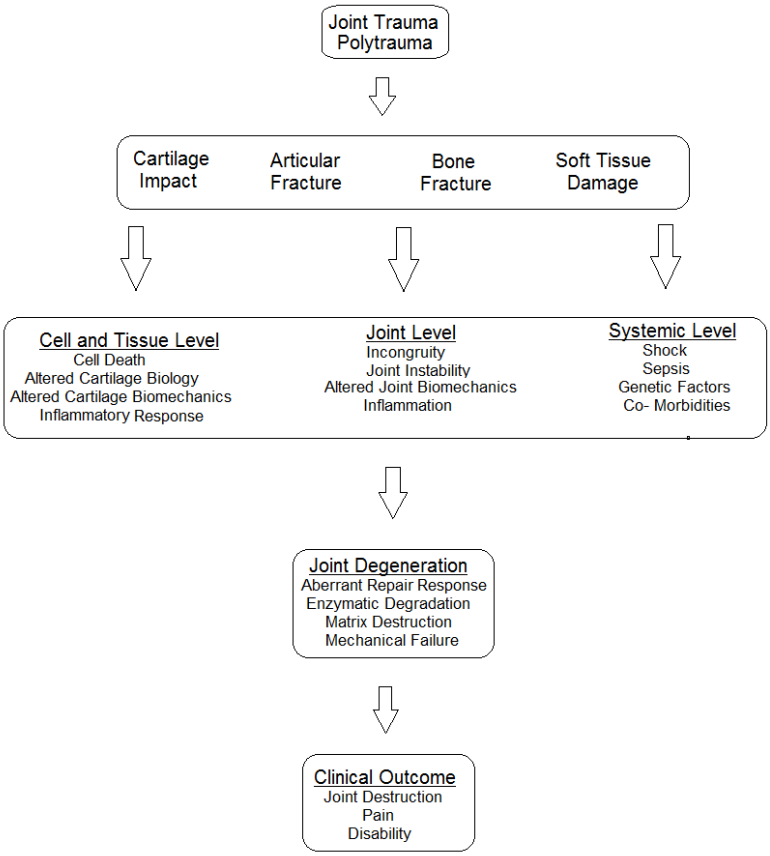

Fig. 5 Development of PTA and its factors involved as proposed by Furman et al. (Furman 2006 [74]).

2.3 Mechanical Properties of Articular Cartilage

In order to understand the mechanical behavior of hyaline cartilage it is inevitable not only to exactly know cartilage's structure and composition but also to gain some insight into basic mechanics, into its behavior under specific types of stress and to take a brief look at the apparatus that have been used in the past to test this "material".

2.3.1 Basic Definitions

2.3.1.1 Stress

Stress (σ) is the intensity of force (P) distributed over a given area (A). Thus, stress in axial loading is defined as:

$$\sigma = P/A$$

A positive sign is used to express tensile stress; a negative sign expresses compressive stress.

P is usually written as Newton (N) and the area as m². Therefore, σ= N/ m² = Pascal (Pa). However, in the United States stress is often expressed as pounds (lb) per square inch (in²) which is abbreviated psi. One pound equals 0.454 kilograms and one inch is the equivalent of 2.54 centimeters (Beer 1992 [24]).

2.3.1.2 Distribution of Stress in Axial Loading

Rather than using the average stress of a given area, in some cases it is necessary to define stress at a given point. We let the area ΔA approach zero:

$$\sigma = \lim_{\Delta A \to 0} \Delta F / \Delta A$$

It must also be noted that, for instance, in a cylinder subjected to the loads P and P' (Fig. 6) the distribution of load far away from the ends will be evenly distributed whereas we find points of high concentration of load at the loading points. Furthermore, for an even distribution of stress it is necessary that the line of action of concentrated loads P and P' pass through the centroid of the sample (Beer 1992 [24]).

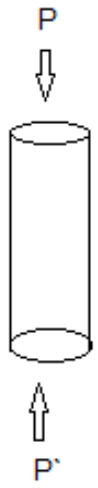

Fig. 6 Cylinder subjected to load P and P´.

2.3.1.3 Shearing Stress

Applying forces P and P' at two different points of a member AB, internal forces referred to as shearing forces (τ) come into being. In this example, P is the magnitude of resulting forces and A is the area of cross section.

$$T = P/A$$

Again, τ is an average value. The shearing stress across the section A are not uniform (Beer 1992 [24]).

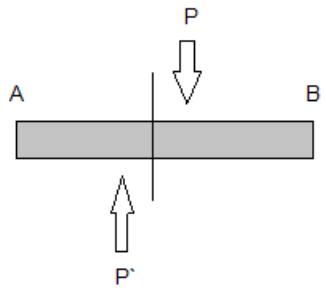

Fig. 7 Shearing stress applied to member AB.

2.3.1.4 Strain

Strain (ε) in a cylinder under axial loading is defined as deformation (δ) per unit length (L).

$$\varepsilon = \delta / L$$

Specific characteristics of a specimen can be seen in a stress-strain-diagram. Different materials result in different stress-strain-diagrams at different temperatures. We generally distinguish between ductile (Fig. 9) and brittle (Fig. 8) materials.

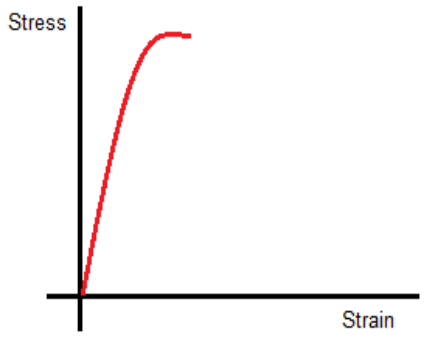

Fig. 9 Stress-strain-diagram of a ductile material with rupture after typical “necking” before rupture (tensile stress applied).

Fig. 8 Stress-strain-diagram of a brittle material such as stone or glass without change of rate of elongation prior to rupture (tensile stress applied).

It must be noted that the area/diameter of the material changes under stress in unconfined compression. Hence, a “true stress” and “true strain” diagram would also take this variation into account. However, it is generally accepted to only use the initial length (L_o) for stress- strain- diagrams (Beer 1992 [24]).

2.3.1.5 Hooke's Law and Young's Modulus

Many materials undergo only little deformation under tensile stress. Therefore, we find stress to be directly proportional to strain in the initial portion of the diagram (Fig. 10). This leads us to the following Hook's Law:

$$\sigma = E*\varepsilon$$

Where σ is stress, ε is strain and E represents Young's Modulus (also called Modulus of Elasticity or Tensile Modulus). E is also expressed in Pascal or psi (Beer 1992 [24]).

Fig. 10 Following Hook's Law, stress and strain are directly proportional during the initial phase in a stress-strain-diagram.

2.3.1.6 Bulk Modulus or Compressive Modulus

The way Young's Modulus describes the characteristics of a material under tensile force, Bulk Modulus describes the compressive stress needed in order to apply a certain strain to a material (Beer 1992 [24]).

2.3.1.7 Shear Modulus or Modulus of Rigidity

Following the above mentioned idea, the shear modulus describes the ratio between shear stress and shear strain (Beer 1992 [24]).

2.3.1.8 Poisson's Ratio

If we compress or stretch any material, strain will not only be found in the axial direction but also laterally. Thus, in a homogeneous material we will find a certain ratio between lateral and axial strain. This ratio is called Poisson's ratio (v) (Beer 1992 [24]).

$$v = \left|\frac{Lateral\ Strain}{Axial\ Strain}\right|$$

2.3.1.9 Elastic and Plastic Behavior of Material

Within the elastic limit of a given material any strain applied will disappear after loading. At the end point of that elastic limit, we find the yield point. Once it has been passed plastic deformation will take place and the original strain will not return. Here,

plastic deformation is not only stress dependent but also time dependent. Time dependent deformation is referred as creep, stress dependent as slip (Beer 1992 [24]).

2.3.1.10 Fatigue

Rupture might occur at a lower stress than the elastic limit after a certain amount of loading cycles. This phenomenon is called fatigue. Depending on the number of loading cycles and the maximum stress of them, an endurance limit can be calculated for a material. Thus, the endurance level is defined as the limit of stress for which failure does not occur even after an unlimited number of loading cycles (Beer 1992 [24]).

2.3.2 A Mechanical Characterization of Cartilage

Structural differences of articular cartilage have been looked at in previous sections. This structural inhomogeneity leads to a complex mechanical behavior which is going to be elucidate in the following text:

2.3.2.1 Permeability of Articular Cartilage

Permeability is a measurement of how easily a fluid can pass through a porous material. Taking into account that cartilage contains fluid, its porosity is defined as fluid volume over total volume. In articular cartilage we find this value to be around 80%. Due to the already described collagen-proteoglycan matrix, nearly all pores in cartilage are interconnected. The large surface of pore walls results in a high frictional resistive force during the movement of fluids within cartilage and thus a very low permeability. Hydrostatic pressure generated by ion electrochemical potential also regulates interstitial fluid flow. Darcy's law states a linear correlation between fluid flux and the pressure gradient. Depending on the applied strain, articular cartilage permeability is found around $8x10^{-15}$ $m^4/N*s$ (very small strain) and $1*10^{-16}$ $m^4/N*s$ (50% strain) (Frankel 2001 [71], Fung 1993 [73], Guilak 2003 [85], Hayes 1997 [95], Huiskes 2005 [104], Mansour 2003 [140], Mooney 2003 [150], Woo 1990 [231]).

2.3.2.2 Aggregate Modulus

The Aggregate Modulus describes the elasticity or stiffness of cartilage after all the fluid flow has ceased, for instance after confined creep loading with a porous indenter. We can find this number to be between 0.5 and 0.9 MPa whereas Young's Modulus is typically located between 0.45 and 0.8 MPa, meaning that cartilage at equilibrium compression is stiffer than before loading (Frankel 2001 [71], Fung 1993 [73], Guilak 2003 [85], Hayes 1997 [95], Huiskes 2005 [104], Mansour [140], Mooney 2003 [150], Woo 1990 [231]).

2.3.2.3 Viscoelasticity of Articular Cartilage

Viscoelasticity describes the cushioning and elastic properties of a material that vary with the magnitude and duration of stress. The collagen-proteoglycan matrix generates internal friction during loading. In addition, the frictional drag between fluid and solid components results in cartilage's viscoelastic properties. Thus, in a typical indentation or stress-relaxation test upon unloading we can observe an instantaneous recovery in size followed by a time-dependent one (Frankel 2001 [71], Fung 1993 [73], Guilak 2003 [85], Hayes 1997 [95], Huiskes 2005 [104], Mansour [140], Mooney 2003 [150], Woo 1990 [231]).

2.3.2.4 Tensile Properties of Articular Cartilage

The collagen mesh in cartilage leads to a wide range of Young's Modulus during tension (between 3 and 100 MPa). Collagen fibrils have a wave form under normal circumstances. Under tension they are stretched and eventually rupture. This means that with increasing tension we find an increased stiffness until failure occurs (Frankel 2001 [71], Fung 1993 [73], Guilak 2003 [85], Hayes 1997 [95], Huiskes 2005 [104], Mansour 2003 [140], Mooney 2003 [150], Woo 1990 [231]).

2.3.2.5 Creep Response of Articular Cartilage

In order to understand the biphasic creep response of cartilage, it is necessary to explain confined compression, which is used in this model: The cartilage explant is placed into an equally sized container, inhibiting deformation in horizontal direction. If stress is applied with a porous indenter, compression equals the loss of fluid. If we take this and the previously mentioned permeability and viscoelasticity theory into account, the biphasic response to axial, confined compression is comprehendible.

Fig. 11 Cartilage deformation under constant stress.

At the point in time A a constant compressive stress is applied to the cartilage sample. Through exudation of fluid (Creep B) the sample reaches its final equilibrium strain (C) (Fig. 11). It has to be noted that exudation is most rapid at the beginning and ceases towards the end due to the increased collagen-proteoglycan stress and frictional drag of the fluid. The time taken to reach the equilibrium strain is directly

proportional to the cartilage thickness (Frankel 2001 [71], Fung 1993 [73], Guilak 2003 [85], Hayes 1997 [95], Huiskes 2005 [104], Mansour 2003 [140], Mooney 2003 [150], Woo 1990 [231]).

2.3.2.6 Biphasic Stress Relaxation Response During Compression

Once the equilibrium strain is reached (A), the compression and thus exudation phase is terminated. As fluid is redistributed within the sample, the phase of stress relaxation begins. We can follow the decrease of stress until the compressive stress within the material equilibrates with the intrinsic compressive modulus (B) (Frankel 2001 [71], Fung 1993 [73], Guilak 2003 [85], Hayes 1997 [95], Huiskes 2005 [104], Mansour 2003 [140], Mooney 2003 [150], Woo 1990 [231]).

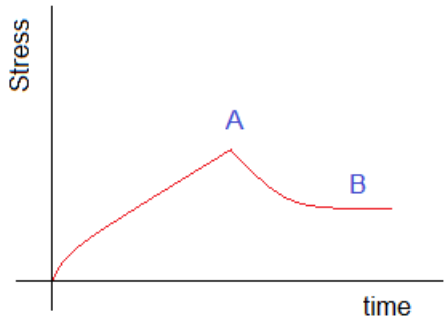

Fig. 12 Biphasic stress relaxation of cartilage during compression.

2.3.2.7 Anisotropy of Articular Cartilage

As already stated, Young's Modulus describes the stiffness of a material. Calculating this property for articular cartilage, provides two different values. In samples harvested parallel to the split lines it is greater than in those ones harvested perpendicular to the split lines. These differences of stiffness indicate that cartilage is an orthotropic material with three major axes: tangent, perpendicular and radial to the surface. Interestingly, these layered variations are not found in immature cartilage (Camosso 1962 [43], Rieppo 2009 [183]). Furthermore, Poisson's Ratio in uniaxial tension is found to be greater than 0.5 which also indicates anisotropy of cartilage (Frankel 2001 [71], Fung 1993 [73], Guilak 2003 [85], Hayes 1997 [95], Huiskes 2005 [104], Mansour 2003 [140], Mooney 2003 [150], Woo 1990 [231]).

2.3.2.8 Articular Cartilage Under Shear Stress

Behavior of cartilage under pure shear stress is of particular interest because it describes only the intrinsic viscoelastic properties of the collagen-proteoglycan matrix. In an ideal model only shear stress and an infinitesimal amount of compression is applied to the sample. Therefore, no volumetric change, no pressure gradients and no interstitial fluid flow occur within the sample and thus only the above mentioned characteristics of the collagen-proteoglycan matrix come into play.

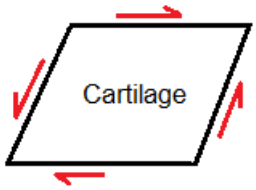

Fig. 13 Cartilage under pure share

In reality one has to imagine the experimental setup as two discs with a certain angle and a certain rotational force at each end of the sample. The dynamic shear modulus (G_{total}) consists of the elastic storage modulus ($G_{elastic}$) and the viscous loss modulus ($G_{viscous}$): $|G_{total}|^2 = (G_{elastic})^2 + (G_{viscous})^2$

The value of the dynamic shear modulus reflects the resistance offered by the collagen-proteoglycan matrix. In bovine articular cartilage it was found between 1 and 3 MPa. The angle between the disc and the sample indicates the total frictional energy dissipation within the sample. Thus, in a fully elastic material the angle would be 0°, in a fully viscous material 90°. In bovine cartilage it has to be located between 9° and 20°.

Characterizing proteoglycans, an interesting observation has been made. Proteoglycan solutions of similar concentrations as in cartilage showed a shear modulus of 10 Pa and a shift angle of 70%. This suggests that shear stiffness in articular cartilage mostly derives from collagen or collagen-proteoglycan interactions (Frankel 2001 [71], Fung 1993 [73], Guilak 2003 [85], Hayes 1997 [95], Huiskes 2005 [104], Mansour 2003 [140], Mooney 2003 [150], Woo 1990 [231]).

2.3.2.9 Swelling Behavior of Articular Cartilage

Looking at cartilage's extracellular matrix, we find a collagen grid and to it attached proteoglycans with negatively charged SO_3^- and COO^- groups. This charge is equalized by electrolytes in the interstitial fluid, leading to an overall tissue charge neutrality. However, compared to its environment cartilage contains more ions and thus creates a higher fluid pressure which is also referred to as Donnan osmotic pressure or swelling pressure. In articular cartilage this Donnan osmotic pressure contributes with 0.15 to 0.17MPa to the compressive stiffness of cartilage (Frankel 2001 [71], Fung 1993 [73], Guilak 2003 [85], Hayes 1997 [95], Huiskes 2005 [104], Mansour 2003 [140], Mooney 2003 [150], Woo 1990 [231]).

2.3.2.10 Lubrication of Articular Cartilage

There are various theories about how articular cartilage obtains its frictional properties.

The fluid film lubrication theory states that each joint surface is covered by a thin fluid film which provides greater surface separation and also protects the surface with its

specific fluid film pressure. There are two types of fluid film lubrication. The first one is called hydrodynamic lubrication. It occurs when two non-parallel surfaces are sliding on top of each other and the fluid is dragged in between those surfaces by the motion. The second one describes the squeezing out of viscous fluid in between two surfaces and is therefore called squeeze film lubrication. However, unlike many industrial materials, cartilage is not rigid but relatively soft. Thus during squeeze film and hydrodynamic lubrication high pressure is generated within the fluid film and the underlying cartilage layer is deformed. This specific case of lubrication is called elastohydrodynamic lubrication and increases the bearing surface area and its congruency and thus allows an increase of bearing capacity. It also has to be stated that the lubricants properties such as viscosity, elasticity and rheology greatly influence this process. Therefore, it was somewhat disillusioning that changing the properties of the lubricant synovial fluid had little effect on lubrication in diarthrodial joints, thus suggesting that the primary mechanism of joint lubrication must be a different one (Frankel 2001 [71], Fung 1993 [73], Guilak 2003 [85], Hayes 1997 [95], Huiskes 2005 [104], Mansour 2003 [140], Mooney 2003 [150], Woo 1990 [231]).

Boundary lubrication occurs when the lubricant is adsorbed into the surface of the joints. Surface-active phospholipids might form the top layer of cartilage. The chemical properties of soluble lubricants such as HA and lubricin characterize boundary lubrication. There is some discussion about which substance within the SF act as main boundary lubricants and how they interact with the phospholipid layer (Frankel 2001 [71], Fung 1993 [73], Guilak 2003 [85], Hayes 1997 [95], Hills 2000 [99], Huiskes 2005 [104], Mansour 2003 [140], Mooney 2003 [150], Woo 1990 [231]).

The exact mechanism of lubrication, however, remains unclear. In another attempt to bridge this gap of knowledge, the theory of mixed lubrication was put forward. As already stated, joint surfaces are not perfectly congruent, neither on a macroscopic nor on a microscopic level. Thus, in areas where the joint surfaces are located closer to each other, boundary lubrication might be more likely. In areas where the joint surfaces are located further from each other, we find more pressurized fluid and thus we can apply the theory of fluid flow lubrication (Frankel 2001 [71], Fung 1993 [73], Guilak 2003 [85], Hayes 1997 [95], Huiskes 2005 [104], Mansour 2003 [140], Mooney 2003 [150], Woo 1990 [231]).

Yet another theory hypothesizes that during weight bearing, synovial fluid is filtrated into the proteoglycan-collagen meshwork of cartilage, leaving behind bigger molecules such as hyaluronic acid. Taking all this into account, it is impossible to define lubrication as a set configuration of different models. Instead it has to be stated that all this depends on the velocity of the moving joints, the actual weight, the individual surface congruity and the presence and production of certain proteins within the synovial fluid and cartilage (Frankel 2001 [71], Fung 1993 [73], Guilak

2003 [85], Hayes 1997 [95], Huiskes 2005 [104], Mansour 2003 [140], Mooney 2003 [150], Woo 1990 [231]).

2.3.2.11 Physiologic Versus Pathologic Loading

Other than in many experimental setups which use static loading, physiologic *in vivo* loading takes places on an intermittent or cyclic basis. Keeping this in mind, every day activities cause maximal contact stresses of around 2 MPa, strenuous activity approx. 6 MPa and the upper limit of non-traumatic loading around 12 MPa (Ahmed 1983 [6], Matthews 1977 [145]). Other studies state the maximal non traumatic stress to be around 18 MPa (Hodge 1989 [100]). However, peak stresses are also expressed in body weight (BW). The lower extremity can account for maximal physiologic stresses of 4.9 BW, the upper extremity for 0.9 BW (Paul 1976 [164], Poppen 1978 [172]). Other than the peak force and BW, research has been done to determine physiologic strains of articular cartilage. Cadaveric studies showed a strain of 20% under 5 BW stress and 6% strain under 1 BW stress (Armstrong 1979 [15], Ateshian 1997 [17]). Furthermore, fluid pressurization plays a key role. Cartilage's very low permeability causes interstitial water to be pushed into the collagen meshwork during loading. This leads to a load distribution throughout the different layers (Mow 1977 [153]).

2.3.2.12 Inhomogeneity of Articular Cartilage Mechanical Properties

Looking at the microscopic cartilage architecture, it becomes obvious that different layers must have different mechanical properties. It is incorrect, however, to define specific mechanical values and properties to each layer without the use of a constitutive testing model. Thus, it is not possible to compare cartilage material properties without referring them to a constitutive model (Guilak 2003 [86]). For my project it is important to focus on variable compressive moduli throughout the cartilage layers. Schinagl et al. (Schinagl 1997 [191]) (Table 3) showed very clearly how overall cartilage strain is mainly absorbed by the superficial layer.

Table 3: Schinagl et al. (Schinagl 1997 [191]) showed different magnitudes of strain in 125µm thick chondral slices beginning at the cartilage surface in bovine ostechondral explants (Z= Displacement). The values ($|du_z/dz|$ or slope of regression fits) indicate a much higher strain in the superficial than in the deeper zones during the same overall strain.

			Distance from Surface in µm								
			0- 125	**126-250**	**251-375**	**376-500**	**501-625**	**626-750**	**751-875**	**876-1000**	**1000-1125**
Strain in %	**32**	$\|du_z/dz\|$	0.58	0.53	0.52	0.46	0.38	0.28	0.24	0.19	0.18
	24		0.52	0.49	0.44	0.38	0.29	0.19	0.16	0.10	0.10
	16		0.46	0.42	0.34	0.25	0.18	0.07	0.06	0.03	0.03
	8		0.36	0.27	0.18	0.07	0.04	0.01	0.01	0.01	0.02

2.4 Apoptosis Versus Necrosis

2.4.1 Introduction

Chondrocyte death or survival plays an important role in the degradation as well as integrity of cartilage. Recent studies have focused on four major types of cell death: apoptosis, necrosis, oncosis and autophagy. Apoptosis describes programmed cell death which can be physiologic or pathologic. Necrosis is always a pathologic process and is characterized by death due to an external stimulus (Table 4). Oncosis describes the morphological changes of necrosis. Recent research suggests that it is induced by a receptor signaling cascade. Autophagy depends on vacuolar proteolysis (Kuhn 2004 [120]).

Table 5: Main differences in terms of morphology, physiology and consequences of apoptosis and necrosis (Kuhn 2004 [120]).

	Apoptosis	Necrosis
Morphology	• Shrinking of cytoplasm and chromatin condensation • Nuclear fragmentation • Formation of membrane enclosed structures (apoptotic bodies)	• Swelling of cytoplasm and mitochondria • Non-specific karyolysis • Total cellular disintegration without formation of vesicles
Physiology	• Induced by physiologic stimuli • Tightly regulated signaling events • Energy dependent • Enzymatically catalyzed changes of cell membrane • Orderly fragmentation of chromosomal DNA (DNA laddering) • Activation of caspases • Late loss of membrane integrity	• Induced by non-physiologic stimuli • Early loss of membrane integrity • No energy requirement • Random digestion of nuclear DNA • DNA degradation occurs after membrane permeabilization
Consequences	• Affects individual cells • Phagocytosis by adjacent cells or macrophages • Typically not associated with an inflammatory response	• Affects groups of cells in a tissue • Associated with an inflammatory response • Disintegrating cells are phagocytosed by leukocytes

2.4.2 Looking at Mechanisms of Apoptosis

In many cases, apoptosis approaches from the outside of the cell (extrinsic pathway) (Fig. 14). In this case the FAS-receptor and other TNF-receptors are examples of plasma membrane receptors of FAS and TNF, respectively. A chain of protein activation and amplification is commenced. The cytosolic protein TNF-receptor-associated-death-domain (TRADD) typically binds on the TNF-R1 receptor after activation. FADD (FAS-associated-death-domain) activates pro-caspase 8 after contact with the FAS receptor. Caspase 8 through BID targets the membrane of mitochondria and causes the release of cytochrome c which potentiates activation of intrinsic pathway. However, both pathways end up with the activation of caspase 3 which induces further apoptosis execution. Looking at the TNF pathway it is important to note that the activation of TNF-R1 can also induce IκB degradation and thus NFκB activation (Cox 2000 [55], Donald Voet 2006 [63]).

The intrinsic or mitochondrial pathway is activated by certain cell stresses such as various cytotoxic stimuli during chemotherapy (Fulda 2006 [72]). This leads to an increase of permeability of mitochondrion's outer membrane and the release of certain substances, most importantly cytochrome c. Adenosine triphosphate ATP together with cytochrome c is able to activate Apaf-1 (pro-apoptotic protease activating factor) which, with the use of a positive feedback mechanism through caspase 7, finally leads to the activation of caspase 3 (Cotran 1999 [54]).

Inside the cell we can find inhibitors and promoters of apoptosis. Bcl-2 and Bcl-XL typically inhibit apoptosis by controlling the permeability of the mitochondrial membrane and thus cytochrome c concentration. Bax and Bad can bind to Bcl-2 and promote apoptosis. Apaf-1 should also be mentioned. It can be bound by cytochrome c and activate a zymogen caspase or be inactivated by Bcl-2.

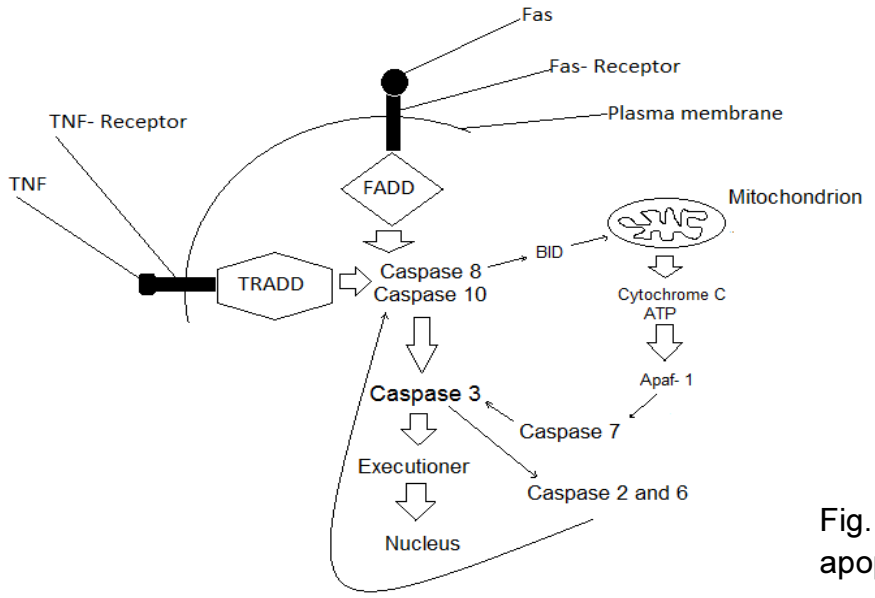

Fig. 14 Basic pathways of apoptotic cell death.

The process of DNA degradation initiates the execution phase. Deoxyribonucleases break down DNA double strands and lead to the formation of equally cut fragments which typically form the DNA ladder in electrophoresis. Morphological changes as described in the table above occur. Apart from budding, the cell is also more easily recognized by phagocytes due to marker molecules on the cell surface (Cotran 1999 [54]).

2.4.3 Apoptosis of Chondrocytes

In theory, chondrocyte death leads to incapability of maintaining homeostasis and integrity of articular cartilage (Mistry 2004 [146]). Furthermore, there is evidence that shows a close correlation between the amount of chondrocyte apoptosis and the severeness of OA (Blanco 1998 [35], Hashimoto 1998 [94], Heraud 2000 [98]). Thus, a treatment that blocks chondrocyte apoptosis during senescence, wear, tear or injury is a possible way to maintain cartilage's characteristics and to prevent OA. There are various studies that deal with apoptosis in OA:

Looking at C57BL/6 mice and Wistar rats at various ages up to 24 months, there was a significant increase of apoptotic chondrocyte death found with increasing age (Adams 1998 [4]). The same observation was made in healthy human cartilage (Blanco 1998 [35]). Hence, a portion of apoptotic cell death in all studies can probably be attributed to senescence.

As opposed to this physiological way of chondrocyte apoptosis we find many other pathways of pathologic apoptotic cell death: As cartilage is an avascular tissue all cell remnants remain within the tissue after cell death. Many studies report membrane enclosed bodies inside the lacunae of dead chondrocytes. Supporting the theory of apoptotic cell death, many reports suggest that these bodies might be apoptotic bodies and that they might even contribute to pathologic cartilage calcification and degradation (Blanco 1998 [34], Hashimoto 1998 [92]).

Nitric oxide (NO) levels were found to be elevated during early stages of OA and thus suggest that they induce chondrocyte apoptosis. Hashimoto et al. (Hashimoto 1998 [94]) describe the formation of peroxynitrite (NO + superoxide radical) which reacts with aromatic amino acids to form products such as nitrotyrosine. This can be used as a NO-depent marker of OA. Findings that Il-1, TNF and lipopolysaccharides induce NO production whereas transforming growth factor β, insulin-like growth factor or fibroblast growth factor are not associated with an increase in NO concentration provide further evidence of NO's catabolic character. In addition, NO is a known inhibitor of proteoglycan synthesis. Evidence also exists that NO donated

from external sources such as sodium nitroprosside or 3-morpholinosynonimidehydrochloride induce apoptosis (Blanco 1995 [36]).

Various reports emphasize the importance of prostaglandins in chondrocytes. For instance, changes in prostaglandins are observed after application of mechanical forces on physeal cartilage (Mankin 1998 [139]). Furthermore, prostaglandins are thought to be the most potent cytokine regulating DNA synthesis and sulfate incorporation (Okeefe 1992 [161]). In addition, increased levels of prostaglandins are found in OA (Sahap Atik 1990 [189]). Finally, both, prostaglandin E2 apparently through the EP2- and EP4-receptors and its downstream products cAMP and proteinkinasis A induce DNA fragmentation und thus apoptosis (Miwa 2000 [147]). Emphasizing this pathway, Il-1 leads to an increase of COX 2 mRNA expression in chondrocytes (Morisset 1998 [152]).

The FAS-ligand is a homotrimeric type II transmembrane protein that after binding leads to trimerisation of the FAS-receptor (CD95 or APO-I). The FAS-receptor belongs to the TNF-receptor family. It is important to state that the FAS-pathway acts independently from the NO-pathway. In addition, it seems that chondrocytes themselves are not able to produce the FAS-ligand, thus a synovial inflammation is probably necessary to activate its pathway (Hashimoto 1997 [93]).
Il-1β is a fundamental anti-apoptotic factor acting on the FAS-pathway. Evidence exists that NFκB, tyrosine kinases and maybe Bcl-2 are involved in this protective effect after FAS-receptor activation (Kuhn 2000 [121]). Another study supports this evidence and adds that apoptosis induced by the FAS-receptor is executed by caspase 3. It is also stated that this mechanism activates caspase 8 which again potentiates caspase 3. Caspase 9 is not involved in FAS induced apoptosis (Kuhn 2001 [122]). However, Heraud et al. (Heraud 2000 [98]) found a significant increase of apoptotic chondrocytes after co-culturing human articular cartilage samples with Il-1β.

In the skeletal system TNF-α stimulates bone and cartilage resorption and inhibits proteoglycan and collagen synthesis. It is also thought to stimulate osteoblasts in the process of endochondral ossification (Aizawa 2001 [8]). TNF-α, Il-1β and anti-FAS antibodies activate endonucleases and thus apoptosis (Fischer 2000 [70]).

Anoikis is Greek and stands for homelessness. Like many other cells, chondrocytes need their surrounding ECM to survive. For instance, lack of collagen II leads to an increase of cell death presumably through apoptosis (Yang 1997 [235]). Besides, mice without collagen II receptor intergrin α1β1 have been shown to be more likely to loose chondrocytes through apoptosis and to develop cartilage degeneration, PG

loss and synovial hyperplasia (Zemmyo 2003 [237]). Finally, lack of hyaluronan also leads to apoptotic chondrocyte death (Lisignoli 2001 [128]).

As already stated, mitochondria play a vital role in the intrinsic pathway of apoptosis. Mitochondrial membrane potential is significantly reduced in OA and in the mitochondria of NO supplemented chondrocytes. This is not associated with increased cell death but does not exclude the possibility that a reduced mitochondrial potential makes chondrocytes more prone to other stimuli (Maneiro 2003 [138], Tomita 2001 [216]).

Many studies have tried to elucidate the influence of the tumor suppressor protein p53 and the protein c-myc. P53 knockout mice were found to show no cartilage degradation during immobilization as opposed to wild type mice which show degenerative changes under the same conditions (Okazaki 2003 [160]). Hydrostatic pressure induces human chondrocyte apoptosis via p53 (Islam 2002 [107]). NO induces apoptosis in rabbit cartilage via p38 and NFκB (Kim 2002 [114]). Findings such as an increase of c-myc concentration together with an increase of the amount of apoptotic cells after application of hydrostatic pressure indicate some sort of correlation (Fig. 15) (Islam 2002 [107]). However, there is no direct evidence that c-myc has an effect on chondrocyte death or survival.

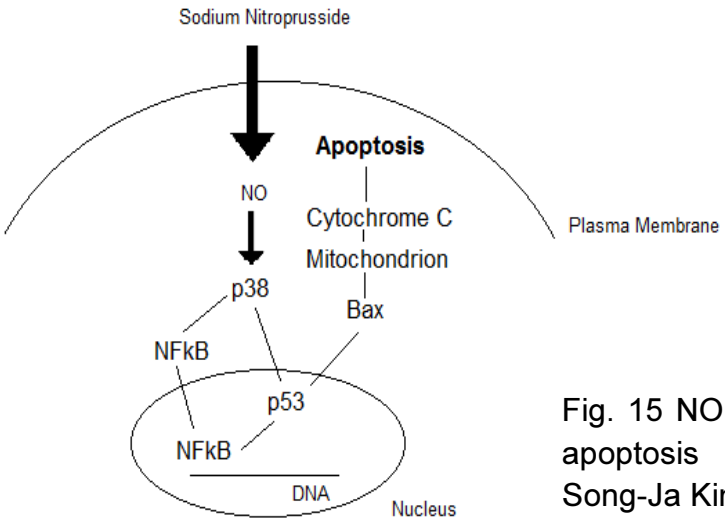

Fig. 15 NO, P38, NFκB, p53 mediated apoptosis pathway as proposed by Song-Ja Kim (Kim 2002 [114]).

Programmed cell death also occurs during normal skeletal development. Calcified matrix is formed just next to the hypertrophic zone in the growth plate. Vascular invasion and chondrocyte death follows. Avian epiphyses are characterized by the formation of “dark chondrocytes” (Erenpreisa 1998 [65]). “Paralyzed chondrocytes”

also show ultrastructural features of apoptosis and necrosis and occur during bone formation (Roach 1999 [185]). Thus, chondrocyte death in the growth plate during skeletal development shows DNA degradation as verified by TUNEL but it also shows ultrastructural changes that suggest a distinct form of cell death other than apoptosis and necrosis.

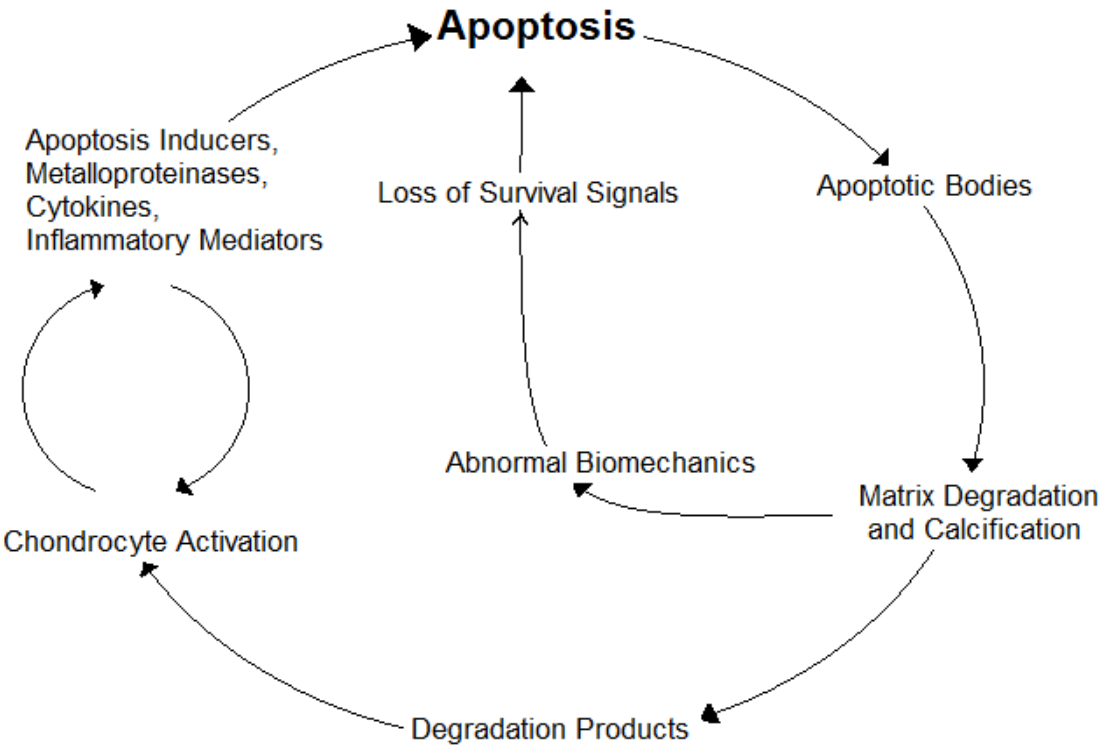

Fig. 16 Cartilage degradation caused by apoptosis: Kühn et al. (Kuhn 2004 [120]) suggest a vicious cycle emphasizing inflammation.

Chondrocyte apoptosis has been detected in OA cartilage in humans as well as in animals. Cell death leads to cartilage degradation and abnormal mechanical properties. Furthermore, inflammatory responses including the production of cytokines, aggrecanases and metalloproteinases cause further matrix destruction and enhance the degenerative cycle (Fig. 16). However, the exact mechanisms of chondrocyte death and their effect on cartilage still remain to be explained in detail. At the same time, forms of treatment are being developed that seem to be particularly promising for apoptotic chondrocyte death (Kuhn 2004 [120]).

2.4.4 Apoptosis in Post-Traumatic Arthritis

Some investigation has been done to find out which role chondrocyte apoptosis plays after intra-articular fracture. Saving these cells would eventually allow them to restore cartilage matrix and thus prevent PTA.

As a first approach, there exists evidence that mere interruption of the cartilage matrix already induces apoptosis (Tew 2000 [214]). Cyclic loading is known to induce cell death in a dose-dependent manner whereby necrosis is dominant in the superficial layer and apoptosis in the deeper layers (Borrelli 2006 [39]). 4 MPa is believed to be the threshold. Cyclic loading at 6.9 MPa has been shown to induce cartilage damage already after 250 cycles whereas cyclic loading at 3.5 MPa does not show any tissue damage even after 120 000 cycles (Zimmerman 1988 [240]).
Lima et al. (D'Lima 2001 [57]) applied single 7 MPa, 14 MPa and 23 MPa compressions to cartilage explants and assessed apoptosis to account for ≈40% and ≈42% of all visible dead cells two days after impact for 14 MPa and 23 MPa, respectively. Further research supports the hypothesis that single impact loads between 15 MPa and 20 MPa induce significant chondrocyte death (Repo 1977 [181], Torzilli 1999 [218]). The loading rate also significantly influences the amount of chondrocyte death. Faster loading is associated with surface fissuring and a high number of dead chondrocytes along these fissures. Slower loading rates distribute cell death more evenly throughout the sample (Quinn 2001 [173]).

In an *in vivo* study on rabbits, single 80 MPa and 66 MPa impacts were applied to femoral condyles causing 11% and 3% apoptotic chondrocytes, respectively. This further emphasizes the importance of apoptosis after mechanical stimulation. It remains unknown, however, if and to which degree this injury results in PTA (Borrelli 2003 [38]).

Various studies have looked at apoptotic chondrocytes in human cartilage fragments after intra-articular fracture and surgery. Hembree et al. (Hembree 2007 [97]) assessed chondrocyte viability in human articular cartilage fragments after intra-articular fracture along the fracture edge in the superficial, middle, deep and osteochondral junction zone to be 24.1%, 37.6%, 43.6% and 36.5%, respectively. The percentage of apoptotic cell death measured by TUNEL showed 42.9%, 25.7%, 25.8% and 28.9% of apoptotic cells, respectively. Murray et al. (Murray 2004 [157]) showed that the apoptosis rate in a similar experimental setup is somewhere around 35%. They also propose that this high rate of apoptotic cells might be the trigger for future PTA.

2.4.5 Cell Injury and Necrosis

Once a cell is stressed so intensely that it cannot adapt anymore, cell injury occurs. The causes for this event are numerous and range from hypoxia over chemical agents to genetic derangements. The first changes to be seen might be cell swelling due to water influx and appearance of lipid vacuoles. This stage, however, might still

be reversible. The mechanism or biochemical event that leads to the point of no return is still unknown.

ATP is produced by oxidative phosphorylation and by the (anaerobic) glycolytic pathway. Once its production is interrupted Na^+-K^+- ATPases fail and Na^+ accumulates inside the cell, K^+ leaves the cell and water enters due to a net gain of ions. Furthermore, the pH decreases as anaerobic glycolysis produces lactic acid and thus changes the metabolic rate of other enzymes. Ca^{2+} also enters the cell due to defect ion pumps. At later stages, ribosomes detach from rER, lysosomal and mitochondrial membranes are damaged irreversibly and mis-folded proteins occur (Kumar 2005 [123]).

Mitochondria play a specific role during necrosis: First of all they can easily be damaged by an increase in Ca^{2+} concentration, oxidative stress, phospholipase A_2 and lipid breakdown products. Secondly, their membrane potential breaks down, cytochrome c is released into the cytoplasm which can induce the apoptotic pathway. A cytosolic increase in Ca^{2+} concentration also activates enzymes such as ATPases, phospholipase, endonucleases and proteases. During mitochondrial respiration, absorption of radiation and through transition metals such as Fe^{2+}, small amounts of reactive oxygen species are formed. NO can also cause oxidative stress. If reactive oxygen species accumulate they can damage the cell through their unpaired electron in the outer shell. Cell membrane damage, protein mis-folding and DNA lesions are some of the consequences (Kumar 2005 [123]).

The morphologic changes described above are initiated through autolysis (own lysosomes) and through immigrating leukocytes. A general inflammatory response can be seen a few hours after necrosis and is most characteristic in vascularized tissue (Kumar 2005 [123]).

2.5 Metabolism of Articular Cartilage

2.5.1 Homeostasis of Articular Cartilage

In healthy cartilage chondrocytes keep the balance between anabolic and catabolic actions. For instance, collagen physiologically has a very long half-life as opposed to PGs which have a much shorter half-life. Both are synthesized by chondrocytes. However, chondrocytes also respond to changes in their environment such as changes in cytokine presence, stress levels and osmotic pressure. Thus, equilibrium is lost very easily possibly resulting in degenerative changes (Guilak 2003 [85], Mow 2005 [154]).

Chondrocytes adapt through cell surface receptors such as integrins, annexin V (also called anchorin CII) and CD 44 to changes in the ECM. They are able to detect changes in loading as well as degradation. As they usually have a rather low metabolic activity, they can only adapt to a limited extent to these changes. Integrins can act as inside-out and outside-in receptors. On the one hand, the cell can alter integrin expression. On the other hand, binding of collagen, fibronectin, thrombospondin and vitronectin on the outside lead to different gene expression within the cell. Blocking of integrin leads to cessation of growth and differentiation. CD 44 binds to HA and regulates the aggrecan retention within the cartilage. Anexin V interacts with collagen II and X and is supposed to be a mechanotransductor (Guilak 2003 [85], Mow 2005 [154]).

Examples for anabolic cytokines in cartilage are Insulin-like-growth factor I (IGF- I), members of the Transforming-Growth-Factor-β/ Bone Morphogenic Protein Family (TGF- β/ BMP) and Fibroblast-Growth-Factor (FGF). They exercise chondro-protective activities such as collagen and proteoglycan synthesis, differentiation, proliferation and down regulation of Il-1 receptors. Il-1 and TNF-α have been found to be typical catabolic cytokines. Synthesized by chondrocytes or mononuclear cells within the synovial lining, they inhibit collagen II, IX and XI synthesis and induce iNOS and COX-2 synthesis and proteoglycan degradation (Guilak 2003 [85], Mow 2005 [155]).

A Disintegrin And Metalloproteinases With Thrombospondin Motifs (ADAMTS) is the family of the group of aggrecanases and leads to early aggrecan cleavage. Later on MMPs (Metalloproteinases) lead to cartilage degradation by, for instance, inhibiting ligation between GAG and aggrecan. In order to fulfill their function MMPs need the presence of Zn^{2+}. Apart from MT1-MMP and MMP-11, all MMPs are synthesized as pro-enzymes and are activated by pro-fragments cleaved by other proteases. Furthermore, MMPs can be inhibited by Tissue Inhibitor of Metalloproteinases (TIMP). It must also be noted that different MMPs have different substrate specifities. MMP-13 has the highest collagenase II activity, others act as gelatinases, stromelysins or specifically on membranes (Guilak 2003 [85], Mow 2005 [155]).

2.5.2 Impact of Mechanical Stimulus to Chondrocyte Metabolism

As already stated, cartilage responds to mechanical stimulus. Furthermore, it even requires mechanical forces within certain magnitude and frequency ranges in order to maintain the ECM balance. Although the pressure on articular cartilage during movement is estimated to be somewhere between 0 and 20 MPa, the threshold above which cartilage begins to degrade is still largely unknown. However, some metabolic changes have been detected under certain well-defined conditions:

Static stress is generally believed to inhibit PG synthesis. It has to be said, however, that static compression leads to a decrease in matrix hydration, a decrease in nutrient and waste transport, an increase of negative charge density and thus an altered osmotic and ionic environment of chondrocytes. Because similar inhibition of PG synthesis has been observed in cartilage explants cultured in osmotically active media, the inhibition of synthesis is most likely associated with a change in osmolarity. Release from a low static stress leads to a return to the same level of PG synthesis as before the stress. After static compression and release of higher magnitudes we find an even higher level of PG synthesis and after very high compression stresses we encounter a decrease in PG synthesis. Osmotic pressure seems to have the highest effect on PG synthesis. 350- 450 mOsmol is thought to be the best pressure and is also physiologically found in articular cartilage. Hydrostatic pressure also has an effect on PG synthesis: Again, there are three different levels: Pressures smaller than 3 MPa usually do not have an effect, 5- 10 MPa increase PG synthesis and 30-50 MPa inhibit biosynthesis (Guilak 2003 [85], Mow 2005 [155]).

Cyclic compression plays a specific role because of its similarity to normal daily activity in a weight-bearing joint. Chondrocyte deformation, fluid flow and streaming potentials, which all occur during cyclic loading, have been found to increase aggrecan synthesis. With increasing magnitude and velocity, fluid flow and streaming potential increase at the periphery of the sample and hydrostatic pressure is highest at the center of the explant. Thus, in a typical experimental setup where cylindrical cores get loaded, the highest rate of biosynthesis will be found near the edges of the sample (Guilak 2003 [85], Mow 2005 [154]).

Impact loading leads to a characteristic cell death pattern only in the superficial zone even after high stresses and strains. At the same time dramatic structural damage is only found in the same superficial zone. This mechanism has been explained by the lower compressive modulus and by trapping of fluid in the superficial zone. Interestingly, cyclic impact loading leads to a cell death area associated with the indenter. Over time the cell death area increases. If the surrounding cartilage is excised after loading we cannot find a similar amount of cell death. This suggests some sort of intercellular communication after impact. This correlates with the observation that already a single impact can lead to degeneration similar to OA (Guilak 2003 [85], Mow 2005 [154]).

Tensile stretch has been shown to induce an increase of aggrecan synthesis. Excessive and continuous stretch is associated with IL-1, MMP-1, -3, -9 and TNF-α up regulation and thus with cartilage degradation. Again, it has to be mentioned that stretch also leads to fluid motion which might influence protein synthesis. Furthermore, the relationship between substrate strain and chondrocyte strain remains unclear. Shear loading has also been found to increase PG synthesis. This

is of particular interest because it shows that chondrocytes are able to respond to pure shear stress. Electric fields have been used to alter protein synthesis in chondrocytes. Different frequencies and strength have been used. 10- 30 mA/cm^2 with a frequency of 10-1 000 Hz, as well as pulsed electromagnetic fields, stimulate aggrecan biosynthesis (Guilak 2003 [85], Mow 2005 [154]).

In conclusion, it has to be said that static compression leads to an inhibition of PG synthesis whereas cyclic compression stimulates its production. In addition to PG synthesis, other proteins are also altered by physical changes of cartilage. Cartilage Oligomeric Matrix Protein (COMP), which is associated with OA and degradation, as well as fibronectin concentration, increase in articular cartilage after long, low-frequency cyclic loading. NO, NO synthase (NOS), MMPs and TIMPs are also elevated in OA in various loading experiments and thus provide us with a valuable link between loading and inflammation (Guilak 2003 [85], Mow 2005 [155]).

2.5.3 Intracellular Signaling After Mechanical Stimulation

As described in the previous text, mechanical loading directly alters the cell shape, hydrostatic pressure, fluid flow, osmotic pressure and Fixed Charge Density (FCD) around the cell. The next question that has to be answered is how does this physical signal cross the plasma membrane, get converted into a biochemical signal and finally lead to a change in gene expression? There are various explanations to this problem.

Stretch Activated Ion Channels are activated by deformation and volume change. Recent studies suggest that their stimulation leads to a cytoplasmic increase of Ca^{2+} and thus a change in membrane potential. Furthermore, the idea has been put forward that stretch activated ion channels bind directly to a second messenger such as cyclic adenosine monophosphate (cAMP) (Guilak 2003 [85], Mow 2005 [154]).

Changes in the ECM might also be detected by proteins such as HA, aggrecan, collagen or fibronectin that bind to their specific plasma membrane receptor. Intracellular signaling might occur through one or more of the traditional signaling pathways such as the cAMP, IP_3 or Ca^{2+} system (Guilak 2003 [85], Mow 2005 [154]).

An additional hypothesis states that mechanical signaling occurs through the physical connection between organelles and ECM. It is believed that the cytoskeleton and adhesion proteins such as α-actinin, vinculin, talin and integrins bridge the distance. Due to chondrocytes complex interactions with all the above stated variables it is a difficult task to further clarify the signaling pathways (Guilak 2003 [85], Mow 2005 [155]).

2.6 Inflammation in PTA

2.6.1 Inflammatory Changes During Joint Degradation

As already stated, OA is believed to be caused by mechanical and biological changes that destabilize the anabolic and catabolic equilibrium. Once degradative changes are initiated, cells in the synovial membrane phagocyte the break down particles and become hypertrophic. Furthermore, clinical signs such as joint space narrowing, osteophytes and subchondral bone sclerosis can be observed.

2.6.2 Pro-Inflammatory Cytokines and Their Inhibition

Pro-inflammatory cytokines which control the synthesis balance between protecting and degradative enzymes are first produced within the synovial lining cells, later in chondrocytes. The most important ones are IL-1α, IL-1β, IL-6, IL-8, IL-11, IL-17, Leukemia Inhibitory Factor (LIF) and TNF-alpha (Martel-Pelletier 1999 [142]).

In OA, Il-1β and TNF-α are the major degradative mediators. They are both secreted as an inactive protein which is activated by Il-1β Converting Enzyme (ICE) and TNF-α Converting Enzyme (TACE). After activation they bind to either the Il-1 receptor or the TNF-receptor. It is important to state that Il-1β and TNF-α do not only induce proteases, inhibit collagen- and TIMP-synthesis but also stimulate reactive oxygen species and other inflammatory mediators such as PGE_2, Il-6, Il-8 and their own production (Caron 1996 [46], Vandeloo 1995 [224]).

Inhibition of the above mentioned mediators can operate on three different points of the pathway. First of all, it can happen directly at the receptor (Il-1Ra). Secondly, Il-1 soluble receptor (Il-1 sR) and TNF-soluble Receptor (TNF-sR) can catch their counterparts before binding to the membrane attached receptor. Cytokines such as TGF-β, Il-4 and Il-10 have anti-inflammatory properties and can thus inhibit inflammation on the first level (Hall 1983 [88], Hall 1991 [89], Helminen 1986 [96], Kuettner 1991 [119], Reginster 1999 [178], Seibel 1999 [192]).

Increased Inducible Nitric Oxide Synthase (iNOS) activity and hence NO concentrations have been found in OA cartilage, both before and after cytokine stimulation. Moreover, NO inhibits cartilage matrix molecules and Il-1R antagonist (Il-1Ra) synthesis, activates a variety of MMPs. INOS inhibition has been associated with MMP reduction *in vivo* (Pelletier 1999 [167]).

2.6.3 Anti-Inflammatory Cytokines

Cartilage homeostasis is also characterized by a number of anabolic cytokines. For instance, IL-4, IL-10, IL-13 and IL-1Ra act as anti-inflammatory cytokines and IGF, TGF-beta as anabolic cytokines (Martel-Pelletier 1999 [142]). Amongst their most important functions we find the decrease of IL-1β, TNF-α, PGE_2 and MMP and an increase of IL-1Ra and TIMP-1 production (Alaaeddine 1999 [9], Shingu 1995 [196]). A better understanding of the balance between protective and degradative events will hopefully enable us to improve the current OA treatment.

2.6.4 Enzyme Activity During Joint Degradation

In the family of the Matrix Metalloproteinases three groups have been identified to be augmented during OA: Collagenase responsible for collagen, stromelysin for PG and gelatinase for denatured collagen degradation.

The group of collagenases contains collagenase-1, -2, -3 (MMP 1,8,13, respectively). The accumulation of collagenase 1 and 2 in the superficial layer and collagenase 3 in the deeper layer suggest a specific role for each one of them. Thus, collagenase 1 is thought to be mainly involved in the inflammatory process whereas collagenase 3 in remodeling activities. Stromelysin 1, 2 and 3 are found in human articular cartilage. Only stromelysin 1 has a major importance for OA. Out of gelantinase 92 and 72 kD, only the 92kD concentration is enhanced in OA (Hall 1983 [88], Hall 1991 [89], Kuettner 1991 [119], Reginster 1999 [178], Vigorita 2008 [228]).

On one hand those enzymes are controlled by Tissue Inhibitor of Metalloproteinases (TIMP 1- 4). It is assumed that there is an imbalance between the above mentioned enzymes and their inhibitors during OA. On the other hand enzymes such as urokinase and cathepsin B activate MMPs and thus contribute to the degradative imbalance and OA. Further families include cysteine proteases such as cathepsin B, L and H, aspartyl proteases such as cathepsin D or serine proteases such as plasmin, elastase or cathepsin G (Hall 1983 [88], Hall 1991 [89], Kuettner 1991 [119], Reginster 1999 [178], Vigorita 2008 [228]).

2.6.5 Inflammatory Response after Articular Cartilage Injury

Taking the above mentioned inflammation mechanisms into account, the following text takes a closer look at inflammation occurring after cartilage injury. Due to cartilage's absence of vascularization, there is a crucial difference between traumata that include the subchondral bone and those ones that do not. Furthermore, additional soft tissue injury plays an important role in the healing process.

Blunt trauma that is greater than physiologic loading but less than necessary to induce cartilage fractures or fissuring has been shown to damage not only the collagen framework but also to induce chondrocyte cell death under some conditions. Depending on chondrocytes ability to restore the ECM, this might be the starting point for further cartilage degradation. Traumata that only induce splits or lacerations within the cartilage will only be recovered to a very small extent. Although chondrocytes might proliferate and form new ECM, there is no formation of a hematoma, nor inflammatory cell or chondrocyte migration. A completely different process takes place after articular fracture that includes the subchondral bone. As during an ordinary bone fracture the “six step” fracture healing mechanism will be started (Table 6) (Bucholz 2001 [41], Vigorita 2008 [228]).

Table 6: Timeline of bone formation after fracture (Bucholz 2001 [41]).

Stage	Time after Fracture	Pathology
1	12h	Fibrin Clot, Hematoma
2	24h	Acute Inflammation
3	48h	Macrophage Invasion
4	2days 4 days 1 week	Granulation Tissue, Soft Callus, Minor Osteoid Formation First Osteoblastlike Cells Change into Hard Callus with first Calcification
5	2 weeks	Primary Callus with Woven Bone
6	4 weeks	Secondary Callus with Mature Bone

The first 24 hours after fracture are decisive as a hematoma rich in kinines, prostaglandins and further inflammatory proteins is formed. The migration of leucocytes, mast cells, fibroblasts and macrophages is equally important later on. They do not only break down cell debris and form a new framework but also secrete tissue factors such as macrophage-derived growth factor, fibroblast growth factor 1 and 2, transforming growth factor-β1, bone morphogenic protein and plated derived growth factor. Aside from osteoblast stimulation and formation of new bone, cartilage regeneration also takes place. The hematoma formed during stage one will also fill in with the chondral lesion. Fibroblasts will migrate and start producing a matrix similar to articular cartilage. The further healing process differs greatly from patient to patient. In an optimal case cells may retain the appearance of chondrocytes and commence the production of PGs, collagen II and collagen I, leaving behind a fibrocartilaginous scar (Bucholz 2001 [41], Vigorita 2008 [227]).

It is important, however, to distinguish origin and destination of inflammatory cells and cytokines. TNF-α, Il-1, and Il-6 contribute in a vital fashion to fracture repair in bones as they stimulate osteoclastogenesis and recruitment and differentiation of osteoblast cell lines (Kon 2001 [117]). Their role in cartilage generation and long term joint inflammation is still largely unknown.
Recent studies showed that mechanical stress activates NO and prostaglandin E_2 production in chondrocytes which, as already mentioned, enhances catabolic processes in the joint (Fermor 2002 [68]). Furthermore, NOS inhibitors and Il-1 receptor antagonists have been shown to decrease OA severity in loading induced osteoarthritic animals (Caron 1996 [46], Pelletier 1999 [165], Pelletier 2000 [166]). Impact loading induces Il-1β, TNF-α, Il-6 and Il-8 production in cartilage (Irie 2003 [106], Pickvance 1993 [169]). Gene expression in these chondrocytes change adequately and degradative enzymes such as metalloproteinases were found in augmented concentrations.

2.6.6 Nitric Oxide

Nitric Oxide (NO) and its derivates seem to have a variety of catabolic and protective effects in a healthy as well as arthritic cartilage. Especially with the occurrence of COX-Inhibiting Nitric Oxide Donors (CINODs) which prevent hypertension and spare damage to the gastrointestinal tract it is of particular interest to evaluate their potential in the treatment of OA (Abramson 2008 [1]).

The overall reaction of NO synthesis can be seen below. There are three different iso-enzymes of Nitric Oxide Synthase (NOS) and they produce NO in either of its forms as S-Nitrosothiol (RS-NO), peroxynitrite ($OONO^-$) or as regular NO. It diffuses into the extracellular space or moves on towards its intracellular targets (Fig. 17).

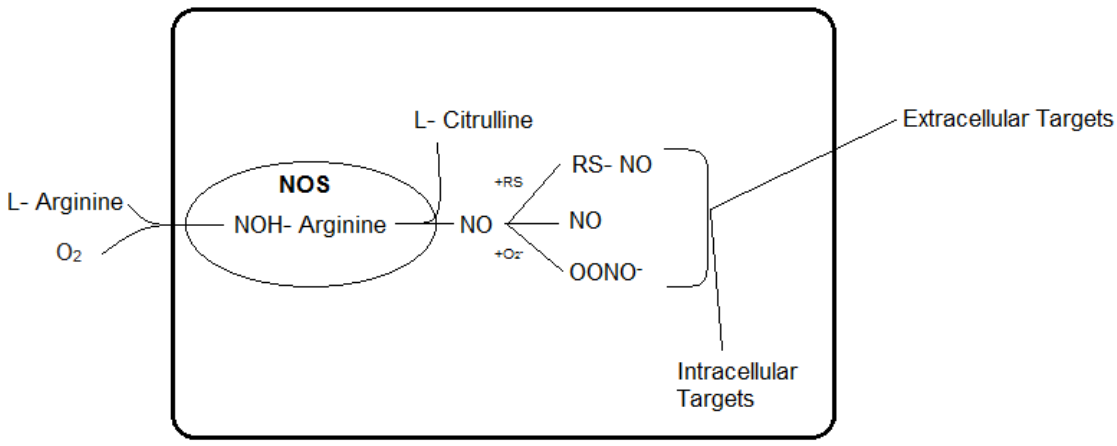

Fig. 17 NO synthesis

Once NO and its derivates diffused into the extracellular space, they typically bind to soluble Cyclic Guanylate Cyclase (sGC) which then forms cGMP from GTP. Numerous biological effects will take place as cGMP induces protein kinases, phosphodiesterases and ion channels. Intracellular reactions and its relevance to OA will be discussed below (Abramson 2008 [1]).

Cytokine-inducible Nitric Oxide Synthase (iNOS) is the only Ca^{2+} independent form of NOS and is characteristic for long lasting high NO output. In hepatocytes it has been shown that iNOS has a regulatory function. NO pre-treatment of those cells leads to a decrease iNOS mRNA expression after inflammatory stimulus, thus, demonstrating that iNOS regulates NO fluctuation (Chang 2004 [50]).

2.6.6.1 Nitric Oxide in Osteoarthritis

The most important inflammatory mediators produced by chondrocytes are TNF-α, Il-1, prostaglandins and NO (Abramson 2006 [3], Pelletier 2001 [168]). Increased NO concentrations are associated with aging and OA (Loeser 2002 [131]). Furthermore, iNOS was found to be augmented preferentially in the superficial zone of OA cartilage, thus promoting degradative changes even further (Amin 1995 [10]). Supporting its inflammatory role, Il-1β, TNF-α and mechanical loading induce iNOS and NO up regulates Il-18 and ICE. In addition, NO inhibits proteoglycan and collagen synthesis, induces metalloproteinases (MMP- 9 even in a concentration dependent manner (Ridnour 2007 [182])), inflammatory responses and chondrocyte apoptosis (Taskiran 1994 [211]).

Looking at NFκB, it is interesting to see that NO is necessary to maintain NFκB activity as a transcription factor inside the nucleus promoting Il-1, TNF-α, iNOS and metalloproteinase synthesis. However, Clancy et al. (Clancy 2004 [52]) found out that peroxynitrite and S-nitrosocysteine have opposed effects to NFκB activation. Thus, during less intense inflammatory stimulus the intracellular redox potential could favor *S*-nitrosothiol or S-nitrosocysteine production by chondrocytes, resulting in inhibitory effects NO production on NFκB activation. This suggests that there might be a more complex interaction which needs further investigation.

2.6.6.2 Nitric Oxide in Post-Traumatic Arthritis

As already stated above, NO is associated with inflammatory responses and in some cases with apoptosis. Chondrocyte death after impact loading is known to be partly due to apoptosis (Hembree 2007 [97]). However, neither causality between apoptosis and cartilage degradation nor the exact apoptotic pathways and their mediators are well studied.

2.6.7 NFκB

The physiological function of Nuclear Factor Kappa-Light-Chain-Enhancer of Activated B Cells (NFκB) is a rapid expression of defense genes. As NFκB is found in nearly every cell in its inactive form it seems suitable for this task. NFκB is a dimeric protein (p50 and p65 subunits) that is expressed by the REL Gene. As a pro-inflammatory transcription factor, it can be found in its inactive form bound to IκB α or β (Inhibitor of NFκB). In response to double RNA, LPS, ROIs (reactive oxygen intermediates), UV- light, gamma irradiation, hypoxia, shear stress and extracellular signals such as TNF-α and Il-1 (selection of huge variety of stimuli (Pahl 1999 [162])), IκB dissociates after phosphorylation. IκB then will be polyubiquitiniated and targeted by a proteasome. NFκB now can be translocated into the nucleus where it binds to specific nucleotides (Renard 1999 [179]).

2.6.7.1 Il-1 Induces NFκB Activation

The functional complex of Il-1, Il-1 Receptor and the membrane spanning protein AcP is called Il-1R-AcP. After activation, it is able to recruit a complex consisting of IRAK 1 and 2 (ser/thr kinases), Tumor-Necrosisfactor-Receptor-Associated Factor 6 (TRAF-6) and Myeloid-Differentiation-Primary-Response-Protein 88 (MyD88) (adaptor protein). Both, NIK (NFκB Inducing Kinase) and MEKK1/ p38 are now able to activate the IKK-Complex and as described above IκB dissociates from NFκB (Fig. 18) (Renard 1999 [179]).

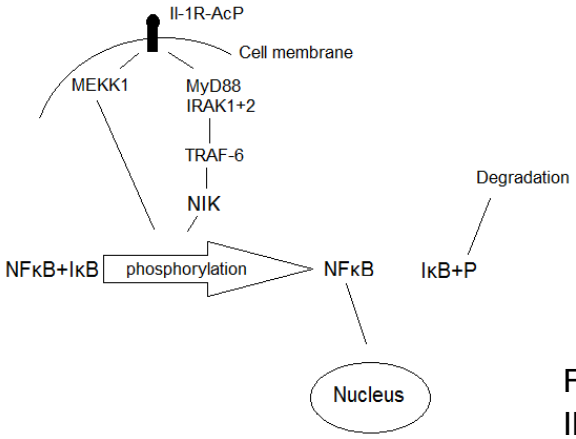

Fig. 18 Activation pathway of NFκB after Il-1 activation (Renard 1999 [179]).

2.6.7.2 TNF Induces NFκB Activation

Binding of TNF to TNFR1 (Tumor Necrosis Factor Receptor 1) leads to the aggregation of TRADD (TNFR associated death domain protein), TRAF 2 (TNFR associated factor 2) and RIP (receptor interacting Protein) (Fig. 19) and finally to the activation of NIK (see above) (Baeuerle 1998 [20]).

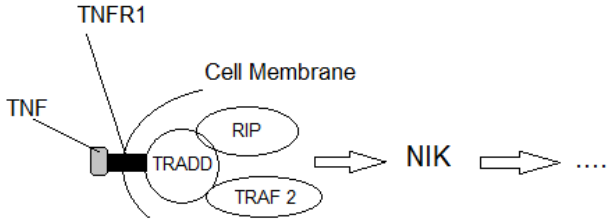

Fig. 19 Activation pathway of NFκB after TNF binding.

Generally, NFκB induces a fast immune response, including the expression of cytokines, acute phase response proteins and cell adhesion molecules. It is also thought that NFκB allows some immune cells such as macrophages, B cells and plasma cells to maintain a differentiated phenotype (Ghosh 1998 [77]).

2.6.7.3 Interaction in the Nucleus

NFκB contains Rel homology domains (RHD). This has an N-terminal 300 amino acid region which is responsible for DNA binding, dimerization and interaction with IκB. However, each p50 consist of two domains joined by a flexible link. Dimerization occurs at the C terminal ends where hydrophobic side chains clamp those regions together. Thus C- and N-terminal ends are involved in DNA binding forming a “NFκB lock”. P65 binds in a similar fashion to DNA (Renard 1999 [179]).

2.6.7.4 NFκB and Apoptosis

Hepatocytes of $p65^{-/-}$ mouse embryos undergo massive necrosis during embryo development, suggesting that NFκB has an apoptosis protecting effect rather than a growth promoting one. TNF-α, ionizing radiation and the cancer chemotherapeutic agent daunorubicin have the potential to induce apoptosis which is prevented by NFκB. Furthermore it is shown that the absence of NFκB during TNF stimulation leads to apoptosis, confirming the anti-apoptotic effect (Baichwal 1997 [21], Ghosh 1998 [77]). However, there are also some studies which suggest a rather pro-apoptotic effect of NFκB (Hasbold 1990 [91], Pahl 1999 [162]).

2.6.7.5 Target Genes of the Transcription Factor NFκB

Just in the same way we find innumerous ways to activate NFκB there seem to be at least as many genes whose transcription will be altered after NFκB activation. Some experts estimate this number to be somewhere around 150 genes. A brief description of the most important functions follows:

NFκB has oftentimes been considered as the central mediator of human immune response. The cytokines Il-1, Il-2, Il-2R, Il-6, Il-8,G-CSF, GM-CSF, TNF-α, TNF-β and IFN-γ, for instance, are induced by NFκB and initiate a general activation of immune cells. It is striking that TNF-α and Il-1 are stimulated and produced by the NFκB pathway, hence suggesting the presence of a positive feedback mechanism.

Furthermore, cell migration and repair is made possible through the adhesion factors VCAM-1, ELAM-1 and ECAM-1 which is also signaled through NFκB. Supporting its inflammatory role, NFκB induces acute phase proteins such as angiotensinogen, serum amyloid protein, α1 acid glycoprotein, C3 complement and complement factor B. Of particular interest is NFκB's role in the response to stress. It has been shown that iNOS and COX-2 are synthesized after NFκB activation (Ghosh 1998 [77], Pahl 1999 [162]).

2.6.7.6 NFκB in Chondrocytes

Extensive research has been done on NFκB as it is thought to be the key inflammatory transcription factor in RA. Hence, activation of pro-inflammatory mediators including NOS2, COX-2, MMPs, IL-1β and TNF-α are caused by NFκB. At the same time aggrecan, collagen type II and TIMP synthesis is down regulated, perpetuating degradative changes even further (Agarwal 2004 [5]). High magnitude cyclic compressive and tensile forces are known to induce NFκB translocation into the nucleus and cause the already described gene expression patterns. Compressive loading at low forces, however, does not only prevent NFκB translocation but also inhibits Il-1β induced pro-inflammatory cascade initiation. It has to be added that low tensile force do not inhibit Il-1β nor TNF-α nor LPS initiated signals (Anghelina 2008 [14]). Emphasizing NFκB's importance further, systemic lupus erythematosus, RA and traumatic injury have been shown to continuously translocate NFκB to the nucleus (Agarwal 2004 [5], Dossumbekova 2007 [64]).

2.6.8 High Mobility Group Box 1 Protein or Amphoterin

The property of high electrophoretic mobility gave High Mobility Group (HMG) Proteins their name more than 30 years ago. Ever since three different families were discovered: HMGA proteins that bind to TA-rich DNA stretches in the minor groove, HMGB proteins that contain HMG boxes of approx. 80 amino acids that bind to DNA with little or no sequence specificity and HMGN Proteins that bind within the nucleosome (Kokkola 2002 [116]).

High Mobility Group Box Proteins (HMGB) act inside the nucleus as well as in the extracellular space. They consist of two HMG box domains with an acid tail (to shield domains before binding to DNA). The box domains are structurally similar but act independently. The B box domain is considered to be pro-inflammatory and the A box domain has anti-inflammatory functionality. Furthermore, they consist of 3 α-helices which can form into a wedge shaped structure that is able to fit into the minor groove of DNA (Kokkola 2002 [116]). The following text is going to elucidate HMGB's function as a nuclear factor and cytokine:

Histones pack human DNA into nucleosomes and control its accessibility. In addition, there are non-histone proteins such as HMGB which contribute to their function by bending and plasticizing DNA. Is has been shown that HMG Box domains can bend DNA up to 90°. However, different functions are classified: First of all, HMGB can interact directly with nucleosomes by loosening the wrapped DNA in order to make it more accessible for other proteins such as transcription factors or to change to overall nucleosome structure. Secondly, HMGB can bind directly to proteins such as TBP, steroids, viruses and NFκB and hence help transcription factors to bind to their specific promoters. Thirdly, HMGB are involved in detection of DNA damage. Taking a closer look at HMGB1, their specific tasks are helping members of the nuclear receptor family, p53- p75 transcriptional complexes to bind to DNA and facilities different transposons to integrate into DNA (Baxevanis 1995 [22], Bianchi 2005 [31], Bianchi 1989 [32], Mollica 2007 [149], Yamada 2007 [233]).

HMGB1 Proteins are also classified as damage-associated-molecular-pattern-molecules (DAMPs) as they are released by natural killer cells, activated macrophages and dendritic cells after injury (Fig. 20). HMGB1 Proteins are also released by necrotic cells and it is important to state that apoptotic cells do not release HMGB1. Hence, HMGB1 do also have a function as cytokine and as such induce inflammation, the expression of adhesion molecules, RAGE (Receptor for advanced glycation endproducts) and Toll-Like- Receptor 2 and 4 (TLR 2 and 4) and promote wound repair and recruitment of leucocytes (Bianchi 2007 [30]).

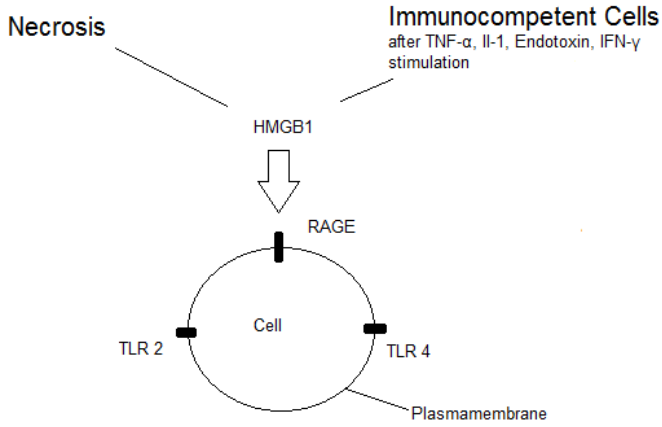

Fig. 20 Origin of HMGB1.

Further investigation was done in order to define the receptors with which HMGB1 interacts in its function as a cytokine. So far we know that HMGB1 binds to RAGE, TLR 2 and TLR 4. Many aspects, however, still need to be clarified (Yamada 2007 [233]). For instance, how does HMGB1 induce a delayed response in macrophages although ligation to their receptors is a process of a few minutes?

As already stated HMGB1 binds to RAGE, TLR-2 and TLR-4. The first steps of this activation pathway are somewhat similar to the NFκB activation by Il-1 (see NFκB): Through the adaptor protein MyD88 IRAK and TRAF 6 Transforming-Growth-Factor-β-Activated Kinase 1 (TAK 1) will be activated. This leads to the activation of the Inhibitor-of-NFκB-Kinase-Complex (IKK-Complex) consisting of NFκB-Essential-Modulator (NEMO), IKK-α and IKK-β. The activated IKK-Complex phosphorylates IκB from the NFκB + IκB complex and thus induces its degradation by ubiquitination and proteasomes. The NFκB molecule now is ready for translocation into and its function as transcription factor inside the nucleus (Fig. 21). There are, however, still unknown signaling pathways that might involve Extracellular-Signal-Regulated-Kinase 1 and 2 (ERK 1 and 2) and the Mitogen-Activated-Protein-Kinase p38 (Lotze 2005 [133]). Some receptor functions of HMGB1 such as an intracrine role leave much room for further speculation.

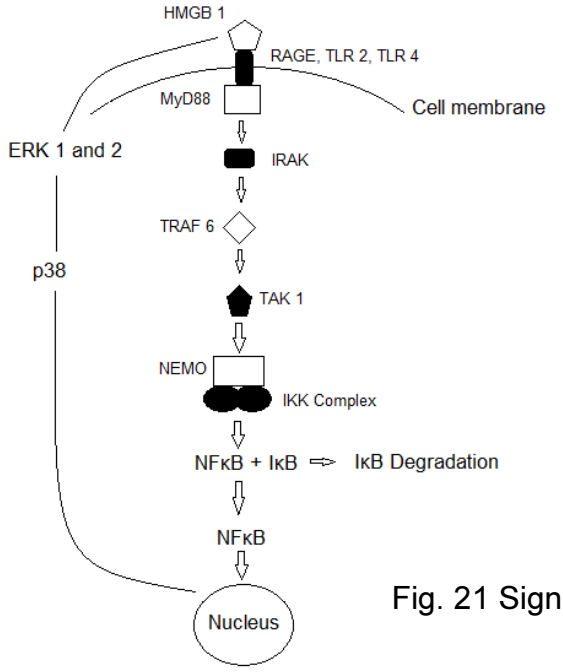

Fig. 21 Signaling pathway of HMGB 1 (Lotze 2005 [133]).

Taking a closer look at the cell response induced by HMGB1, it is striking that HMGB1 attracts leucocytes through endothelial barriers by the induction of the expression of integrin signaling. Free HMGB1 as well as HMGB1 expressed on the surface of macrophages binds to RAGE expressed on endothelia and in that manner leads to expression of molecules such as Vascular-Cell-Adhesion-Molecule 1 (VCAM1), Intercellular-Adhesion-Molecule 1 (ICAM1) and Endothelial-Cell-Selectin (E-Selectin) in vascular tissue. Here, its role as promoter of wound repair might also come into action although it is still largely unknown. Finally, it also has to be said that the effects of HMGB1 can be modulated by the presence of other cytokines (Lotze 2005 [133]).

Physiologically we find a concentration of 5 ng/ml in human blood. This number increases to 150 ng/ml in blood of patients with severe sepsis and to an even higher amount in patients after death. Apart from being a general pro-inflammatory cytokine, however, HMGB1 also has its specific roles in different tissue pathology: After toxin related liver damage, for example, we find augmented HMGB1 levels in the blood. Furthermore, animals with autoimmune hepatitis present Perinuclear-Anti-Neutrophil-Cytoplasmic-Antibodies (pANCAs) specific for HMGB1 (Lotze 2005 [133]).

In cartilage tissue HMGB1 is of particular interest. Elevated HMGB1 levels have not only been found in blood of patients with rheumatoid arthritis but there exists also evidence from animal studies that HMGB1-Antibodies protect the cartilage from collagen-induced-arthritis. Direct injection of HMGB1 leads to arthritic changes as well (Kokkola 2002 [116]). HMGB1 can be released by macrophages (in synovial tissue or fluid) or stimulate them to produce Il-1β, Il-6 and TNF, amongst other cytokines. HMGB1 causes a delayed and biphasic release of TNF in comparison with that detected after LPS activation and thus is associated with the induction of chronic arthritis. It is also released by dying cells, an event which we also find in chronic arthritic joints, frequently accompanied by synovial inflammation. In addition, necrotic $\mathrm{hmgb}^{-/-}$ cells show less inflammatory stimulus to the surrounding tissue. Finally, HMGB1 enhances the activity of tissue plasminogen activator and matrix metalloproteinases 2 and 9. All those findings emphasize HMGB1's importance as an inflammatory cytokine in arthritis and thus it is not surprising that recent studies focus on it. We already find promising therapy suggestions such as the use of anti-HMGB1 antibodies addressing this protein (Andersson 2004 [13], Kokkola 2003 [115], Kokkola 2002 [116]).

After an extensive search there was no literature found that elucidates the role of HMGB1 in PTA.

2.6.9 Toll-Like Receptors

In 1985 Christiane Nüsslein-Volhard identified Dorsophilia fruit fly larva with a wired looking ventral plate. Her first comment was:" Das ist ja toll". As it turned out, a mutation in the toll gene caused underdevelopment in the ventral portion. Ever since the new group of pattern recognition receptors (PRR) was called Toll-Like Receptors (TLRs) (Hansson 2005 [90]).

TLRs are an evolutionary highly conserved part of the innate immune system. As such byproducts of fungal and bacterial infection seemed to activate inflammatory processes. Only TLRs-1, 2 and 4 are expressed on the cell's surface. They are

thought to respond mainly to bacterial ligands. TLRs-3, 7, 8 and 9, however, are found only in intracellular compartments and thus (viral) ligands have to be internalized by phagosomes or endosomes before binding. Primary binding of, for instance, LPS seems to have a stronger effect than later binding, meaning that there is a modulating effect by the cell itself (Rakoff-Nahoum 2009 [176], Takeda 2007 [209]).

Acquired and innate immunity are the key players in the host defense system. T- and B-Lymphocytes, for instance, use antigen receptors and mechanisms like diversity, clonality and memory in order to build up an efficient (acquired) immune system. On the other hand macrophages and dendritic cells are part of the innate immune system. It has been know that they can be activated by components such as LPS. The responsible receptor, however, was unknown until the discovery of TLRs (Takeda 2005 [210]).

Evolutionary, TLRs primary function is host defense by antimicrobial response. As such, they can be numerously found in epithelial cells, being involved in regulation of factors such as defensins (α and β), phospholipase A2, lysozymes, enhancing microorganism uptake by phagocytes, generation of reactive oxygen and nitrogen intermediates and mediating leucocyte recruitment via E-selectin and intercellular adhesion molecule 1. TLRs are also involved it the host adaptive immune response. Not only antigen-presenting cells such as dendritic cells are activated by TLRs but also activation and maturation of B-cell response, immunoglobulin isotype class switching and somatic hypermutation can be influenced by TLRs (Rakoff-Nahoum 2009 [176]).

2.6.9.1 Toll-Like-Receptors and Their Ligands

TLRs are best known to bind to ligands of the general group of pathogen-associated molecular patterns (PAMPs) (Table 7). Regardless of their pathogenicity PAMPs can be found in nearly all microorganisms. A useful differentiation can also be made between microbial (exogenous) or host-derived (endogenous) ligands (Rakoff-Nahoum 2009 [176]).

2.6.9.2 Endogenous Ligands of TLRs

Necrosis as opposed to apoptosis is associated with release of cell content and activation of resident immune cells. Uncontrolled release of proteases that cleave surrounding tissue is contributing to this process. Unlike in the event of a microbial assault, necrosis is related to other circumstances like sterile injuries or mechanical trauma. It will only lead to the release of endogenous ligands and finally to inflammation (Table 8).

Table 7: Toll- Like receptors and their ligands (Takeda 2007 [209]).

Toll- Like Receptor	Ligands
TLR 1	Triacyl Lipopeptides
TLR 2	Peptidoglycan, Lipopeptides, Lipoteichoic Acid, Lipoarabinomannan, Glycosylphosphatidylinositol Anchors, Phenol- Soluble Modulin, Zymosan, Glycolipids
TLR 3	dsRNA
TLR 4	Lipopolysaccharides, Taxol, Respiratory Syncytical Virus Fusion Protein, Mouse Mammary Tumor Virus Envelope Protein, Endogenous Ligands (Heat Shock Proteins, Fibronectin, Hyaluronic Acid)
TLR 5	Flagellin
TLR 6	Diacyl lipopeptides
TLR 7	ssRNA, Imidazoquinolines
TLR 8	ssRNA, Imidazoquinolines
TLR 9	CpG DNA
TLR 11	Profilin

Table 8: Endogenous stimuli to TLRs, their function and cellular response as stated by Beg et al. (Beg 2002 [25]).

Endogenous Stimulus	Functions	TLRs Involved	Cellular Responses Triggered
HSPs, HSP60, HSP70, GP96	Numerous, including protein folding, assembly of protein complexes, stress responses	TLR4 (HSP60) TLR2/4 (HSP70, GP96)	NF-κB activation, DC maturation, cytokine synthesis
Hyaluronan	Extracellular matrix component	TLR4	NF-κB activation, DC maturation, cytokine synthesis
Lung surfactant protein-A	Pulmonary surfactant	TLR4	NF-κB activation, cytokine synthesis
Necrotic cells	Not applicable	TLR2	NF-κB activation, induction of inflammatory and tissue repair genes, DC maturation
HMGB1	Chromatin binding	Not determined	Inflammation
Chromatin–IgG complexes	Multiple	TLR9	B-cell activation
Others: fibronectin, fibrinogen, heparan	Multiple	TLR4	Inflammatory-gene induction, DC maturation

- Heat Shock Proteins are involved in proper protein folding and contain well defined binding domains for TLR-2 and 4.
- As a DNA binding and bending protein, HMGB1 is found in nearly every cell. It is known to bind directly to TLR-2 and 4.
- Uric acid has been known for years to cause inflammation in gout. Recent research indicates that TLR-2 and 4 bind to it.
- Endogenous RNA binds to TLR-3. DNA binds to TLR-9. Unmethylated (CpG) DNA which is predominantly derived from pathogenic organisms also binds to TLR-9 and is frequently used as a positive control (Beg 2002 [25], Kariko 2004 [110], Rifkin 2005 [184], Sloane 2010 [197]).
- As important component of articular cartilage, HA has been shown to induce dendritic cell (DC) maturation via TLR-4 (Termeer 2002 [213]). Its action depends on the molecular size. Low molecular weight HA signals via TLR-4. High molecular weight HA acts anti-inflammatorily via cluster of differentiation (CD-) receptors (Campo 2010 [44]).
- Extracellular matrix fragments such as fibronectin have been found in high quantities in the joint space following trauma. Only fibronectin containing type III repeat extra domain A (EDA) has been found to bind to TLR-4 (Lotz 2010 [132], Okamura 2001 [159]).
- Extravascular Fibrin deposition is involved in the blood clot formation and is an early hallmark of inflammation. Fibrinogen has been shown to act as a ligand to TLR-4 (Smiley 2001 [198]).
- Heparan Sulfat is an acid polysaccharide, normally found in cell membranes and extracellular matrices and rapidly shed after cell injury and inflammation binds to TLR-4 (Johnson 2002 [109]).
- Chromatin–IgG complexes can activate rheumatoid factor+ B-lymphocytes via Ag-receptor and TLR-9 (Leadbetter 2002 [124]).

2.6.9.3 TLRs and HMGB1

Recent studies have discovered that HMGB1 signals through TLR-2 and 4. Macrophages typically react to HMGB1 with the release of TNF in a dose dependent manner. MyD88 and TLR-4 knockout mice released significantly less TNF after HMGB1 stimulation. The same applies for Il-8 release after TLR-2 stimulation with HMGB1 in human embryonic kidney cells (Yu 2006 [236]). Underlining this process, HMGB1 exposure to macrophages, monocytes and neutrophils leads to an increased nuclear translocation of NFκB (Park 2004 [163]). Confirming this mechanism, there are many reports describing organ specific effects of TLR and HMGB1 interaction. For instance, HMGB1 release after liver ischemia activates reactive oxygen species production via TLR-4 (Tsung 2007 [221]).

Summarizing, it has to be said that the list of endogenous TLR-ligands varies somewhat depending on the author. The most important ones, however, are named above. Furthermore, there exists some doubt if the discovery of these endogenous ligands might be distorted by bacterial contamination. Thus, results have to be interpreted very carefully (Tsan 2004 [220]).

2.6.9.4 Signalling Pathways of Toll-Like-Receptors

Signaling pathways can generally be divided in a MyD88 dependent (Fig. 22), independent (Fig. 23) (also called TICAM1 and TRIF), TIRAP (also called MAL) and TIRAP 2 (also called TRAM or TIRP) pathway. All TLRs but TLR-3 signal through the Myd88 dependent pathway. TLR-3 signals through the MyD88 independent pathway and TLR-4 through both (Rakoff-Nahoum 2009 [176], Takeda 2007 [209]). For reasons of clarity I outlined only the two most important pathways:

MyD88 Dependent Pathway

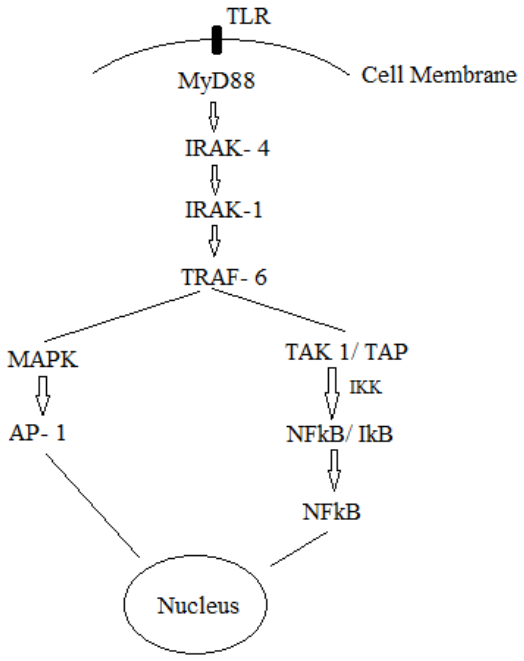

Fig. 22 MyD88 dependent TLR activation (Takeda 2007 [209]).

MyD88 Independent Pathway

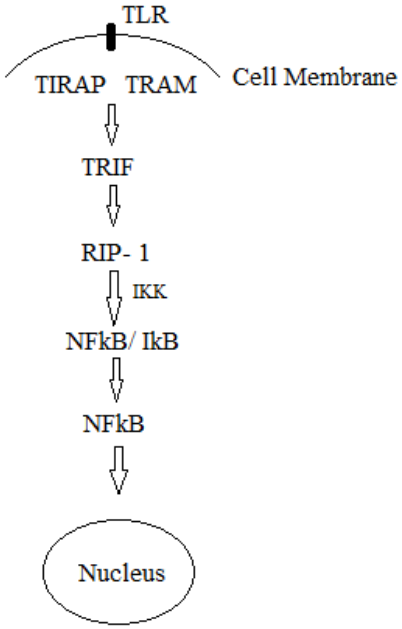

Fig. 23 MyD88 independent TLR activation pathway (Takeda 2007 [209]).

TLR=Toll-Like-Receptor, MyD88= Myeloid-Differentiation-Primary-Response-Protein 88, IRAK= interleukin-1 receptor-associated kinase, TRAF= Tumor- Necrosisfactor- Receptor-Associated Factor, MAPK= Mitogen-activated protein kinases, AP-1=Activator Protein 1 (Transcription Factor), TAK1/TAP= TAK1/TAP Complex, NFκB/IkB=Nuclear Factor-kB/ Inhibitor of kB complex, TIRAP= TIR domain-containing adaptor, TRAM= additional TIR domain-containing adaptor; TRIF= additional TIR domain-containing adaptor, RIP= kinases receptor interacting protein, IKK= IkB kinase complex

2.6.9.5 Toll-Like-Receptor and Articular Cartilage

Recent studies give evidence for the presence of TLR 1-9 in human chondrocytes. They were found in human articular chondrocytes on mRNA level. Additionally, TLR-4 was found on protein level. Furthermore, it was shown that TLR-4 activation by LPS leads to Il-1β mRNA synthesis increase as well as a PG and collagen synthesis decrease, indicating TLR's catabolic function (Bobacz 2007 [37], Su 2005 [207]).
Kim et al. (Kim 2006 [111]) found a TLR-2 and 4 up-regulation in OA cartilage and after Il-1 and TNF-α stimulation. Emphasizing TLR's inflammatory role, they confirmed that MMP-1,-3,-13, NO and PGE_2 also increased after TLR ligand treatment. Another study confirmed TLR's degradative function. Collagen resorption was found after TLR-1/2 activation with Pam3CSK4.3HCL and TLR-6/2 activation with macrophage-activating lipopeptide-2 (Zhang 2008 [238]). Furthermore, TLR-2 and 4 activation has been shown to induce chondrocyte hypertrophy (Liu-Bryan 2010 [129]). High shear stress induces an up-regulation of TLR4 expression, whereas prolonged shear down-regulates TLR4 (Wang 2011 [229]). So far there is no study elucidating TLR's importance in PTA.

3 Materials and Methods

3.1 Preparation of Osteochondral Explants

3.1.1 Opening of Joints

Porcine knee joints were obtained from a local abattoir within 6 hours after death. Only female skeletally mature 2 to 3 year old pigs were utilized. Their weight has been estimated at around 200 Kg. Just after arrival in the laboratory the whole leg (complete femur, attached tibia and fibula) were first washed with antimicrobial soap (VWR Soft Cide, Sargent Welsh, Buffalo, NY, USA) dried with paper towels and then placed in a laminar flow hood. Using sterile technique in a first step the patella was removed by making the first incision above the patella in the tendon of the rectus femoris muscle (Fig. 24). The patella was then carefully cut free and finally separated at the tuberosity of the tibia. The lateral and medial collateral ligaments of the knee were dissected without injuring the subjacent cartilage and cut off at the proximal end (Fig. 25). The last step consisted of carefully inserting the scalpel between the lateral and medial femoral condyle with the blade facing cranial cutting the anterior and posterior cruciate ligament (Fig. 26). The last supporting structures were dissected. The cartilage of the femur was covered with Phosphate-Buffer-Solution (PBS) soaked 4 x 4 inch gauze and stored inside the hood. The tibia and patella were discarded.

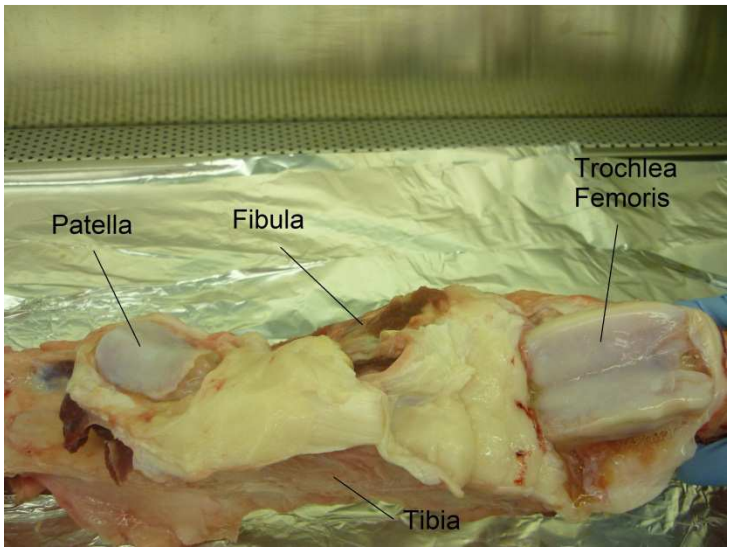

Fig. 24 View from frontal. Right leg: At the left hand side tibia and fibular with dissected patella. On the right hand side femur trochlear femoris.

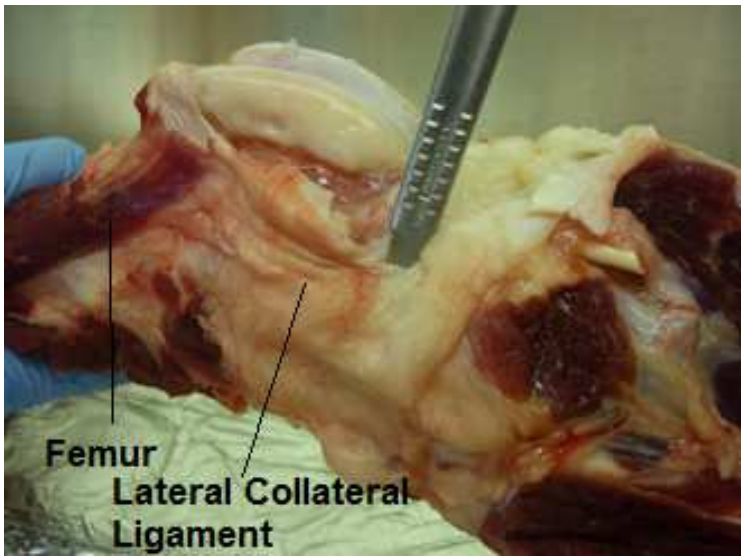

Fig. 25 View from lateral on right leg: On the left hand side femur and trochlear femoris. On the right hand side fibula and tibia. Just in front of the scalpel lateral collateral ligament.

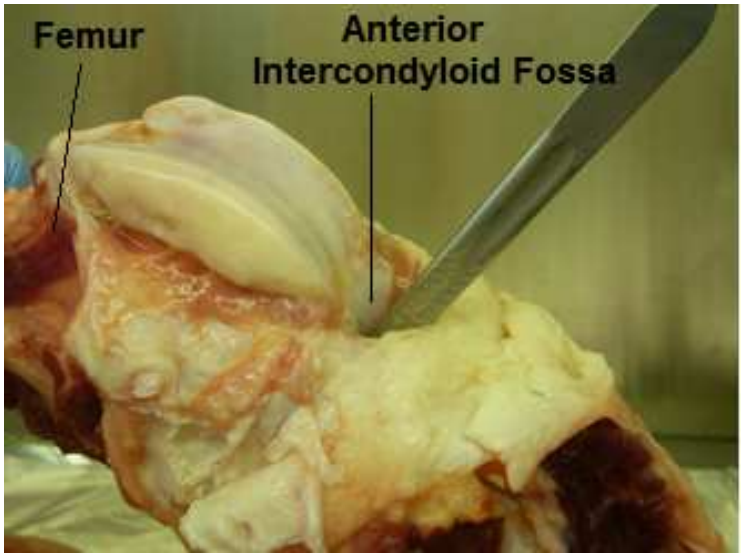

Fig. 26 The anterior and posterior cruciate ligaments are cut by carefully inserting the blade in the intercondyloid fossa.

3.1.2 Obtaining Osteochondral Cores

A bench vice was used to firmly clamp the diaphysis of the femur. Using an electrical saw (Black & Decker Navigator Saw SC500G) the distal femoral epiphysis was separated from the diaphysis at the height of the epicondyles (Fig. 27). A vertical drill press (Mini Vertical Milling/ Drilling Machine, Little Machine Shop, Pasadena, CA, USA) with a ¼ inch diameter sterile coring tool was used to obtain osteochondral cylinders (Fig. 28). We chose the number of revolution to be 2500 per minute in order to cut sharp and clear edges. To liberate the osteochondral cylinders from the underlying bone an osteotome was used to break the cylinder free at the bottom of the sample. These cylinders were immediately placed in PBS (Fig. 29).

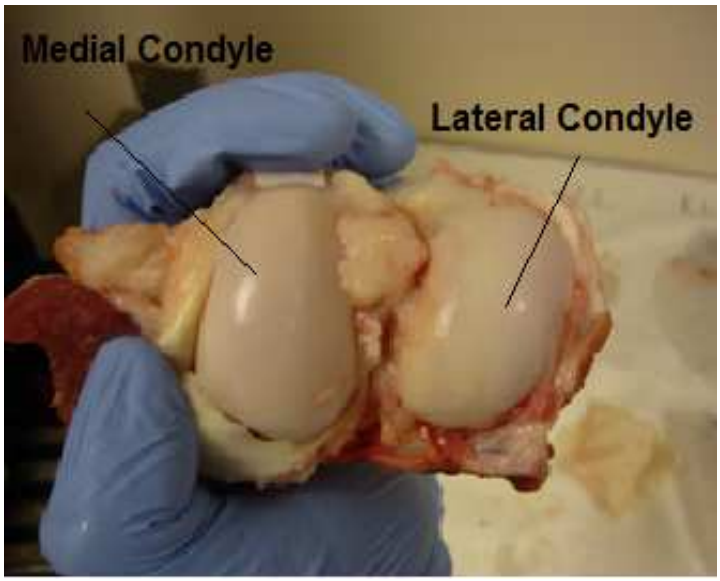

Fig. 27 Joints were examined for pathologic changes. This sample does not show any arthritic changes neither in the lateral nor in the medial condyle.

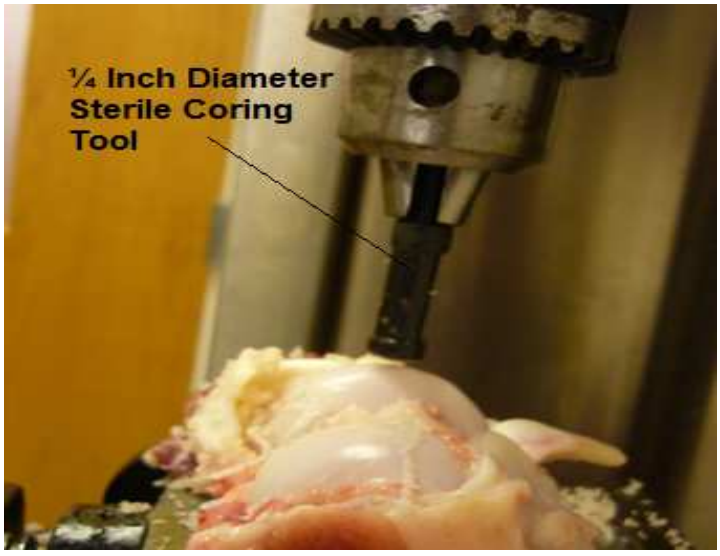

Fig. 28 A ¼ inch diameter coring tool was used to obtain osteochondral cylinders.

Fig. 29 After liberating osteochondral cylinders from underlying bone with an osteotome forceps were used to carefully place them in PBS solution.

3.1.3 Preparation of Osteochondral Cores

Osteochondral cores were stored in PBS keeping them moisturized at all times. Each cylinder was taken out individually and residual cartilage hangovers were carefully removed with a scalpel (Fig. 30). The cartilage surface was not touched at any time. The trimmed cores were now separated in two groups: The first groups consisted of cores whose cartilage layer was parallel to the attached subchondral bone. These cores were fixed in a custom made sawing jig and the bone was cut to a height of approximately 1 to 2 mm (Fig. 31). The second group contained all the slanted cylinders. They were fixed in a bench vice and the bone was also trimmed to a height of 1 to 2 mm.

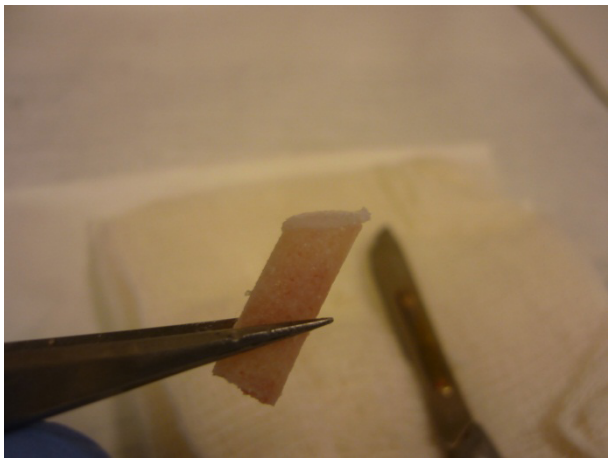

Fig. 30 This image shows a slanted core after trimming with scalpel.

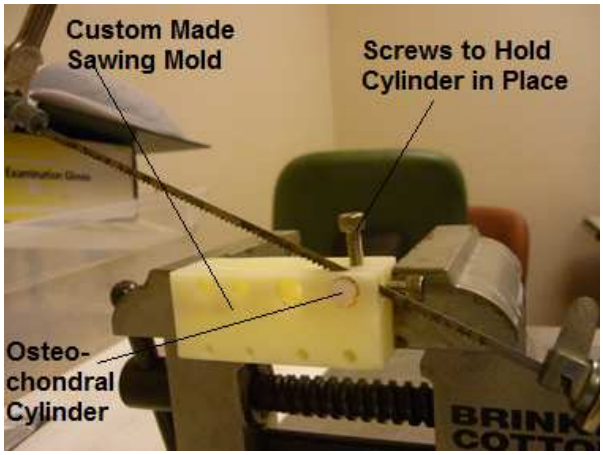

Fig. 31 A custom made sawing jig was used to obtain samples with perfectly parallel bone to cartilage layers.

3.1.4 Cartilage Height Measurement

Ostechondral cores were stored in PBS between preparation and height measurement. Cores were placed on a platform which was covered with a sterile aluminum foil. A camera system (Sony Electronics, Park Ridge, NJ) fitted with a 94-

mm video lens (Infinity, Boulder, CO) was set up and connected to a laptop. NI Vision Builder software (National Instruments Corporation, Austin, TX) was calibrated at the beginning of each testing day and then used to find the exact cartilage height (Fig. 32).

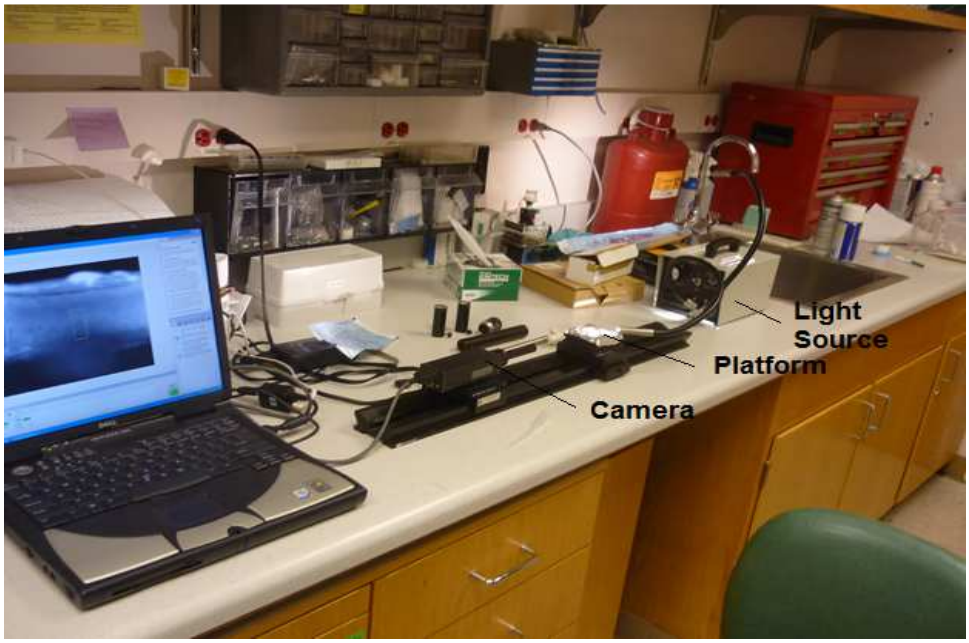

Fig. 32 A camera system was set up to determine cartilage height. From left to right: Laptop, camera, platform, light source.

For a series of cores values obtained with the camera system (Fig. 33) were compared to cartilage height measurements from the Differential Interference Contrast (DIC) mode of the confocal laser scanning microscopy (LSM 510, Zeiss, Thornwood, NY) (Fig. 34) in a previous test. The results were found to be nearly equal. Cartilage height was measured at one point including the dense layer of calcified cartilage. Whenever delineation of the calcified cartilage was not clearly visible, further measurements were taken to confirm height value.

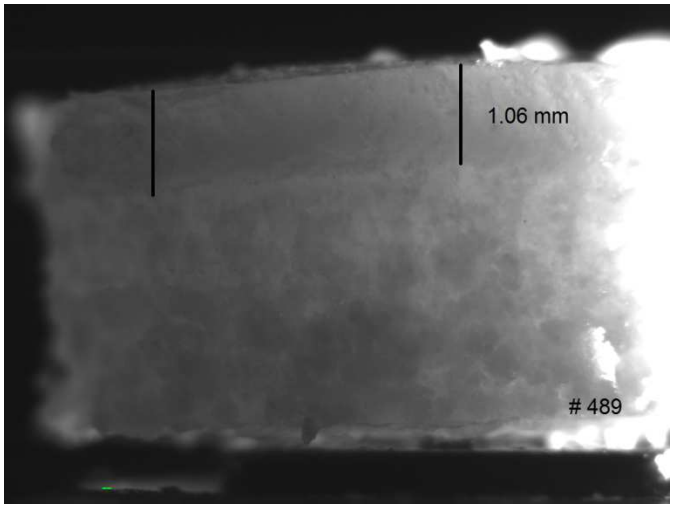

Fig. 33 Core #489: Image taken by camera system: Cartilage + calcified cartilage = 1060 µm.

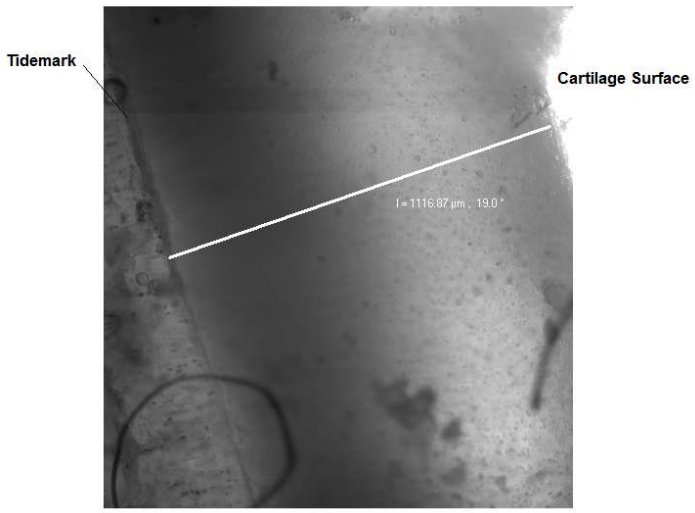

Fig. 34 Core #49: Image taken by DIC Mode Confocal: Cartilage 1116 µm, cartilage + calcified cartilage = 1405 µm

3.1.5 Serum Free Media

Looking at previous studies culturing chondral or osteochondral cores, usually Dulbecco's modified eagle medium (DMEM) containing 10% heat-inactivated fetal bovine serum, 0.1 mM nonessential amino acids, 10 mM HEPES buffer solution and 37.5 mg/ml of L-ascorbic acid 2-phosphate (AAP) at 37°C and 5% CO_2 have been used. Particularly the ingredient fetal bovine serum gave cause to search for new media with better defined elements. Bian et al. (Bian 2008 [29]) tested a new composition of fetal bovine serum free medium in 2008. Mechanical, biochemical properties and viability after 2 weeks in SFM were shown to be superior to serum supplemented media.

Hence, all our experiments were run in serum free media, containing high glucose DMEM with 50 mg/ml L-proline, 0.9mM sodium pyruvate (DMEM, high glucose, Invitrogen, Carlsbad, CA), 1% ITS + Premix (BD Bioscience, Bedford, MA, USA), and AAP (35.7 mg/ml) (Sigma–Aldrich, St. Louis, MO) at 37°C and 5% CO_2. As the only change to the recipe we left out dexamethasone as it has been shown that it inhibits apoptosis (Borrelli 2006 [39]).

3.1.6 Wash with Penicillin/Streptomycin/Fungizone

The following step consisted of 2 x 1 h washes in 2 ml Serum Free Media (SFM), AAP and 1,000 U/ml of penicillin/streptomycin/fungizone (Invitrogen). The purpose of this step was to liberate the cores from bacteria and fungi which might have adhered to them during the previous steps. At the same time we did not want to culture the cores for a longer time after loading with these antibiotics to prevent the unlikely event of interference with any of the inflammatory or apoptotic pathways.

3.2 Loading

3.2.1 Blunt Impact Model

“A sterile 9.525 mm diameter stainless steel hemisphere (model no. 357-TB, Bal-tec, Los Angeles, CA) was placed on the articular surface of an osteochondral core. A concave adaptor attached to the load-frame (Bose EnduraTEC SmartTest, Eden Prairie, MN) applied a maximum preload of -5 N(Fig. 35a). This set-up allowed the hemisphere to self-align with the articular surface of the sample. Cores were loaded at 70%, 80% and 90% strain by applying a single ramp compression at a strain rate of 100% sec^{-1} (Fig. 35b)”(Stolberg-Stolberg 2013 [203]).

3.2.2 Fracture Model

“A sterile 6.35 mm diameter truncated ball (Bal-tec Div., Los Angeles, CA, USA) mounted to the load-frame applied a maximum -5 N preload to the bone surface of an inverted sample (Fig. 35c). A 90% compressive strain was applied with a single ramp compression at a strain rate of 100% sec^{-1} (Fig. 35d)” (Stolberg-Stolberg 2013 [203]).

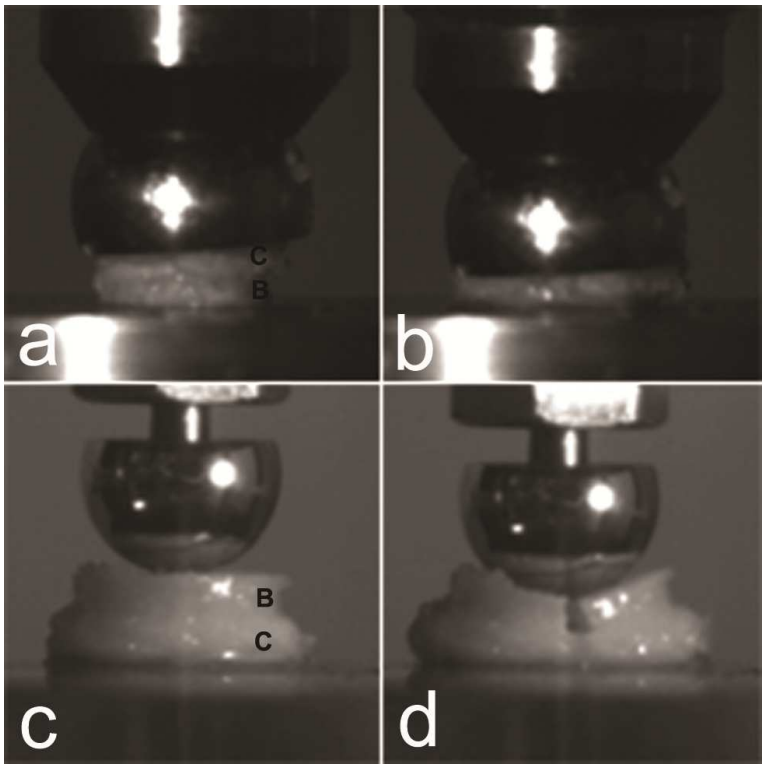

Fig. 35 Loading of osteochondral cores (C = cartilage, B = bone). For the blunt impact model (a) a hemisphere was placed with the flat face on the cartilage surface. The concave adapter attached to the loadframe allowed self-alignement and completely blunt loading (b). For the fracture model (c) a truncated ball in contact with bone caused sample frature (d) (Stolberg-Stolberg 2013 [203]).

3.2.3 Blunt Fracture Model

Samples were loaded equally to the blunt impact model. Displacement was programmed to reach 90% strain. In some samples the subchondral bone fractured before full displacement was reached.

3.3 Necrosis Induction

Samples were frozen at -80°C for at least 3 days. Preliminary experiments confirmed this to be the time point when all chondrocytes have died.

3.4 Apoptosis Induction

Osteochondral cores were cultured in SFM, AAP and 10 µM staurosporine (Invitrogen, Carlsbad, CA). Staurosporine is a well-known inducer of apoptosis (Belmokhtar 2001 [27]).

3.5 Strain Measurement

3.5.1 Computerized Strain Measurement

Videos of all loading procedures were taken. Using Matlab R2009b (MathWorks, Natick, MA, USA) cartilage surface, osteochondral junction and bone surface were determined during preloading and hold down time. Strain was calculated by averaging all values of each group.

3.5.2 Compressive Modulus of Bone Only

10 osteochondral explants were prepared as described previously. Cartilage was cut off and bone only was placed into blunt impact apparatus. At a strain rate of 100% sec^{-1} bone was loaded up to -2500 N. Stress-strain diagrams were recorded by Bose EnduraTec software.

3.6 Viability Assessment

Osteochondral cores were first washed in 3 ml PBS for 5 minutes and then cut in half perpendicular to the surface using a straight edge razor blade (Fig. 36). One half was conserved in formalin solution for later histologic evaluation. The other half was placed into 4 µM ethidium homodimer and 4 µM Calcein AM (Invitrogen, Carlsbad, CA) in PBS for 30 minutes. Calcein AM is membrane permanent and is cleaved by esterase activity to Calcein only in live cells before yielding the green fluorescence.

Ethidium homodimer is not membrane permanent and binds to nucleic acids. It fluoresces red with a 40 fold intensity after binding.(Molecular Probes 2005 [148]) An additional wash step in PBS for 5 min was carried out before mounting the sample onto the confocal microscope.

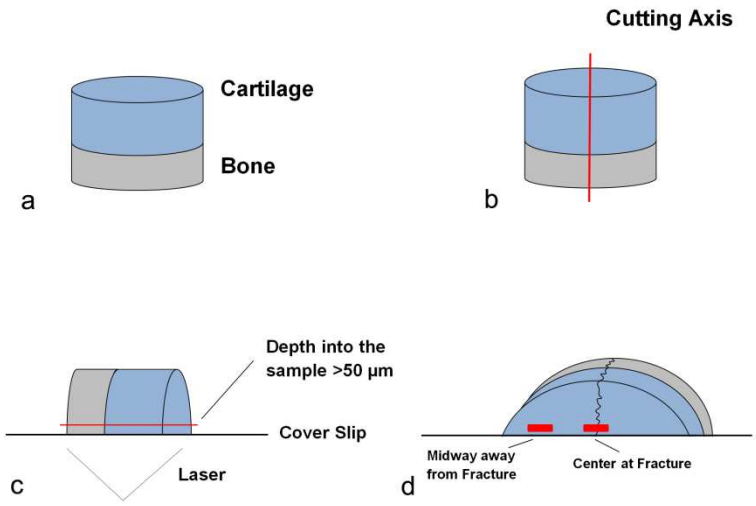

Fig. 36 Preparation of osteochondral cores: A cut was made perpendicular to the surface (Cutting Axis) (b). After staining the sample was mounted onto the microscope with the cut surface facing down. Chondrocyte Viability was measured at a minimum depth of 50 µm to avoid accounting for cells that died due to the cut (c). For fractured cores viability was measured at two locations: at the fracture edge and at the midpoint between fracture and outer edge (d) (Stolberg-Stolberg 2013 [203]).

Confocal laser scanning microscopy (10 x objective, numerical aperture of 0.30, LSM 510, Zeiss, Thornwood, NY) was used to obtain viability values. A depth of at least 50 µm was chosen to avoid counting dead cells from cutting. The size of the pinhole/ optical slices was set to 15 µm for the green as well as for the red laser. This thickness has previously been described to account for one layer of chondrocytes as their diameter is assumed to be between 7 and 15 µm (Backus 2010 [19], Darling 2006 [59]). Images were taken from the surface and from the area around the tidemark. For later analysis the different regions were defined as follows: The superficial zone accounts for the first 100 µm from the surface down into the cartilage, the middle zone lies 200 to 300 µm from the surface into the cartilage (Fig. 37).

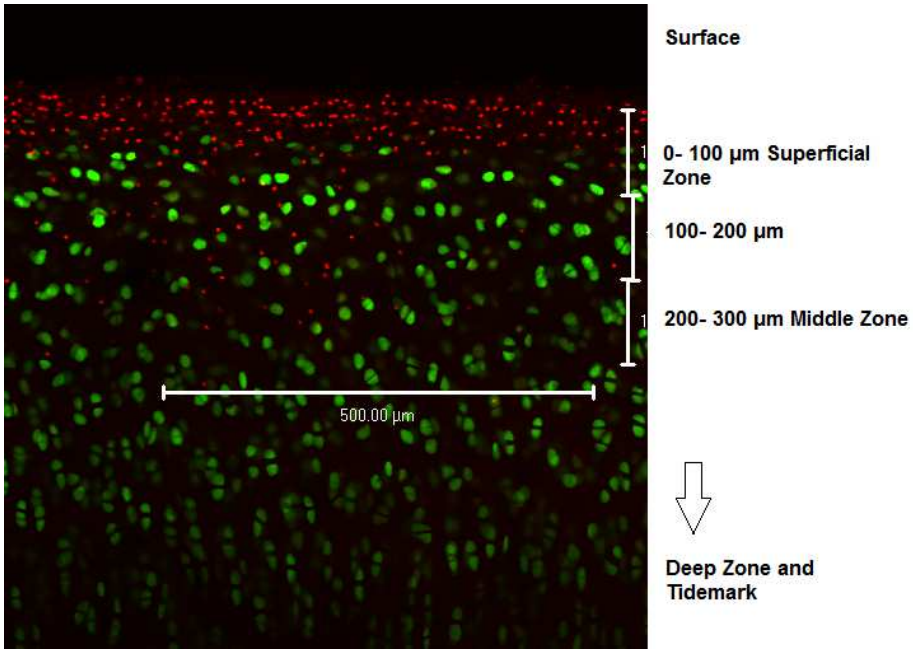

Fig. 37 Core #215: Superficial and Middle Zone.

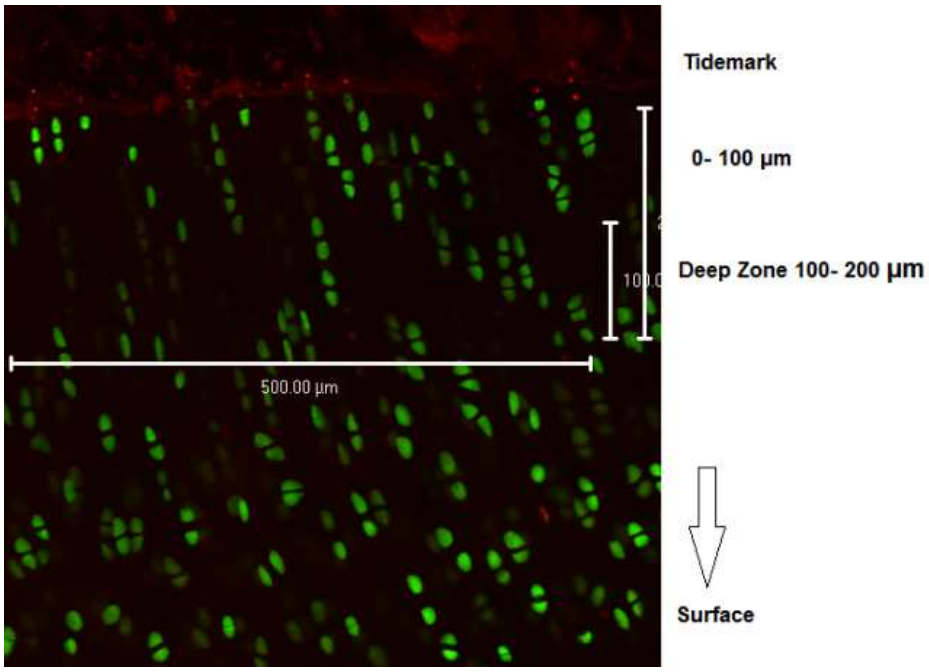

Fig. 38 Core #215: Deep Zone.

The deep zone is located 100 to 200 µm from the tidemark in direction to the cartilage surface (Fig. 38). For all areas the second dimension was set to be 500 µm to make up for an area of 50 000 µm^2. Before saving the data all images were rotated so that the cartilage surface and the tidemark were perfectly parallel to the upper image border. This was important for later image analysis.

3.6.1.1 Cell Count

Images were opened using Zeiss LSM 5 Image Browser (Jena, Germany). Green and red channels were switched off and the images with only the green or only the red stain visible were saved to a new file (Fig. 40 and Fig. 41). This data was opened again with Adobe Photoshop Limited Edition (Adobe Photoshop, San Jose, CA) and was converted into gray scale (Fig. 43 and Fig. 42). In a last step the images were opened with Scion Image (Scion, Inc., Frederick, MD), the white to black scale was inverted. Chondrocytes were now seen as grey/ black dots. The functions smooth and remove streaks were applied to all images that showed strong background staining. The intensity threshold was set to 30 for live and 25 for dead cells (Fig. 44 and Fig. 45). Cells in the selected area were then counted by the analyze particle function accounting a minimum particle size of 3 for dead and 5 for live chondrocytes. Viability was calculated using the following formula:

$$\%\,Viablity = \left(\frac{Live\ Cells}{Live + Dead\ Cells}\right) * 100$$

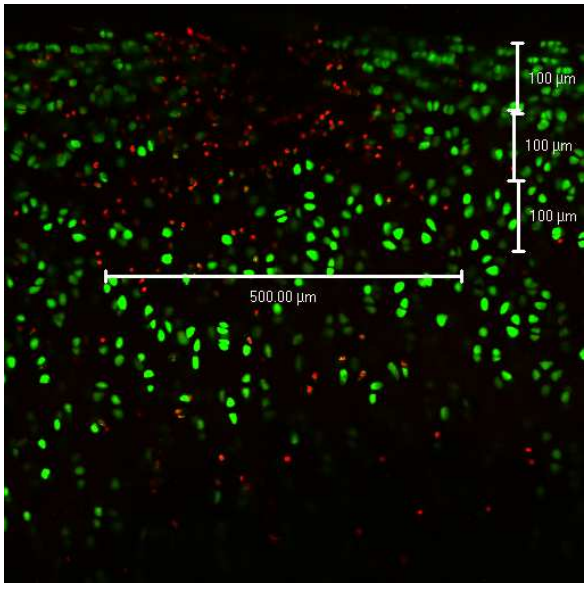

Fig. 39 Sample # 112, Superficial and Middle Zone.

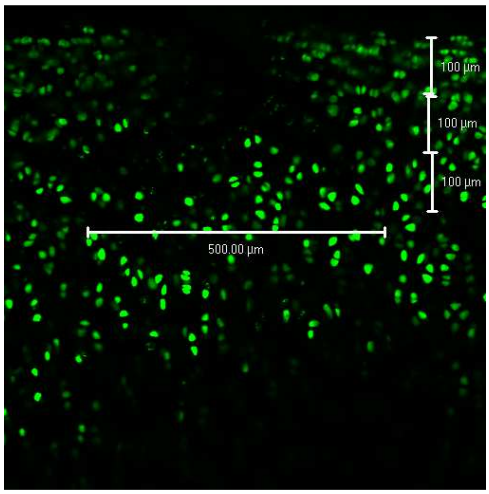

Fig. 41 Green channel only.

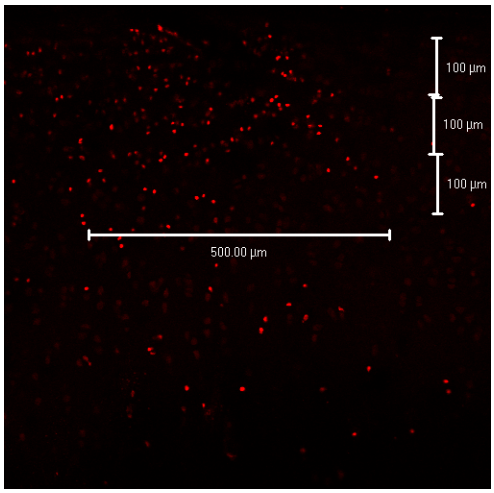

Fig. 40 Red channel only.

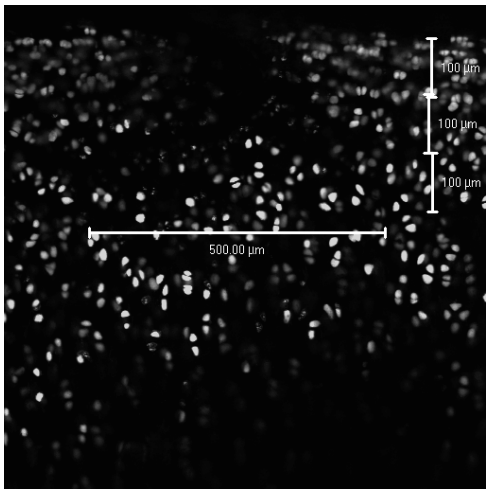

Fig. 43 Conversion into grey scale of live cells.

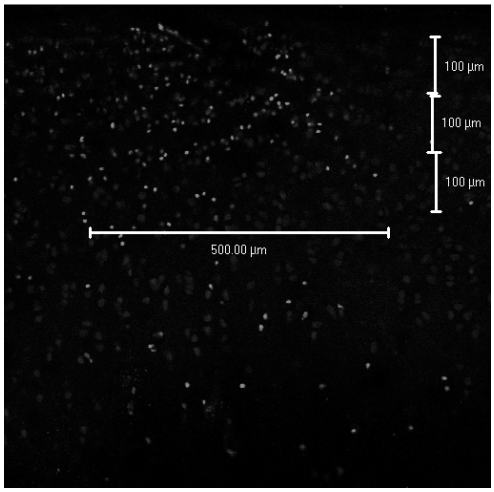

Fig. 42 Conversion into grey scale of dead cells.

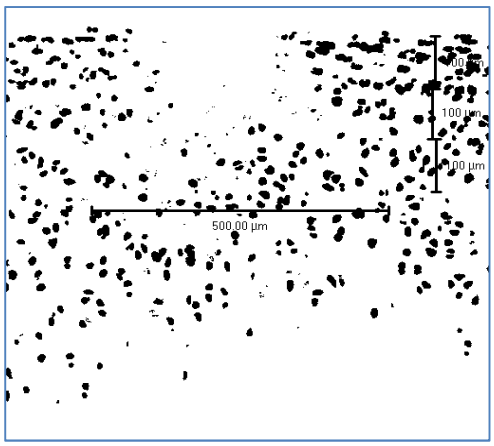

Fig. 44 Live cells after black-white inversion.

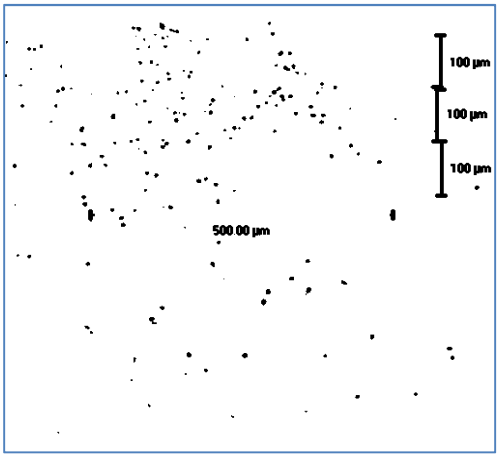

Fig. 45 Dead cells after black-white inversion.

3.7 Apoptosis Detection

3.7.1 Tissue Fixation

After cutting samples perpendicular to the articular surface with a razor blade the second half was preserved for histologic processing. It was fixed for 3 days in 10% neutral buffered formalin and then stored in 70% Ethanol until further processing. Samples were decalcified for 3 days (Cal-Ex; Fisher Scientific, Fair Lawn, NJ), dehydrated and embedded in paraffin. 7 µm tick sections were taken perpendicular to the articular surface. The first 50 µm of the sections were discarded to avoid counting of incision related cell death.

3.7.2 TUNEL

Sections were labeled using the TUNEL assay kid (ApopTag Peroxidase In Situ Apoptosis Detection Kit; Chemicon International, Temecula, California). The following protocol was used:

1. Deparaffinize slides in a coplin jar
    a. 3 changes of xylenes for 5 minutes each wash
    b. 2 changes of 100% Ethanol for 5 minutes each wash
    c. 1 change of 95% Ethanol for 3 minutes each wash
    d. 1 change of 70% Ethanol for 3 minutes each wash
    e. 1 change of PBS for 5 minutes each wash
2. Circle sections for staining with pap pen
3. Pretreat tissue with proteinase K (Roche)
    a. Dilute stock IHC proteinase K to 20µg/ml (0.75µL of 20mM Proteinase K in 999µL of 10mM Tris HCl pH 7.4; 70µl per slide)
    b. Apply directly to specimens for 10 minutes in humidified tray at room temperature
    c. Wash slides in 2 changes of PBS for 2 minutes
4. Create positive control slide with DNase I recombinant (Roche)
    a. Apply 50µL of 1500 U/mL DNase I (7.5µL of 10,000 U/mL DNase I + 4.3µL of 10x Incubation Buffer + 38.2µL of RNase-free H_20) per individual tissue section for 20 minutes
    b. Wash slides in 2 change of PBS for 5 minutes
5. Quench endogenous peroxidase
    a. Apply 3% hydrogen peroxide in methanol to slides for 5 minutes at room temperature
    b. Wash slides in 2 changes of PBS for 5 minutes each wash
6. TdT Reaction mixture
    a. Prepare 51µL of TUNEL reaction mixture per section
        i. Nucleotide mix = 0.25µL biotin-aha-dUTP + 0.5µL dATP + 4.25µL TE Buffer
        ii. To nucleotide mix, add 45µL TdT Buffer + 1µL TdT Enzyme

b. Apply TdT Buffer (NOT TdT enzyme/nucleotide mixture) for 10 minutes.
c. Apply TdT Reaction mixture (enzyme/nucleotide/buffer) for 75 minutes
d.
Prepare ABC reagent here, it needs to be mixed 30 minutes prior to use

e. Wash in 3 changes of PBS for 2 minutes each

7. SSC stop wash buffer
    a. Prepare 50µL of SSC per section
        i. 5µL of 20x SSC + 45µL of UltraPure deionized H_20
    b. Apply SSC for 15 minutes
    c. Wash slides in 1 change of PBS for 2 minutes
8. Mix ABC Reagent 30mins prior to using
    a. Add exactly 1 drop of Reagent A (Avidin DH, orange label) to 5ml of PBS in the ABC Reagent mixing bottle
    b. Add exactly 1 drops of Reagent B (Biotinylated Horseradish Peroxidase H, brown label) to the same mixing bottle, mix immediately, and allow VECTASTAIN ABC Reagent to stand for approx. 30 minutes before use.
    c. Add enough ABC Reagent to cover tissue sections (1-2 drops)
    d. Incubate at RT for 30 minutes
    e. PBS: 3 washes 3 minutes each
9. DAB Substrate for Peroxidase
    a. To 2.5ml of distilled water, add 1 drops of Buffer Stock Solution and mix well
    b. Add 2 drops of DAB Stock solution and mix well
    c. Add 1 drop of the Hydrogen Peroxide Solution and mix well
    d. Add enough Substrate mixture to cover tissue (2 drops)
    e. Incubate at RT for 8 minutes
    f. Gently dip sections in distilled H_20
10. Counterstain
    a. Rinse slides in tap water.
    b. Add Vector Hematoxylin QS counterstain to completely cover tissue sections
    c. Incubate for 3 seconds
    d. Immerse in tap water for appoximately 10 seconds
    e. Hold slides in tap water until all slides are stained
11. Clear and mount slides
    a. 1 change of 70% Ethanol for 3 minutes each wash
    b. 1 change of 95% Ethanol for 3 minutes each wash
    c. 2 changes of 100% Ethanol for 5 minutes each wash
    d. 1 change of xylenes for 5 minutes each wash
    e. Mount with Permount and 50mm cover glass

3.7.3 ISOL

Samples were deparaffinised, rehydrated as for the TUNEL assay. The ISOL protocol (ApopTag® ISOL Dual Fluorescence Apoptosis Detection Kit (DNase Types I & II), Millipore, Billerica, MA) (carboxyfluoroscein excitation-emission at 492/518 nm, Cal Fluor Red 590 excitation-emission at 569/591 nm) was used: Samples were incubated in proteinase K (150µl of 0.05 mg/ml per section) for 15 minutes. ISOL labeling reaction mix (15 µl Dual reaction buffer 2X, 10 µl Vaccinia Topoisomerase I, 4 µl T4 DNA Ligase and 1 µl Dual Labeled Oligo) was prepared and applied to each section. Samples were then incubated in a humidified chamber for 12 hours at room temperature. As counterstain 30 µl of 1:200 of To-Pro-3-Iodide (Invitrogen, Carlsbad, CA) (Excitation-Emission: 642/661 nm) and PBS were applied to each section 40 minutes before imaging. Before confocal analysis each slide was washed in PBS 1 time for 10 minutes. For confocal imaging the optical slice was set at 8 µm and lasers were set at FITC/Rhod/Cy5. Images were taken at 10 x magnification and zones were defined as described above.

3.8 Wet Weight

In order to adapt the amount of NO, PG, MMP and aggrecanase release of each core to the actual weight of cartilage, we cut the cartilage from the bone and weighed the cartilage on a high precision balance. This was only done for the conditioned media experiments because cartilage was not needed for further processing. For all other experiments, results were normalized using cartilage height.

3.9 S-GAG Measurement by DMB Assay

Sulfated-glycosaminglycan concentrations were measured by using the 1,9-dimethylmethylene blue (DMB) assay. Briefly, this assay is based on a metachromatic shift in absorption after s-GAG and DMB complex formation (Farndale 1986 [67], Taylor 1969 [212]). Standards were made up at the concentrations of 100, 80, 60, 40, 20, 10 and 0 µg/ml. Bovine Trachea chondroitin 4 (A) Sulfate (Sigma- Aldrich), SFM and AAP were used.

The assay was run by adding 40 µl of standards and samples in duplicates to a 96 well plate. 125 µl 1,9-dimethylmethylene blue (DMB) was added to each well and absorbance was measured within 5 minutes at 540 nm wavelength (Tecan GENios Plate reader, Switzerland). This test was repeated for samples that showed a concentration below 40 µg/ml or above 80 µg/ml (most accurate reading range) at an adequate dilution with SFM.

3.10 NOX Assay

Total nitrate (NO_3^-) and nitrite (NO_2^-) (NOX) concentrations were measured by a NOX assay using nitrate reductase in order to measure total nitrite concentration (Granger 1999 [81]).

The first step for the NOX assay was the preparation of standards. $NaNo_3$ (Sigma) was diluted in SFM and AAP to concentrations of 320, 160, 80, 40, 20, 10 and 0 µM solutions, pipetted into 500 µl Micron Ultracel YM-10 filters (Millipore) and centrifuged at 14000 g for 30 minutes.

50 µl of the standard or the sample (after centrifugation, 14 000 g, 30 minutes) were pipetted into a 96 well transparent plate. Now 7 µl of 1 molar Tris Buffer solution, 10 µl of 0.2 molar NADPH, 23 µl of a G6P and G6PH solution and 10 µl of nitrate reductase (Roche Diagnostics, Mannheim, Germany) were added chronologically. The solutions in this plate were mixed thoroughly by placing the plate on a plate ruttler. The plate was then incubated for 30 minutes at 37°C. 100 µl of Greiss I (Sigma) and 100 µl of Greiss II (Sigma) reagent were added to each well. After 10 minutes incubation time at room temperature the color change was measured using plate reader at an absorbance of 540 nm. Data was adapted to the wet weight of the cartilage of each sample (Fermor 2002 [68]).

3.11 MMP Assay

MMP activity is involved in major catabolic processes during cartilage degradation. Total specific MMP activity was measured in media collected from our samples. This assay is most specific for MMP- 13. The peptide substrate might also be cleaved by MMP-1, MMP-2, MMP-3 and MMP-9 (Rasmussen 2004 [177]).

Duplicates of 50 µl samples were added into a 96 well plate. A 20 µM solution of consensus peptide was made up in assay buffer. In two different batches to each ml 50 ng of GM6001 (EMD Biosciences Inc.) or 50 ng of GM6001 negative control (EMD Bioscience Inc.) were added. Either GM6001 or its negative control was pipetted into each well. The plate was then incubated at 37°C for 2 hours. Fluorescence was measured at 485 nm excitation and 535 nm emission on the plate reader.

Total specific MMP activity was determined by subtracting the negative control from its GM6001 sample and by normalizing it to the cartilages wet weight. If the fluorescence of the negative control or fresh SFM was found to be higher than the samples one, MMP activity was defined as 0.

3.12 Aggrecanase Activity Assay

The fluorescent peptide WAAG-3R (AnaSpec, San Jose, CA) at a concentration of 25 µM was used to measure aggrecanase-1 (ADAMTS- 4) activity (Zhang 2004 [239]).

Briefly, a 96 well plate was used. 50 µl of sample was added to each well. One of the remaining wells was used to add 50 µl buffer. After pipetting another 50 µl of the peptide (40 µl peptide + 10 ml WAAGER assay buffer) the plate was incubated at 37°C in the dark for 30 minutes. Fluorescence was measured at 340 nm excitation and 405 nm emission on the plate reader.

Again, aggrecanase activity was normalized to wet weight. If the buffer control showed more activity, aggrecanase activity was defined as 0 for that sample.

3.13 PicoGreen Assay

“Culture media was diluted 1:10 in PBS making up 70 µl. 50 µl of diluted media and standards were added to a black 96-well microtitre plate (Costar, Corning Incorporated, Corning, NY, USA). PicoGreen dye (Molecular Probes, Eugene, OR, USA) diluted to 1 : 200 in Tris-EDTA buffer (10 mM Tris, 1 mM ethylenediaminetetraacetic acid, pH 8) was added. TECAN GENios microplate fluorescence reader (Salzburg, Austria) was used to measure fluorescence. At an excitation wavelength of 485 nm and an emission wavelength of 535 nm values were obtained as relative fluorescence units according to a standard curve made from dsDNA from calf thymus (Sigma). Total dsDNA concentration was normalized to the cartilage height for each sample” (Stolberg-Stolberg 2013 [203]).

3.14 Conditioned Media

The idea of conditioned media is to pool media which has already been used for culturing of several cores of a specific group. This pooled media was then supplemented with 50% fresh SFM. This mixture was chosen due to test runs which showed a slight change in color (indicates lack of nutrients) using higher percentages of already used media.

After three days of culturing, media from necrotic, loaded (90% strain blunt impact) and sham cores was pooled for each group. The pooled media was then added to sham cores. Sham cores were then cultured from day 3 to day 6. At day 6 the media was harvested. NOX and PG measurements were then done for the media of each core individually. Concentrations were adapted to wet weight and concentrations from pooled media from day 3 were subtracted from day 6.

3.15 Ramos Blue Cells

“Ramos-Blue Cells, stably expressing an NF-kB/AP-1-inducible SEAP (secreted embryonic alkaline phosphate) reporter construct, was purchased from InvivoGen (San Diego, CA). These cells express nucleic acid-sensing TLRs, (e.g. TLR-3, 7 and 9) and selectively respond to agonists of nucleic acid-sensing TLRs. Ramos-blue cells were cultured in Iscove's Modified Dulbecco's Medium supplemented with 2 mM L-glutamine, 10% heat-inactivated fetal bovine serum, 50 U/ml penicillin and 50 µg/ml streptomycin (all from Life Technologies, Grand Island, NY) at 37°C in a 5% CO2. TLR-mediated stimulation of Rasmos-Blue cells was performed according to the manufacturer's instructions. Briefly, cells were suspended at a density of 2 x 10^6 cells/ml in the growth media. 140 µl of cell suspension was mixed with 60 µl of culture media from loading experiments and incubated for 18 h in a 96-well flat bottom plate. NFκB activation was accessed by quantifying SEAP level in cell culture supernatant. To quantify SEAP, 180 µl of SEAP substrate (QUANTI-Blue) (InvivoGen) was mixed with 40 µl of Ramos Blue cell culture supernatant in a 96-well flat bottom plate. After 5 hour incubation, SEAP level in Ramos-blue cell culture supernatant was determined by measuring absorbance at 650 nm using a BioTek Power Wave XS2 ELISA plate reader (BioTek, Winooski, VT)”(Stolberg-Stolberg 2013 [203]).

3.16 HEK Blue hTLR-4 Cells

HEK Blue hTLR-4 Cells also stably express an NF-kB/AP-1-inducible SEAP reporter construct were purchased from InvivoGen (San Diego, CA). These cells express TLR-4. They were cultured identically to the Ramos Blue Cells. HEK Blue hTLR-4 Cells were suspended at a density of 140 000 cells per ml. 180 µl of cell suspension and 20 µl of media were added to a 96-well flat bottom plate and incubated for 24 hours. NFκB activation was accessed as described in the previous section.

3.17 Statistics

Statistica 7 (StatSoft, Tulsa, OK, USA) was used for statistical analysis. A two-factor ANOVA and Tukey post-hoc test were performed to determine significant differences. For analysis of dsDNA release, Ramos Blue and HEK-293 Cell activity repeated measures ANOVA and Fisher LSD were used.

4 Results

4.1 Results Strain Measurement

4.1.1 Results Computerized Strain Measurement

In order to assess total strain applied to cartilage, videos were taken while loading. Briefly, change in length of cartilage and bone were measured using Matlab R2009b (MathWorks, Natick, MA, USA). For images at -5 N preload and during 2 second hold-down cartilage surface, osteochondral junction and bottom of bone were tagged manually. As shown in this pilot (Fig. 46), with increasing stress total bone strain increases. Total cartilage strain, however, decreases. This happens due to radial extension and bulging over of the cartilage. Thus, in the video documentation cartilage strain is shown false low whereas bone strain is shown false high.

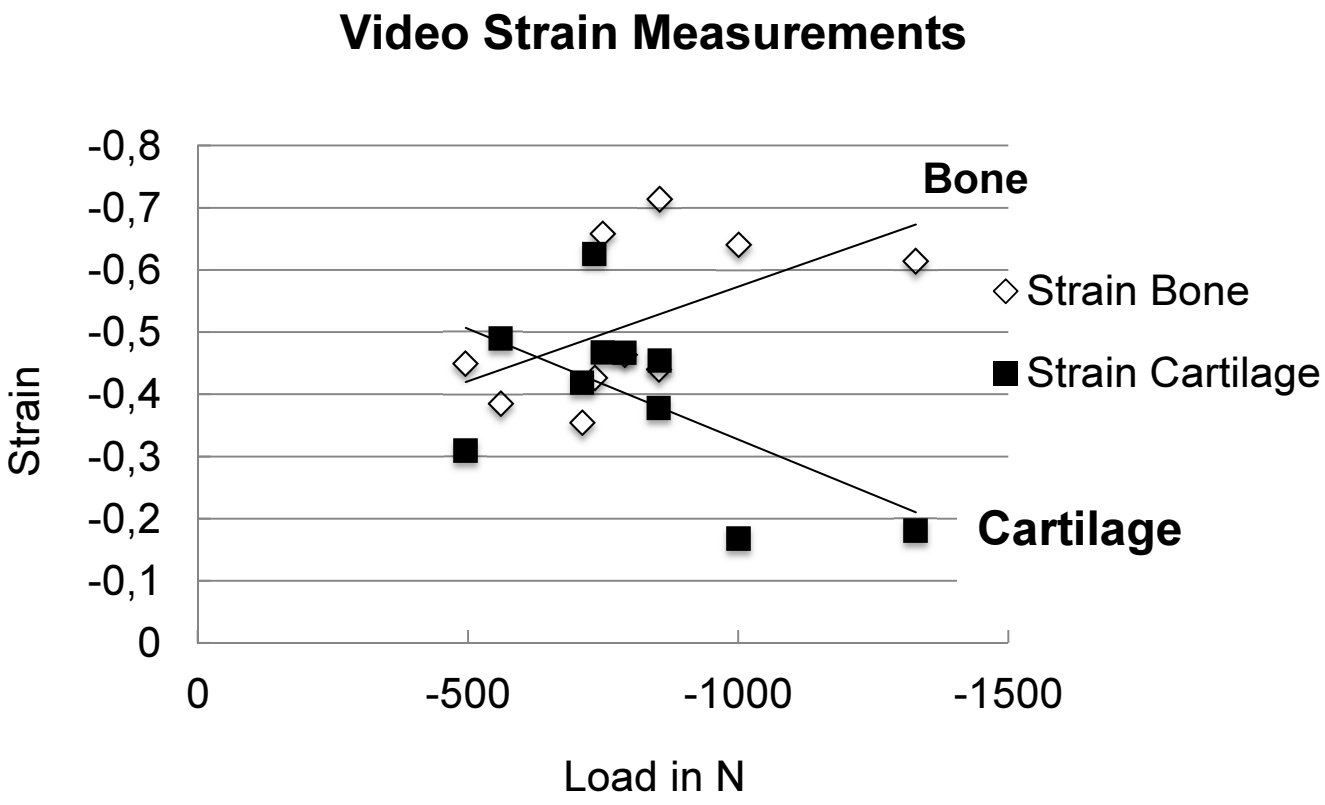

Fig. 46 Stress-Strain curve shows decreasing cartilage strain with increasing stress.

4.1.2 Results Compressive Modulus of Bone Only

1 mm thick samples of bone only were loaded to a maximum stress of -2500 N at a rate of 1 sec^{-1} (Fig. 47). The decrease of steepness of some samples might be caused by fracture of the bone. Taking this data into account, roughly 10-20% displacement of the 70%, 80% and 90% strain samples will be absorbed by the bone. Thus, the real cartilage displacement is lower than indicated by the name of each group.

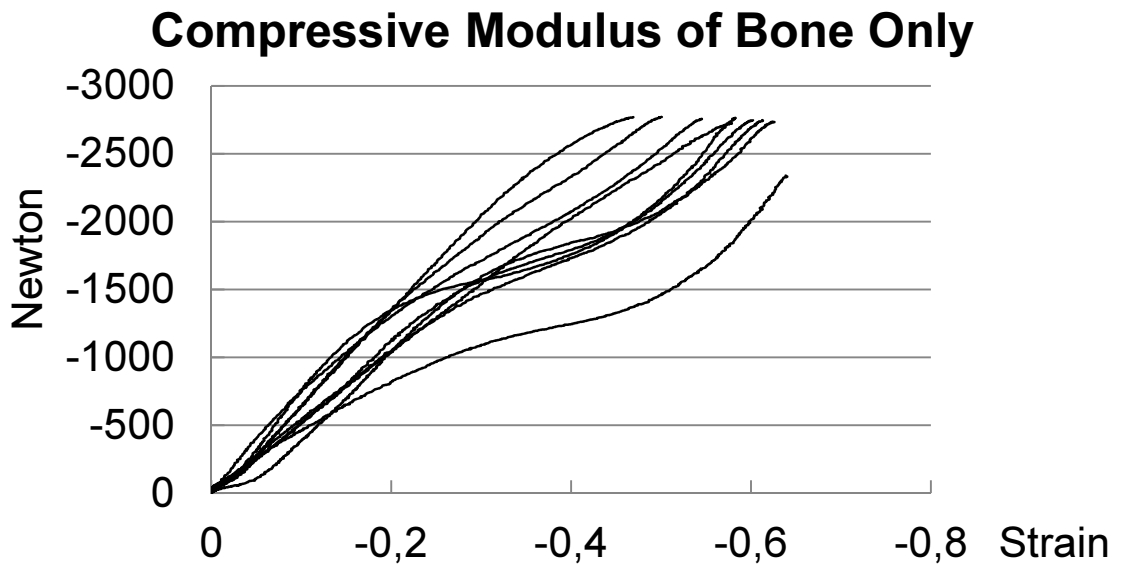

Fig. 47 The stress-strain curve of bone only shows the compressive modulus of bone.

4.2 Viability

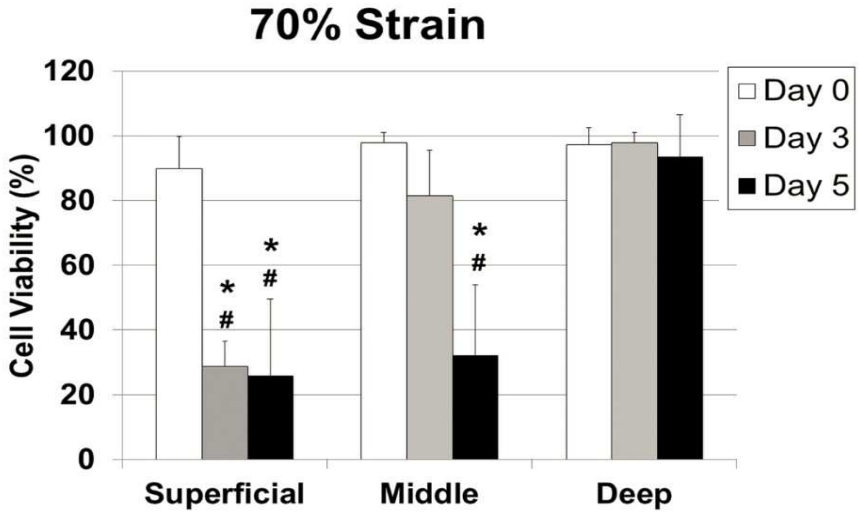

Fig. 48 Viability data after 70% Strain Loading (# indicates statistically significant differences from sham controls; * indicates statistically significant differences from day 0) (Stolberg-Stolberg 2013 [203]).

“At 70% strain (Fig. 48), viability at day 0 was not significantly different from controls in any cartilage zone (Fig. 53). However, the superficial zone at days 3 and 5 and the middle zone at day 5 showed significant decreases in viability from controls ($p \leq 0.0001$) with no significant differences from controls in the deep zone. Viability decreased with time in the superficial and middle zones. In the superficial zone, viability significantly decreased following loading from day 0 to days 3 and 5 ($p \leq 0.001$). No significant loss of viability was detected in the deep zone with time. 70% strain was the only blunt impact loading condition in which viability decreased with time” (Stolberg-Stolberg 2013 [203]).

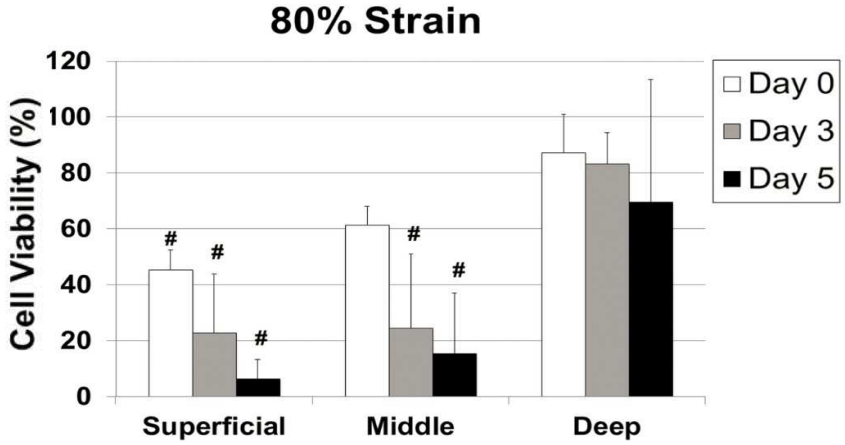

Fig. 49 Viability data after 80% Strain Loading (# indicates statistically significant differences from sham controls) (Stolberg-Stolberg 2013 [203]).

“At 80% strain (Fig. 49), viability at day 0 was significantly different from controls only in the superficial zone (p=0.048). The superficial and middle zones showed significant decreases in viability from controls at days 3 and 5 (p≤0.0001) with no significant differences from controls in the deep zone. However, within cartilage zones, no statistical differences in viability were detected with time. Compared to 70% strain, there were significantly less viable chondrocytes in the middle zone at day 3 (p=0.006)” (Stolberg-Stolberg 2013 [203]).

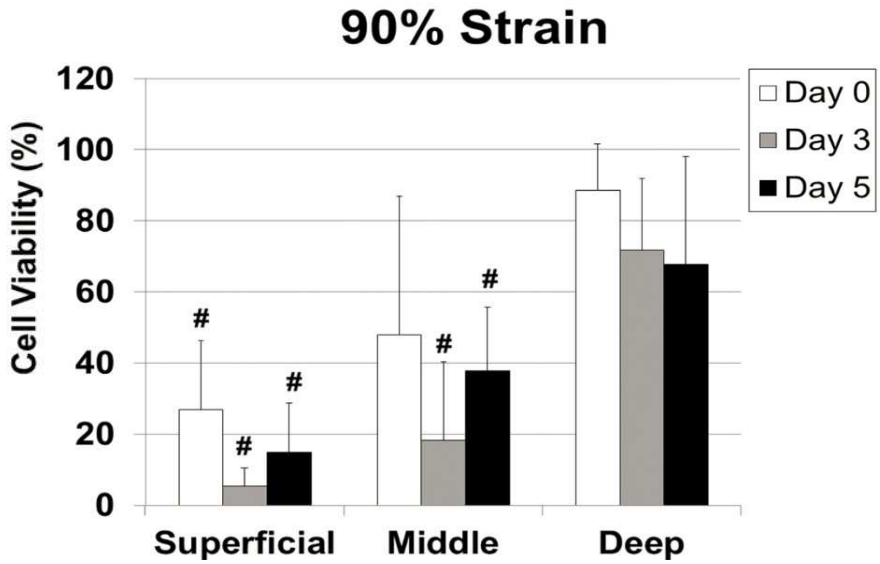

Fig. 50 Viability data after 90% Strain Loading (# indicates statistically significant differences from sham controls) (Stolberg-Stolberg 2013 [203]).

“At 90% strain (Fig. 50), viability in the superficial zone was significantly decreased compared to controls at all days (p≤0.0001). The middle zone at day 3 and day 5 showed significant decreases in viability from controls (p≤0.006). Again, there were no significant differences in viability from controls in the deep zone. Similar to 80% strain, loss of viability with 90% strain was immediate, and no statistically significant differences in viability with time were found in any cartilage zone. Compared to 70% strain, there was a significant decrease of viability in the superficial zone at day 0 (p=0.0007) and the middle zone at day 3 (p=0.0006). However, compared to 80% strain, there were no statistical differences in viability in any cartilage zone for all days”(Stolberg-Stolberg 2013 [203]).

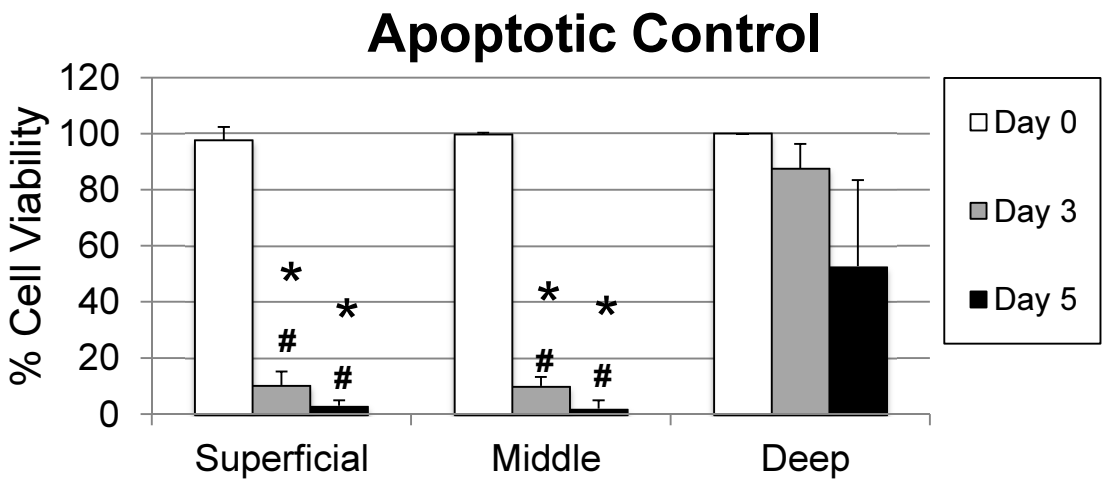

Fig. 51 Viability data after culturing in 10 µM Staurosporine (# indicates statistically significant differences from sham controls; * indicates statistically significant differences from day 0).

Staurosporine: The application of 10 µM staurosporine induced apoptotic cell death beginning in the superficial and middle zone. There was a significant loss of viability in the superficial and middle zone from day 0 to day 3 ($p \leq 0.000031$) and day 5 ($p \leq 0.000031$). The superficial and middle zone of days 3 ($p \leq 0.000031$) and 5 ($p \leq 0.000031$) were also different to the corresponding sham control. In the deep zone no significant differences could be observed (Fig. 51).

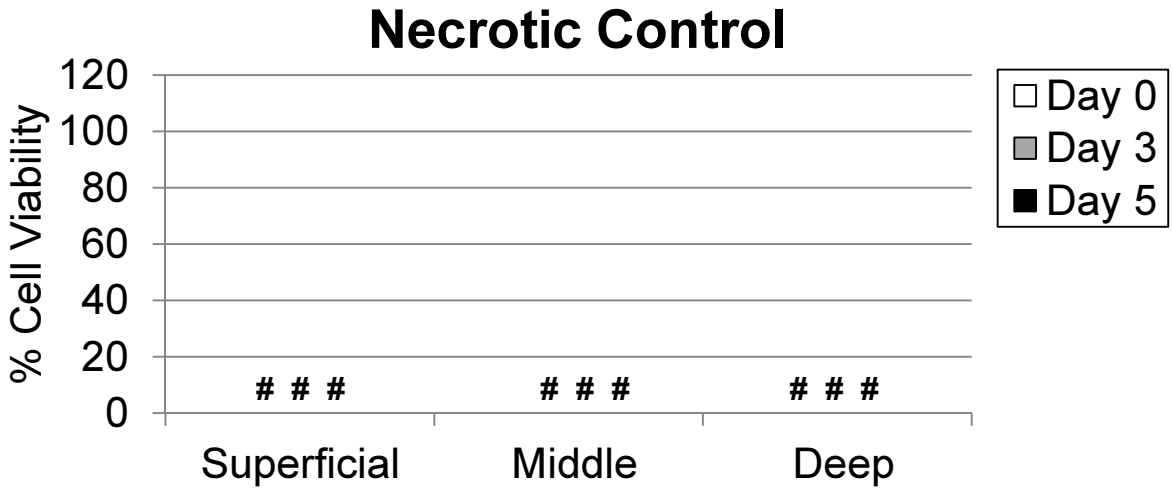

Fig. 52 Viability after 3 days at -80°C (# indicates statistically significant differences from sham controls).

Necrotic cores showed 0% viability in all zone from the first day of culturing and thus were different to sham controls at all time points and zones ($p \leq 0.000031$) (Fig. 52).

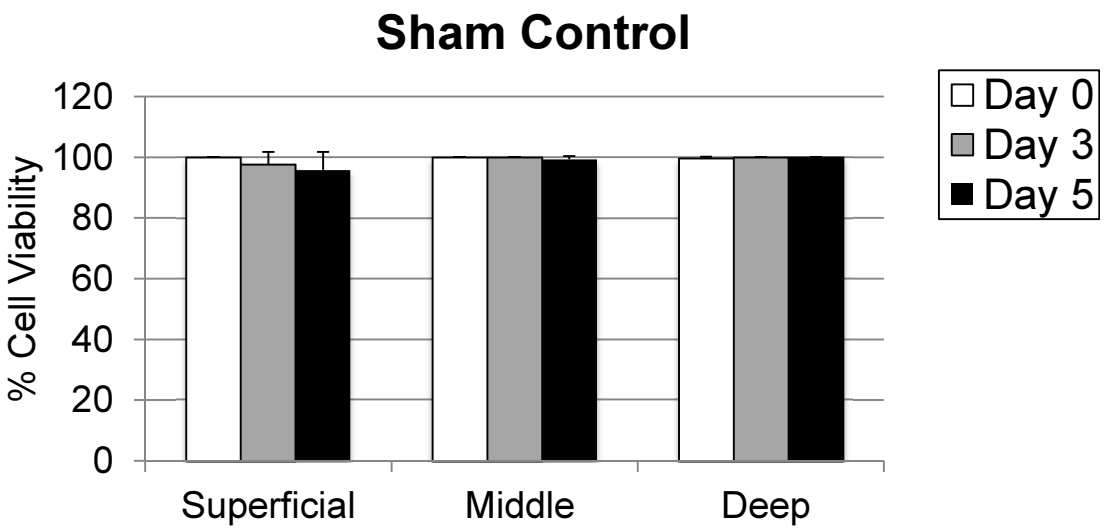

Fig. 53 Viability of sham controls.

"In the sham control samples, the overall viability of the cartilage was 99.2±2.5% (day 0: superficial 97.6±4.8%, middle 99.6±0.8%, deep 100±0%; day 3: superficial 97.6±4.1%, middle 100±0%, deep 100±0%; day 5: superficial 95.8±5.9%, middle 99.4±1.1%, deep 100±0%) (Fig. 53) "(Stolberg-Stolberg 2013 [203]).

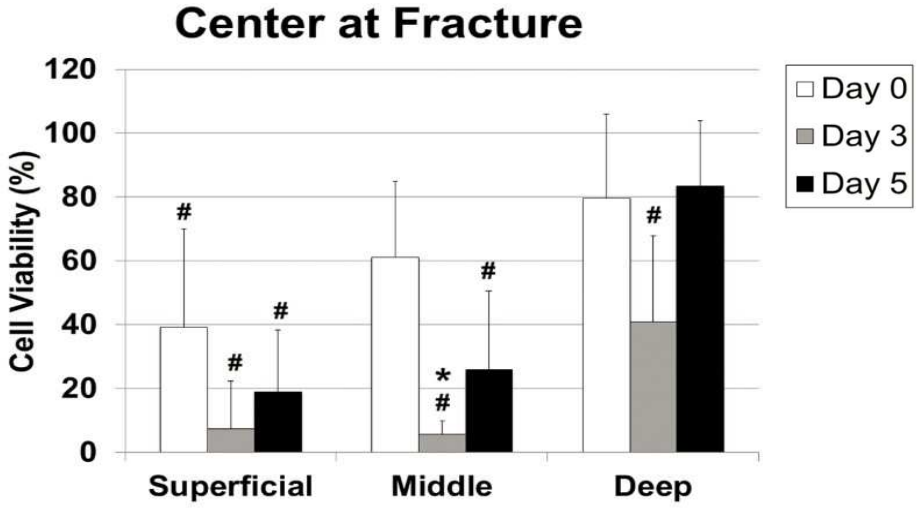

Fig. 54 Viability 250 µm to each side of the fracture edge (# indicates statistically significant differences from sham controls; * indicates statistically significant differences from day 0) (Stolberg-Stolberg 2013 [203]).

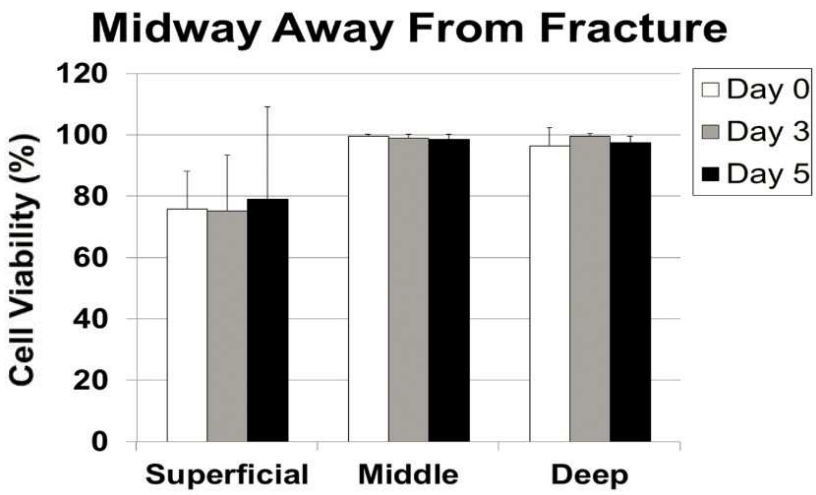

Fig. 55 Viability at the midpoint between fracture and outer edge (Stolberg-Stolberg 2013 [203]).

“In fractured cores, a high level of chondrocyte death occurred along the fracture edges with high variability due to variations fracture patterns (Fig. 54). At the fracture, viability at day 0 decreased significantly compared to controls only in the superficial zone ($p=0.008$). The superficial and middle zones showed significant decreases in viability from controls at days 3 and 5 ($p\leq0.0001$) with significant differences from controls in the deep zone only at day 3 ($p=0.013$). In the middle zone, viability significantly decreased following loading from day 0 to day 3 ($p=0.011$). Away from the fracture, viability was not significantly different than controls in any cartilage zone for all days (Fig. 55; $p\geq0.999$)” (Stolberg-Stolberg 2013 [203]).

4.2.1 Live-Dead Assay Images

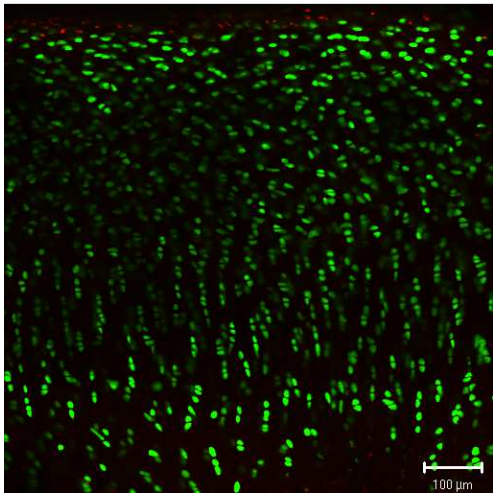

Fig. 57 #289: Viability after 70% strain blunt impact at day 0.

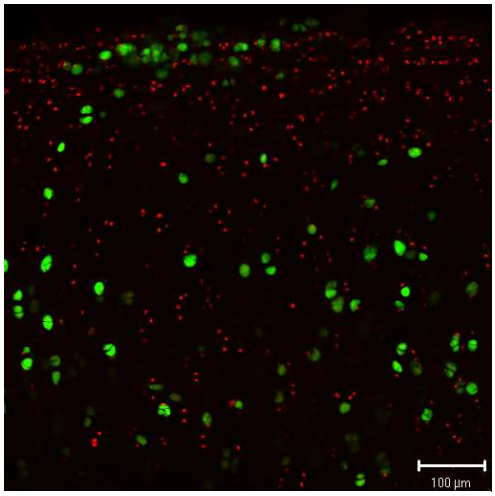

Fig. 56 #381: Viability after 70% strain blunt impact at day 5.

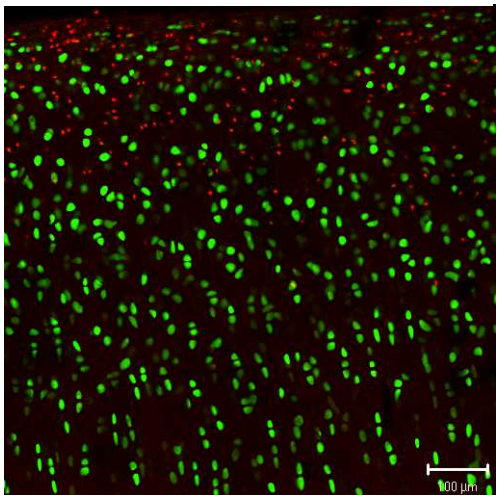

Fig. 59 #306: Viability after 80% strain blunt impact at day 0.

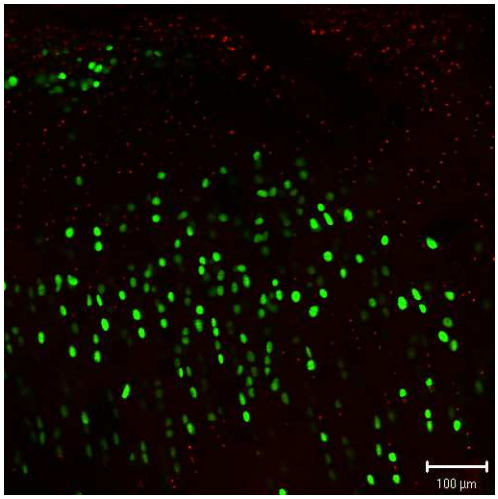

Fig. 58 #361: Viability after 80% strain blunt impact at day 5.

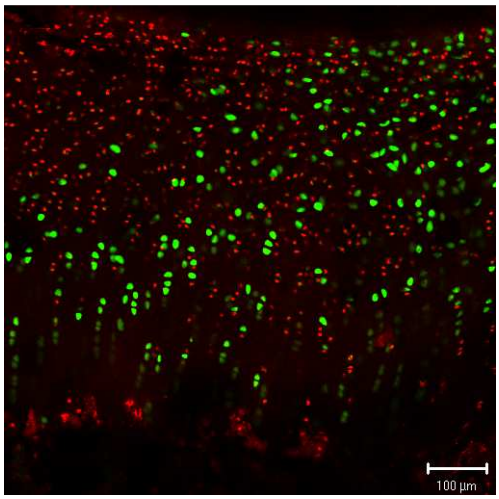

Fig. 61 #301: Viability after 90% strain blunt impact at day 0.

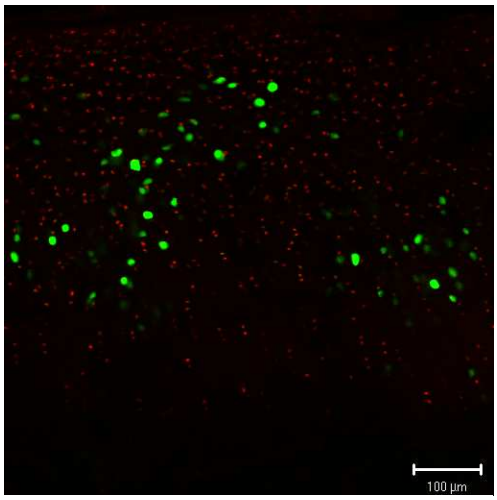

Fig. 60 #441: Viability after 90% strain blunt impact at day 5.

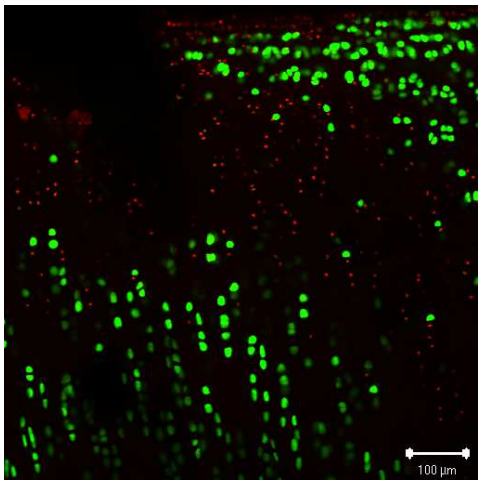

Fig. 63 #467: Viability after fracture at fracture at day 3.

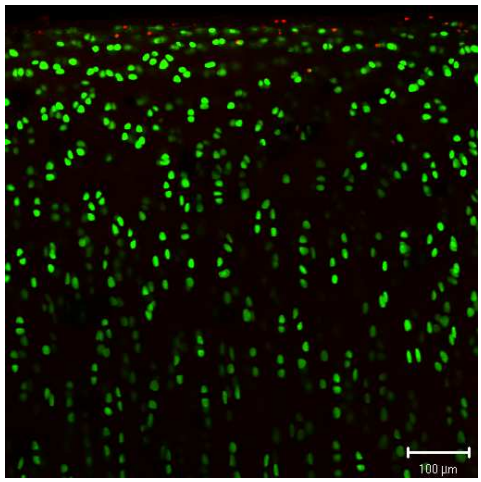

Fig. 62 #467: Viability after fracture away from fracture at day 3.

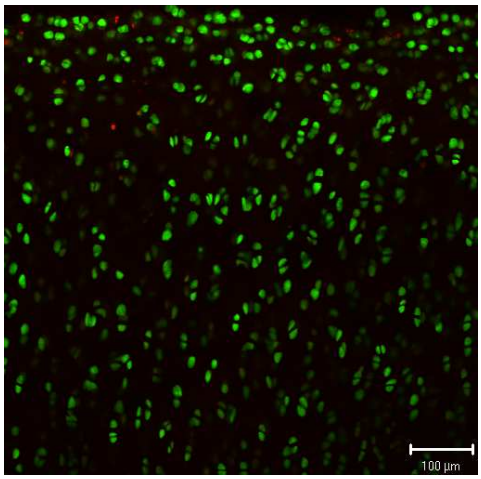

Fig. 64 #370: Viability of sham core at day 5.

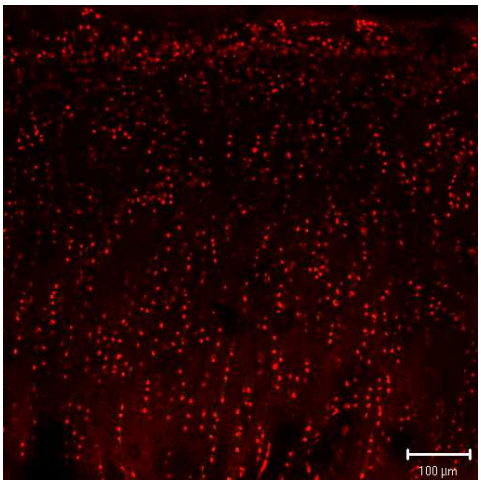

Fig. 65 #405: Viability of necrotic core at day 0.

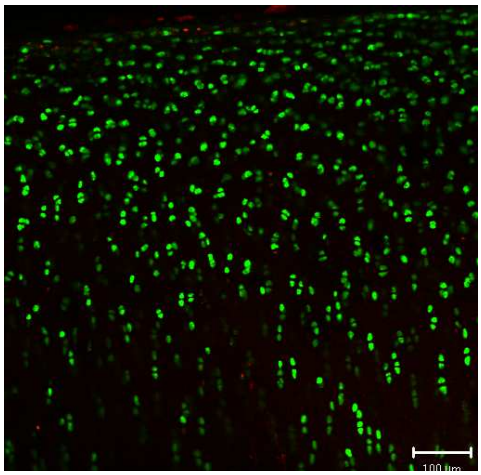

Fig. 66 #461: Viability of apoptotic control core at day 0.

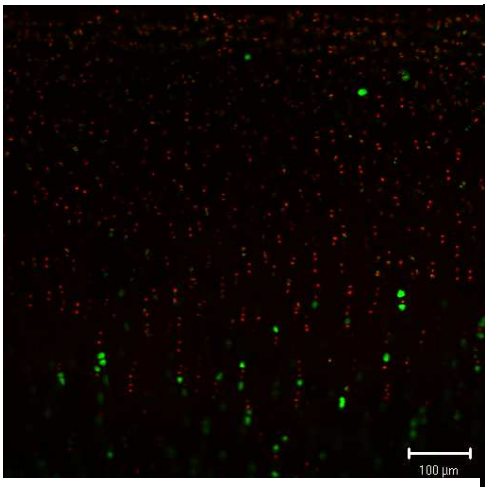

Fig. 67 #472: Viability of apoptotic control core at day 5.

4.3 Apoptosis Detection

4.3.1 Results TUNEL Assay

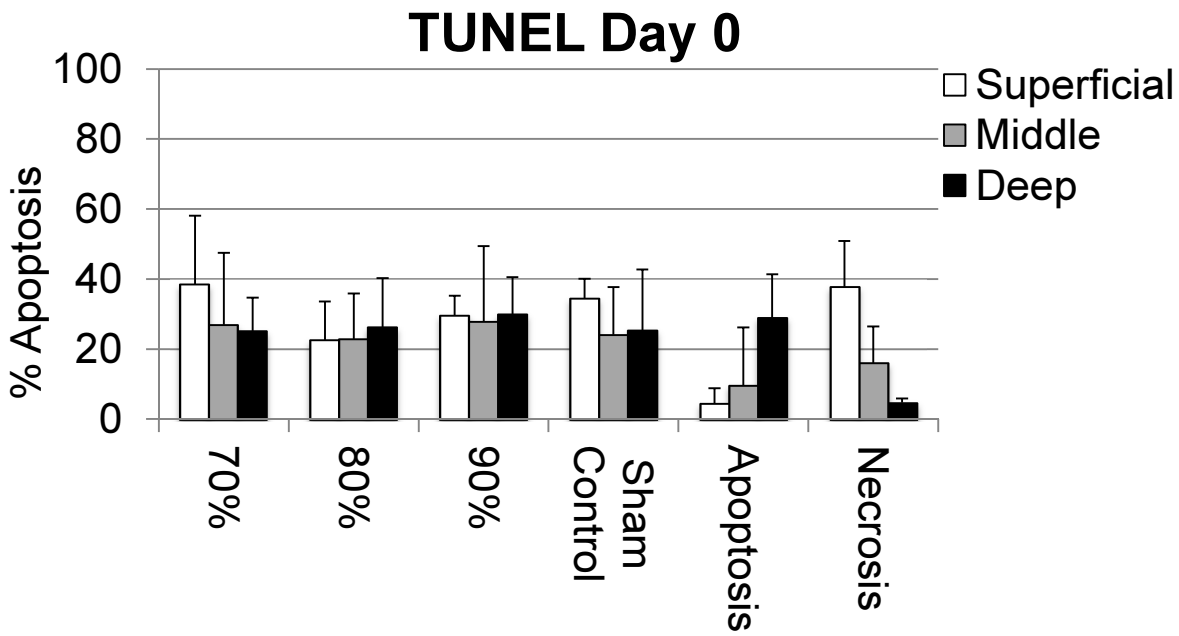

Fig. 68 Results of TUNEL assay at day 0.

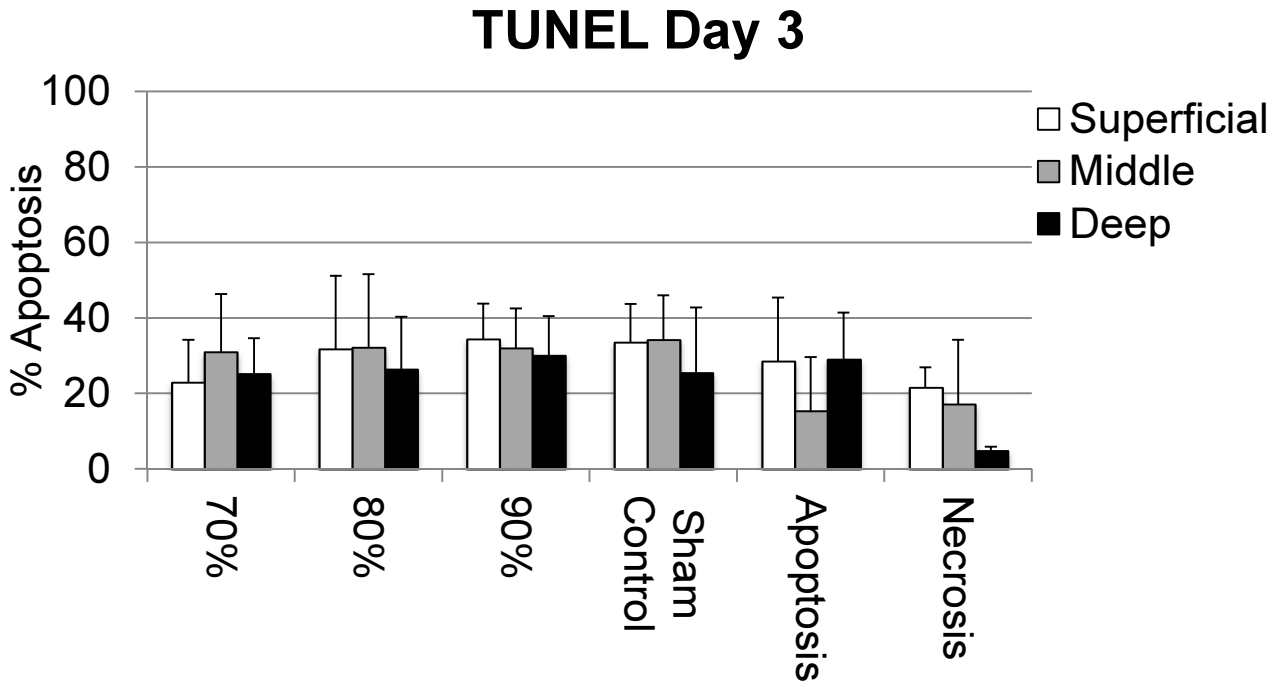

Fig. 69 Results of TUNEL Assay at day 3.

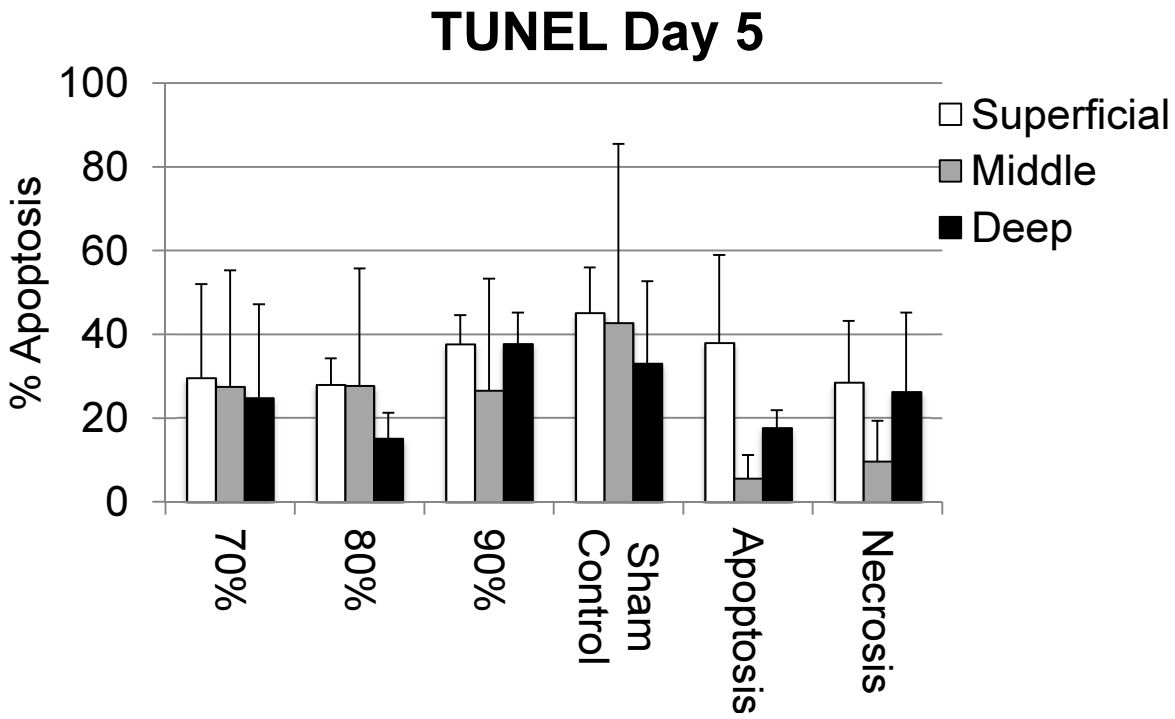

Fig. 70 Results of TUNEL assay at day 5.

Despite extensive troubleshooting on the TUNEL assay, at none of the time points there was a significant difference between apoptotic and necrotic control samples, nor at day 0 (Fig. 68), nor day 3 (Fig. 69) nor day 5 (Fig. 70). This led us to the final conclusion that this assay is not working on our tissue. Thus, no further statistical analysis was done.

4.3.2 TUNEL Images

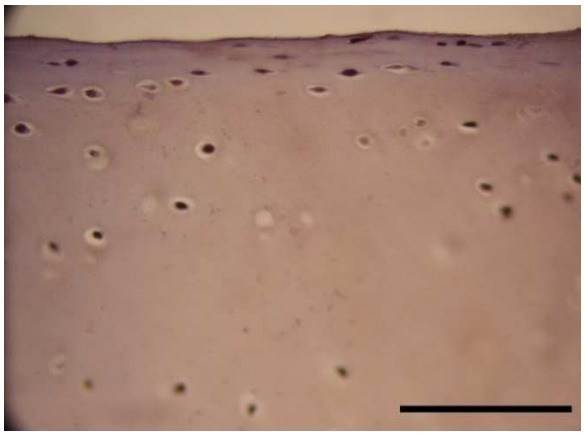

Fig. 72 #363: Not loaded control sample from day 3 treated with DNase showing positively stained dark brown nuclei. Scale bar 100 µm

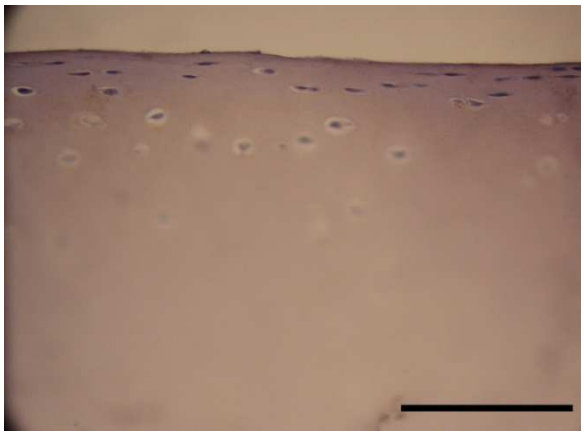

Fig. 71 #363: Not loaded control sample from day 3 without DNase treatment showing negatively stained blue nuclei. Scale bar 100µm

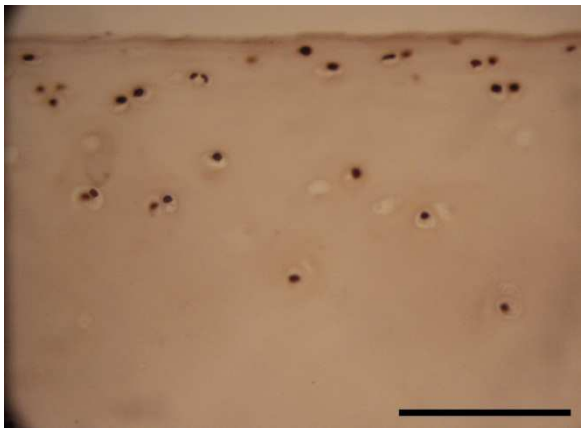

Fig. 73 #398: Necrotic control slide from day 0 showing primarily false positive apoptotic nuclei. Scale bar 100 µm

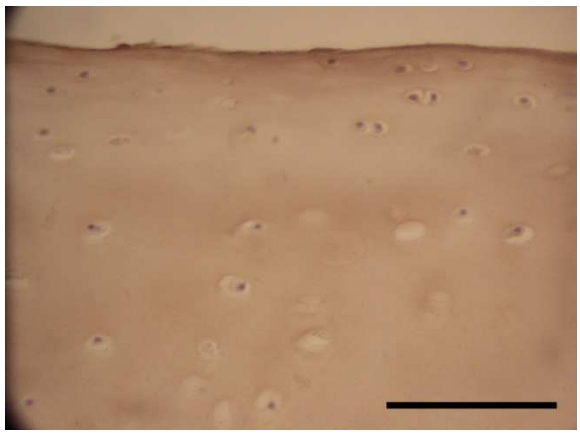

Fig. 74 #398: Control slide of necrotic control slide from day 0 showing blue nuclei only. Scale bar 100 µm

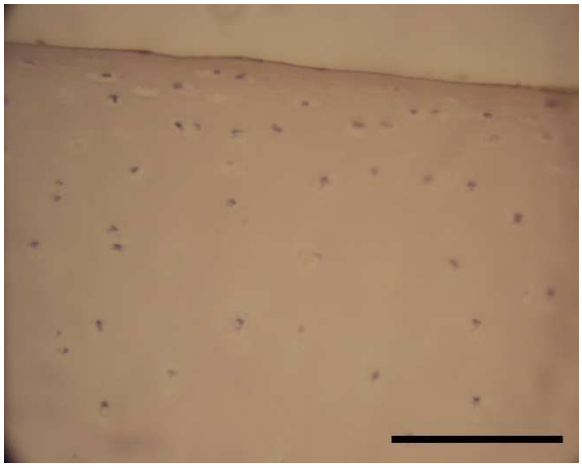

Fig. 76 #461: With staurosporine treated apoptotic control from day 0 shows no (false negative) apoptotic nuclei. Scale bar 100 µm

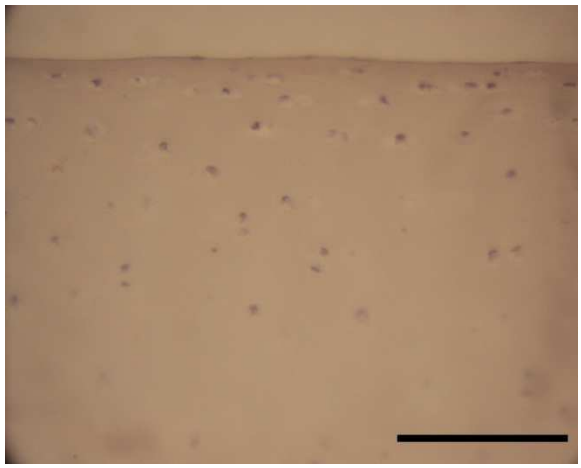

Fig. 75 #461: Nuclei of negative control slide from day 0 looks just as the positive slide. Scale bar 100 µm

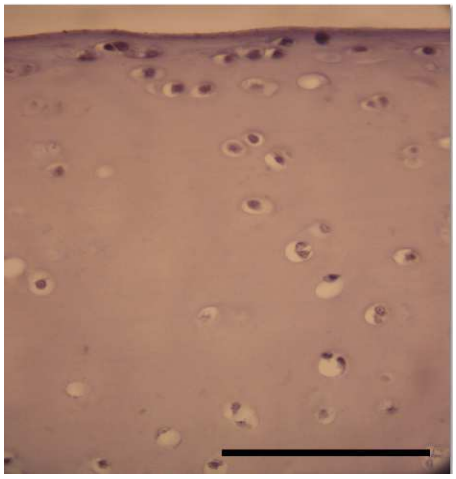

Fig. 78 #370: sham control slide from day 5 showing apoptotic nuclei particularly in superficial zone. Scale bar 100 µm

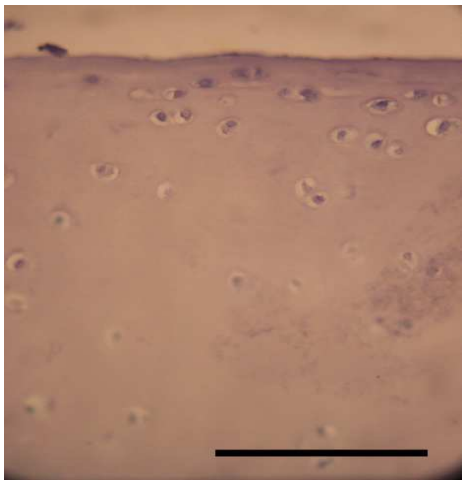

Fig. 77 #370: Negative control. Scale bar 100 µm

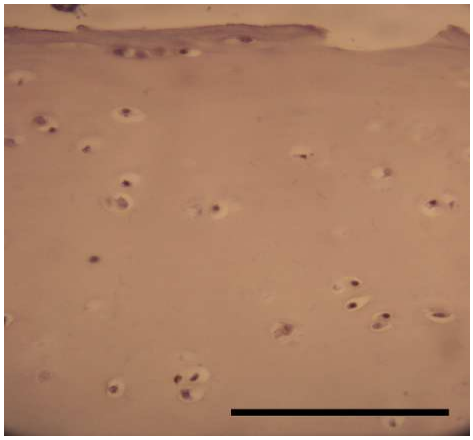

Fig. 80 #381: Sample after 70% strain at day 5. Scale bar 100 µm

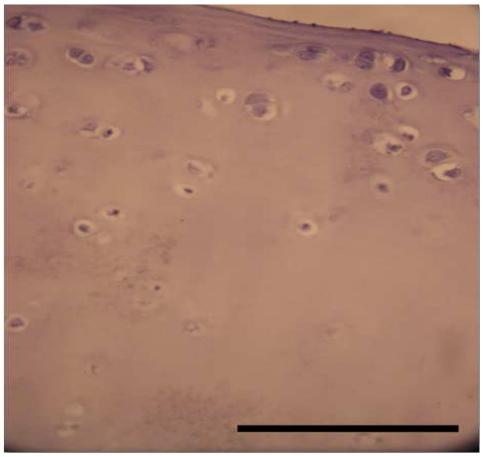

Fig. 79 #381: Negative control. Scale bar 100 µm

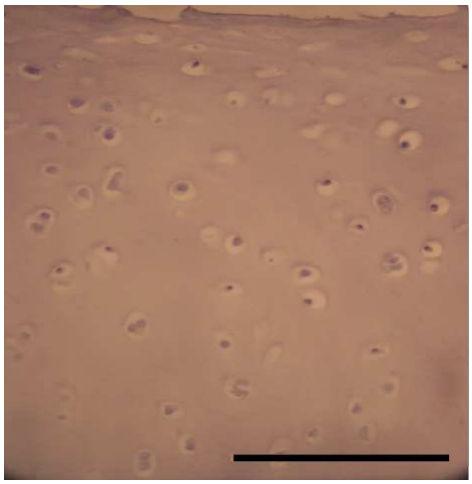

Fig. 82 #383: 80% strain day 5. Only very few apoptotic nuclei can be suspected, Scale bar 100 µm

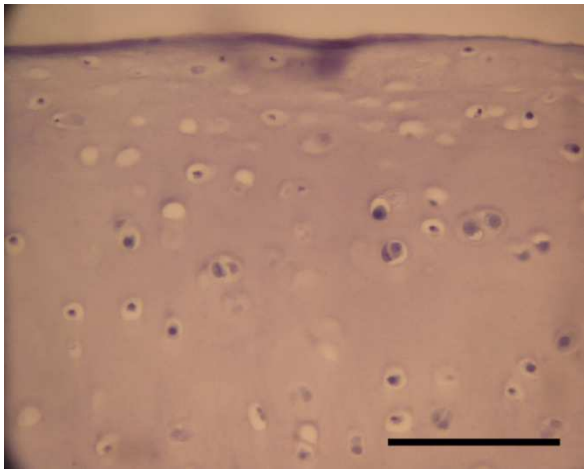

Fig. 81 #383: Negative control slide. Scale bar 100 µm

4.3.3 Results ISOL Assay

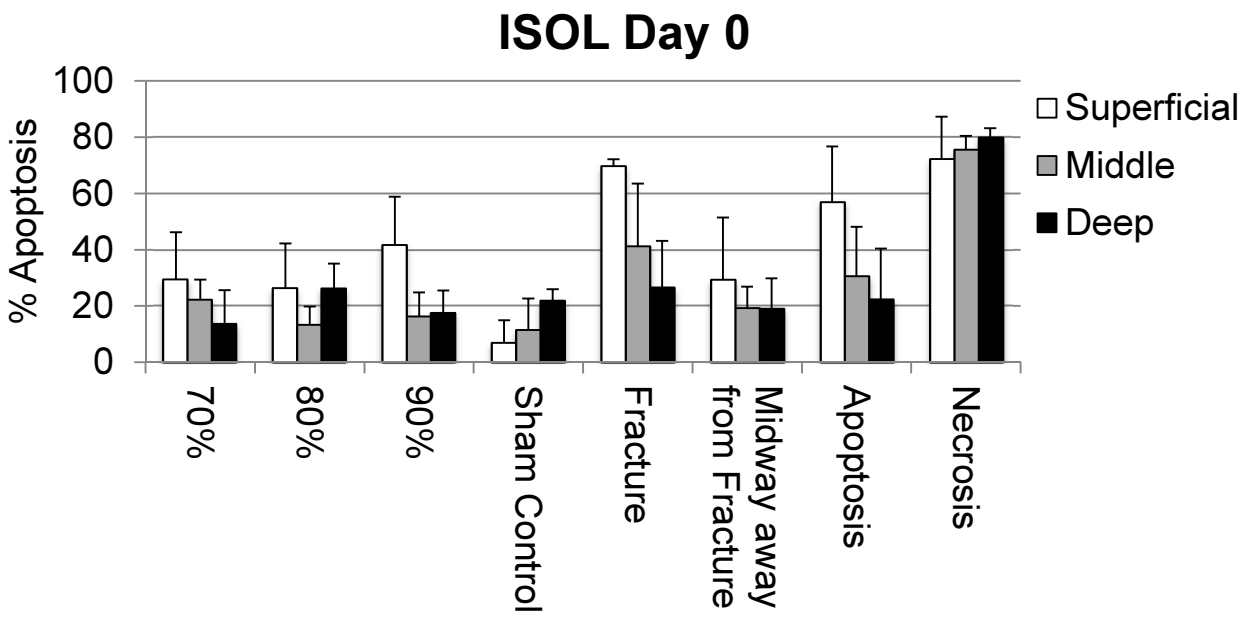

Fig. 83 Results of ISOL assay at day 0.

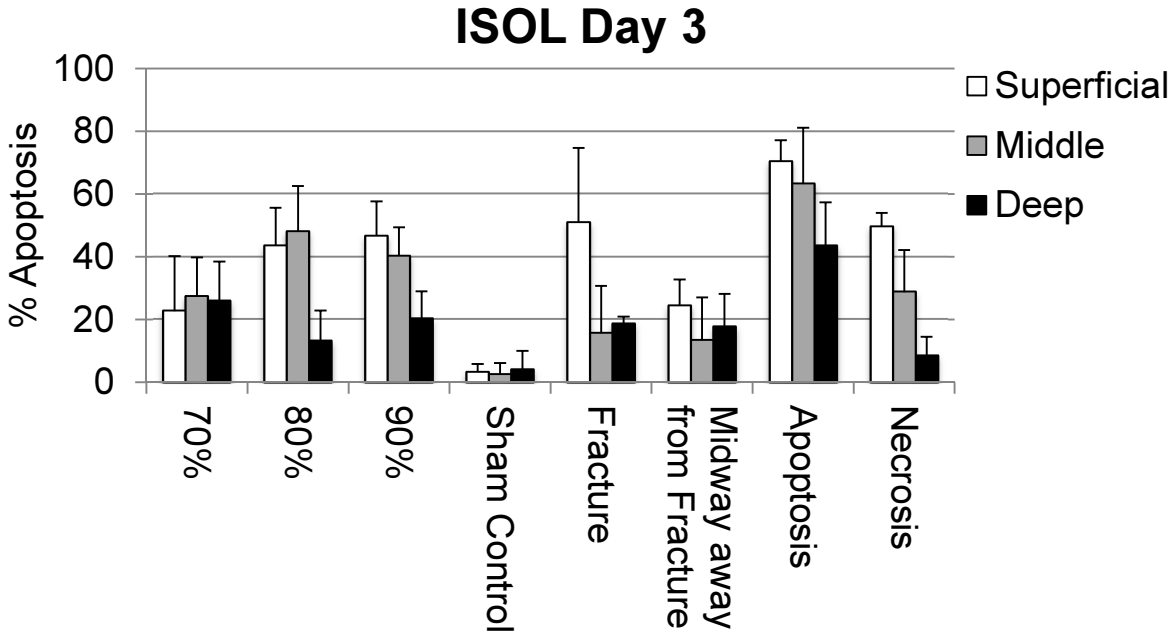

Fig. 84 Results of ISOL assay at day 3.

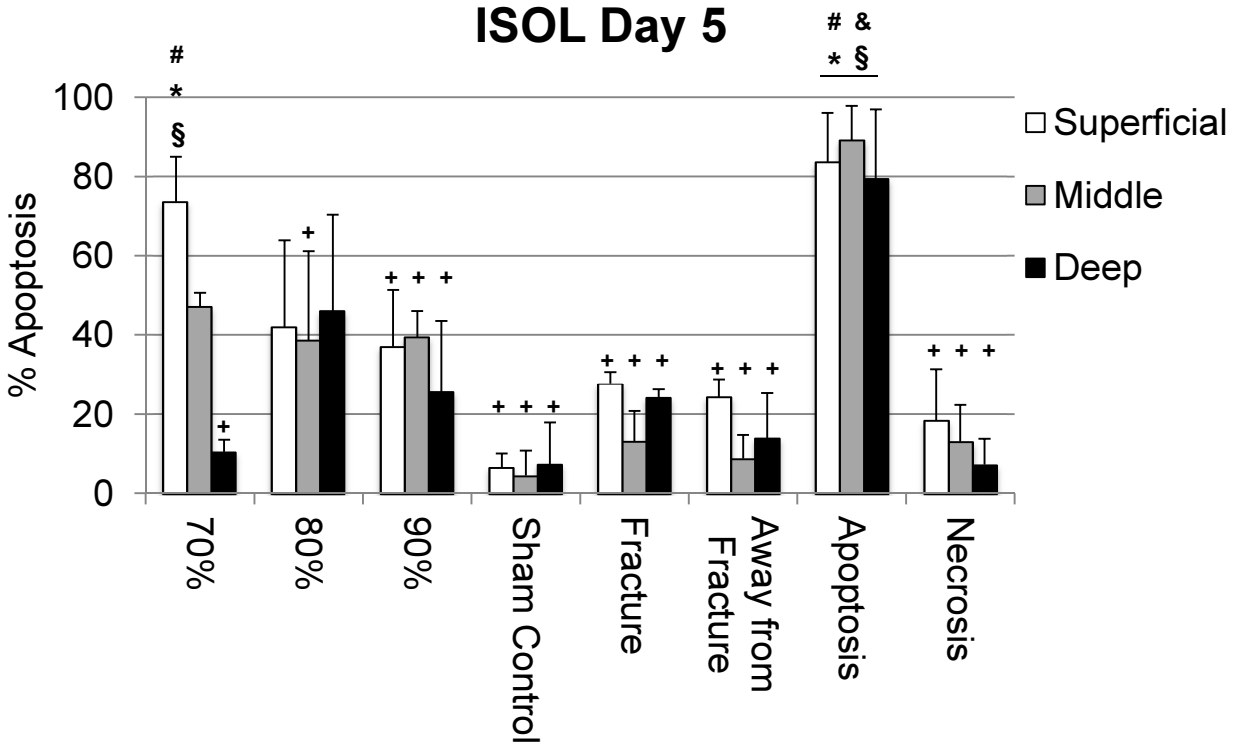

Fig. 85 Results of ISOL assay at day 5. (# indicates statistically significant differences from sham controls; *indicates statistically significant differences from necrosis; + indicates statistically significant differences from apoptosis, & indicates statistically significant difference from fractured edge, § indicates statistically significant difference from midway between fracture and outer edge) (Stolberg-Stolberg 2013 [203]).

As with the TUNEL assay, ISOL days 0 (Fig. 83) and ISOL day 3 (Fig. 84) did not show a significant difference between the apoptotic and necrotic control samples.
“At day 5 (Fig. 85), apoptotic controls demonstrated significantly higher levels of apoptosis than sham controls ($p \leq 0.000032$). Additionally, levels of apoptosis in necrotic controls were similar to sham controls ($p=1$) and significantly lower than the apoptotic controls ($p \leq 0.000053$). Based on these validation results of the ISOL detection method for identifying apoptosis in osteochondral tissue, data from day 5 is presented for all loading conditions”(Stolberg-Stolberg 2013 [203]).

“At 70% strain, the superficial zone had significantly higher levels of apoptosis than the sham and necrotic controls ($p \leq 0.0027$). The middle zone showed no statistical differences to controls, and the deep zone was had significantly lower levels of apoptosis to only the apoptotic control ($p \leq 0.00003$). Compared to other loading conditions, 70% strain had significantly more apoptosis than the fractured cores in

regions of the superficial zone located midway away from fracture (p≤0.0023)"(Stolberg-Stolberg 2013 [203]).

"At 80% strain, the levels of apoptosis were similar to sham and necrotic cores (p≥0.444). The only significant difference was found in the middle zone, which had significantly lower levels of apoptotic cells than the apoptotic controls (p≤0.0036). At 90% strain, all cartilage zones had significantly less apoptosis than the apoptotic controls (p≤0.018) and showed no significant differences to any other group"(Stolberg-Stolberg 2013 [203]).

"In the fractured cores, apoptosis at the fracture edges was significantly less compared to the apoptotic controls in all cartilage zones (p≤0.0033) and showed no significant differences to any other group. Away from the fracture at the midpoint between fracture and outer edge, all cartilage zones showed significantly less apoptotic cells than the apoptotic control (p≤0.0004), and the superficial zone had significantly less apoptosis than 70% strain (p≤0.0023)" (Stolberg-Stolberg 2013 [203]).

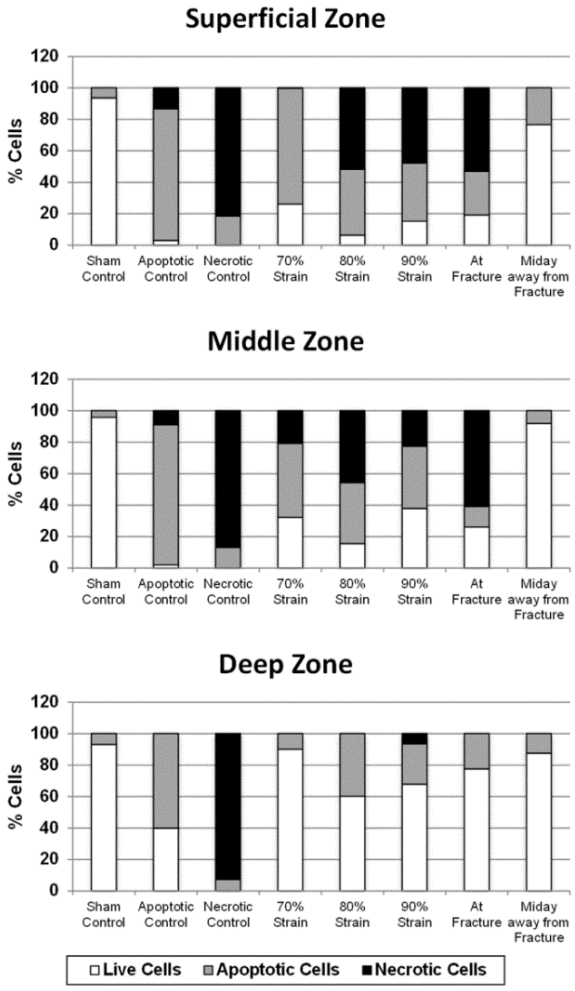

Fig. 86 Relative percentage of live, apoptotic, and necrotic cells at day 5. 70% low-strain blunt impact lead to predominantly apoptosis whereas 80% and greater high-strain blunt impact and fracture caused predominantly necrosis in addition to apoptosis (Stolberg-Stolberg 2013 [203]).

4.3.4 ISOL Images

Blue Channel • To-Pro-3-Iodide • Counterstain: Stains all nuclei	Green Channel: • FAM labeled oligonucleotide • Binds to DNase II induced DNA strand break with 5'-OH hangovers
Red Channel: • CR-590 labeled oligonucleotide • Binds to DNase I induced DNA strand breaks with 5'-PO_4 hangovers	All Channels: • Overlay of all three channels

Table 9 Allocation of channels and stainings.

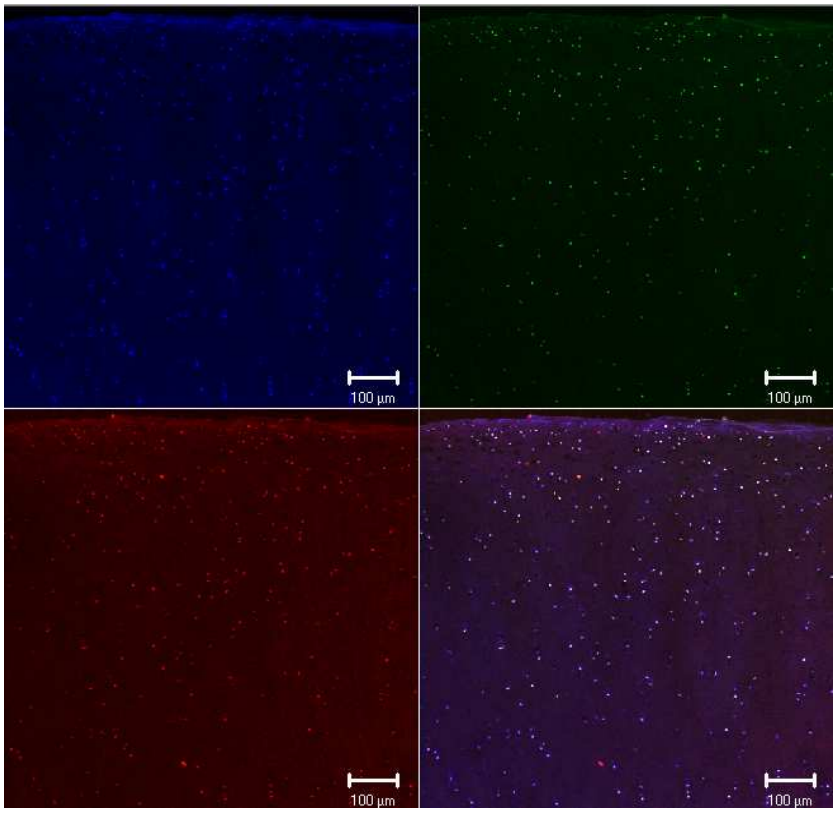

Fig. 87 #482: With staurosporine treated apoptotic control at day 5. Red and green channel show plenty of positively stained apoptotic cells.

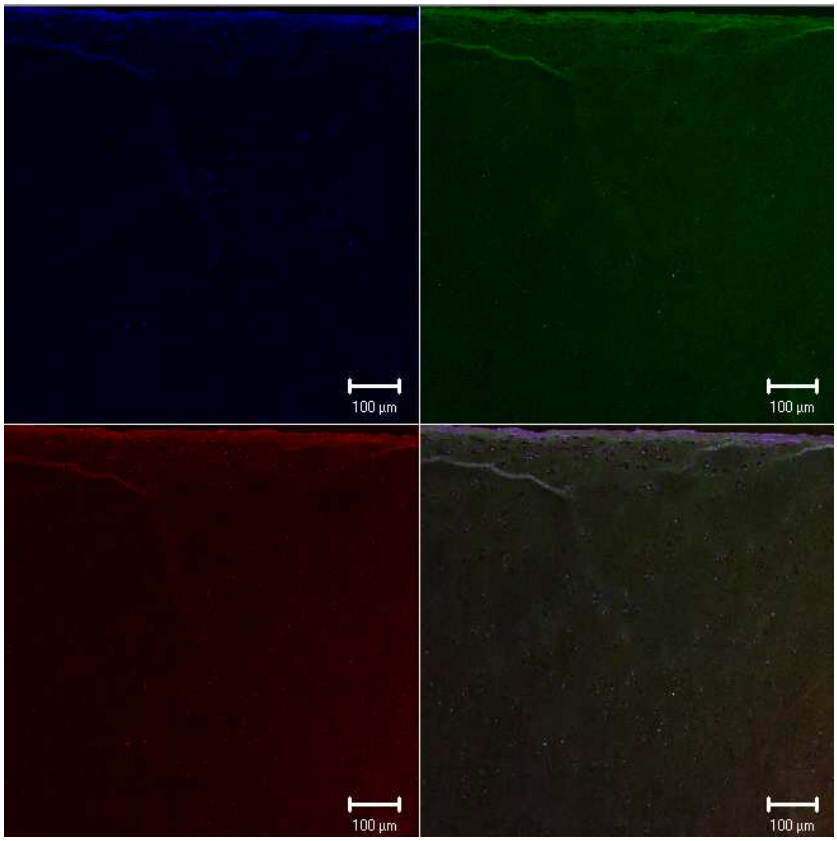

Fig. 88 #408: Frozen negative control slide showing nuclei only in the blue channel. None of the nuclei stained for apoptosis in the green or red channel.

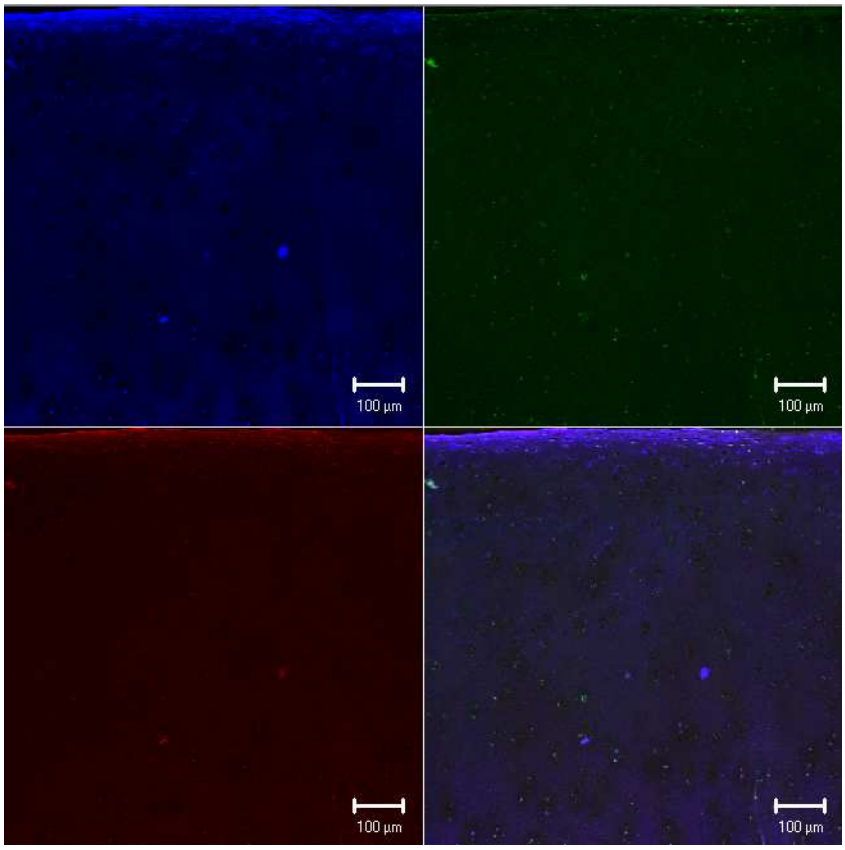

Fig. 89 #364: Sham control slide from day 5. Only very few apoptotic nuclei can be discovered in the middle and deep zone.

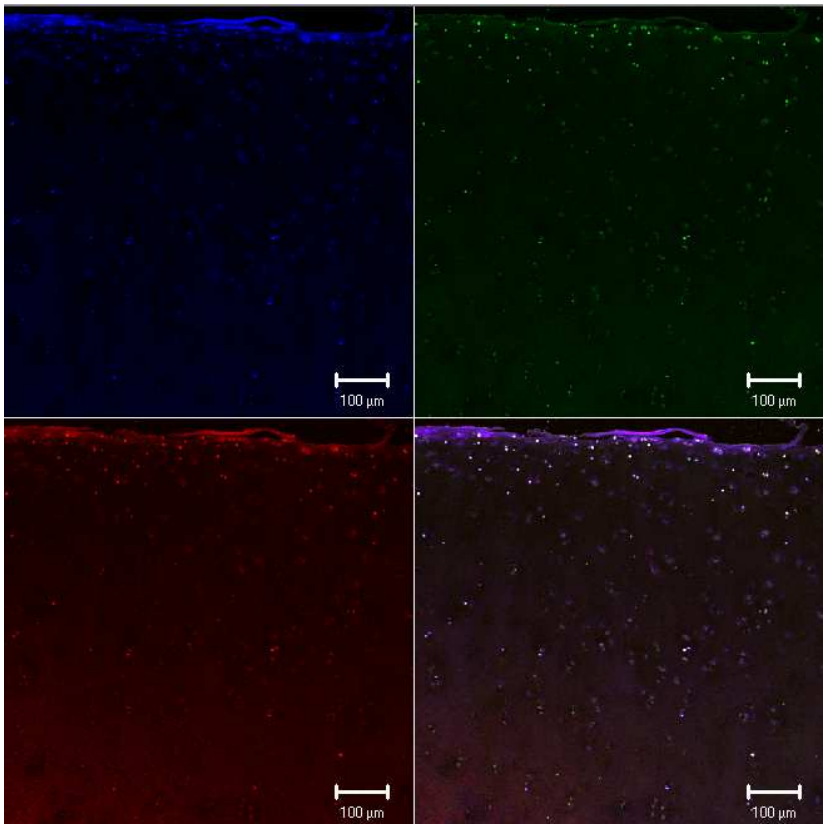

Fig. 90 #381: Sample after 70% strain at day 5. Plenty of apoptotic cells can be seen in the superficial layer.

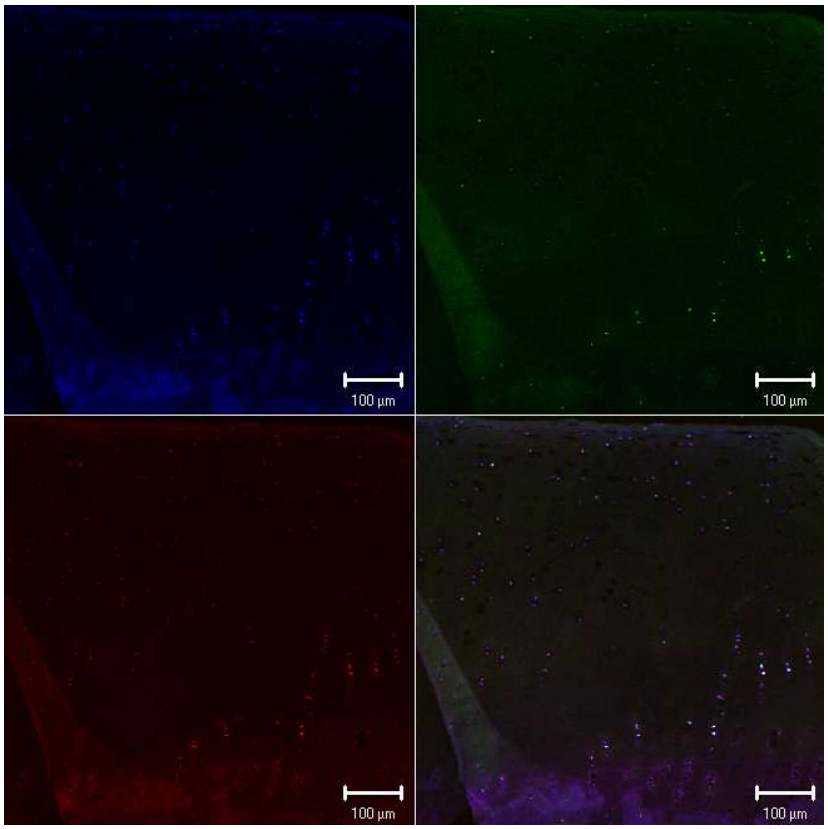

Fig. 91 #416: Sample after 80% strain at day 5. Only very few apoptotic nuclei can be discovered throughout all layers.

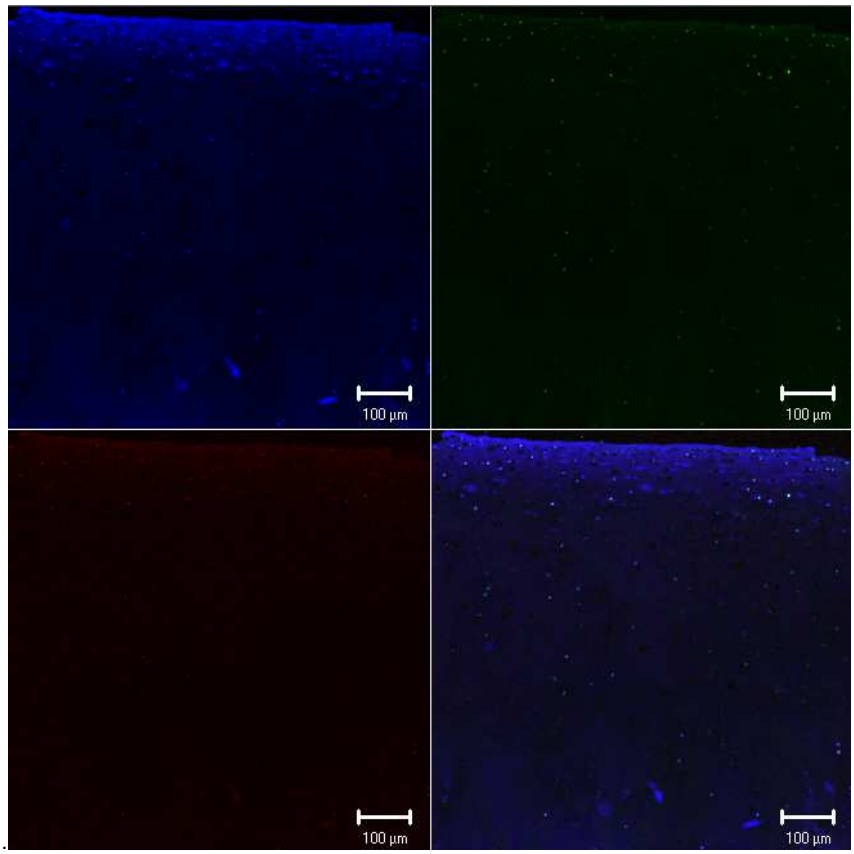

Fig. 92 #455: Sample after 90% strain at day 5. As with 80% strain only very few apoptotic nuclei can be discovered.

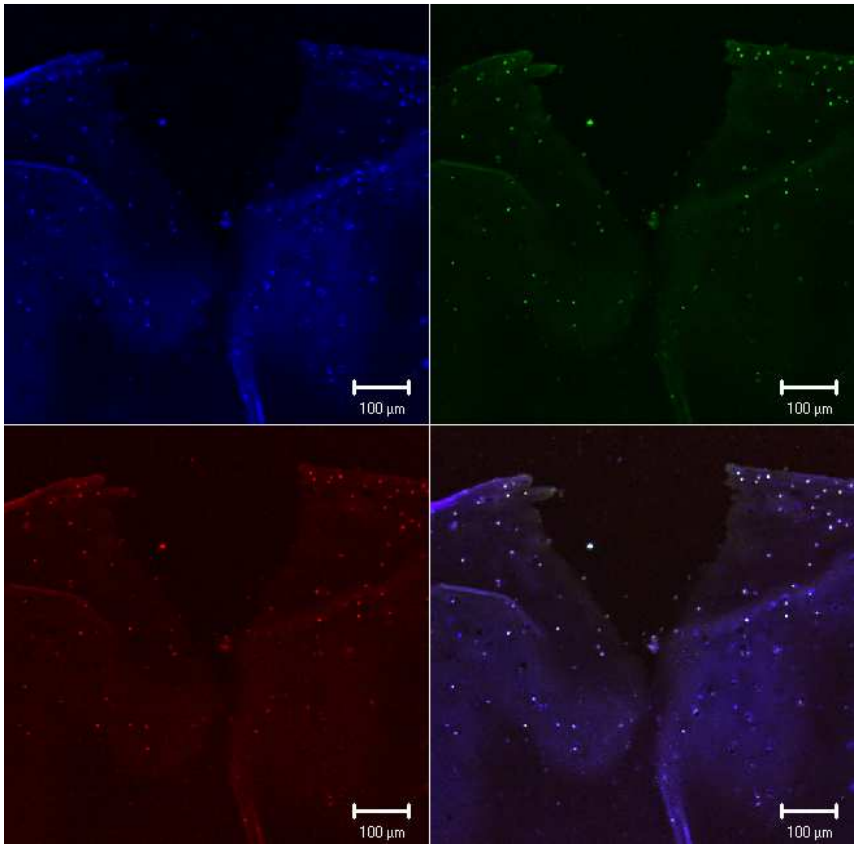

Fig. 93 #481: Sample after fracture. Several apoptotic nuclei can be seen along the fracture edge.

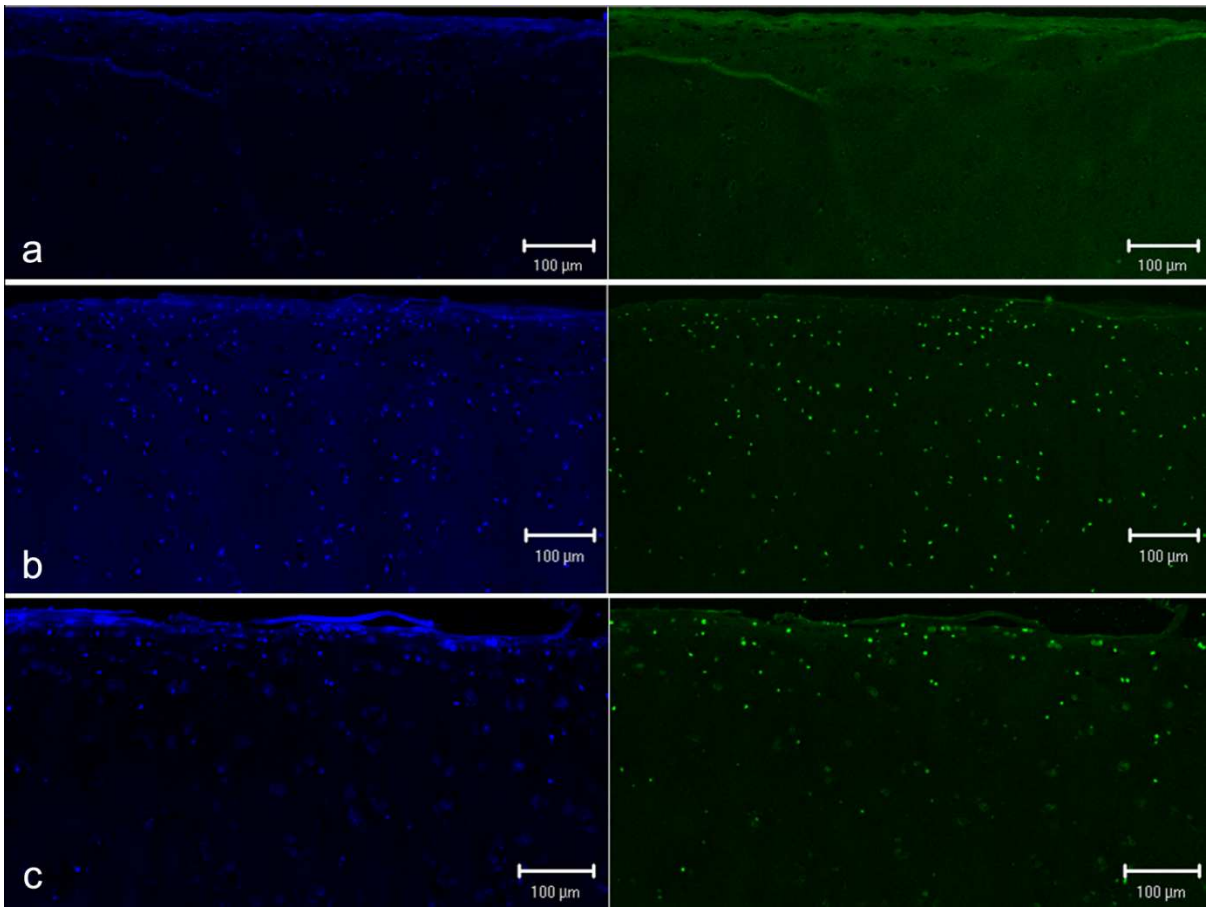

Fig. 94 Apoptotic Cell death was confirmed by ISOL. The blue channel on the left shows all nuclei within the section. The green channel on the right shows apoptotic nuclei. Only very few positively stained chondrocytes could be found in the necrotic control samples (a). The apoptotic control samples treated with staurosporine (b) showed similar fluorescence as the superficial layer of samples loaded with 70% strain blunt impact (c) (Stolberg-Stolberg 2013 [203]).

4.4 Degradative Changes after Blunt Loading and Fracture

4.4.1 S-GAG Release

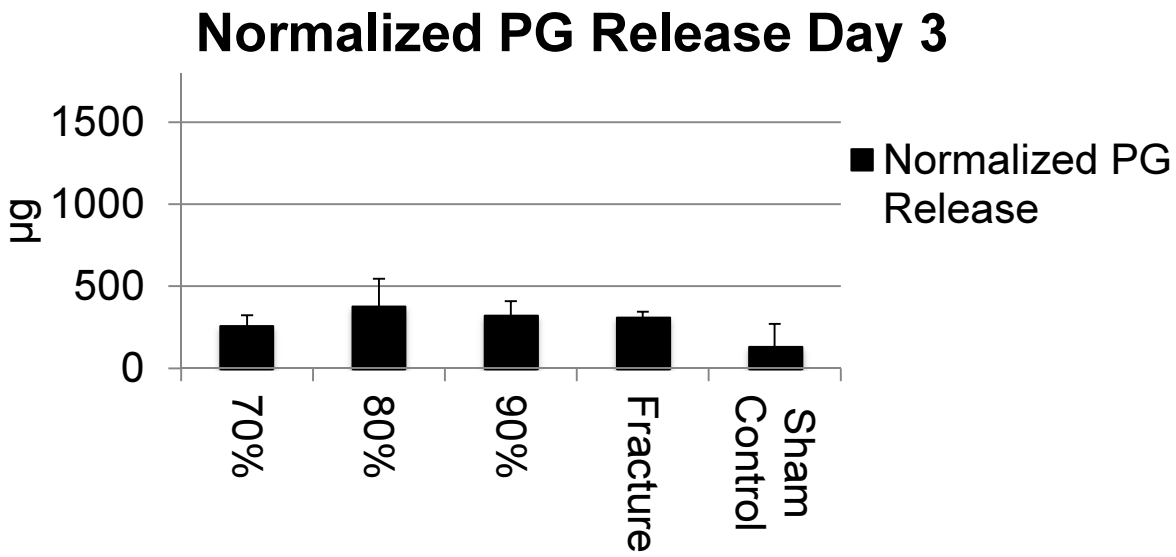

Fig. 95 Results of DMB assay showing PG release until day 3.

There was not statistical significant difference in PG release at day 3.

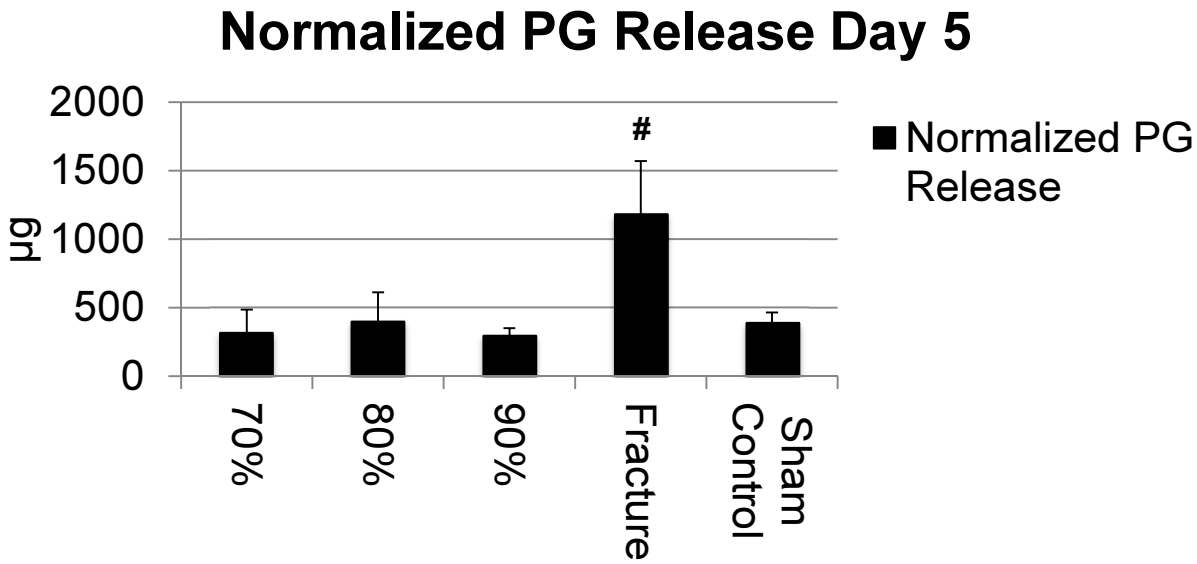

Fig. 96 Results of DMB assay showing PG release until day 5.

Significant differences could only be found at day 5 (Fig. 96). Fractured cores were significantly different to all other groups ($p=0.344$). No difference could be detected between any other group ($p \geq 0.344$).

4.4.2 Enzyme Activity

4.4.2.1 MMP Activity

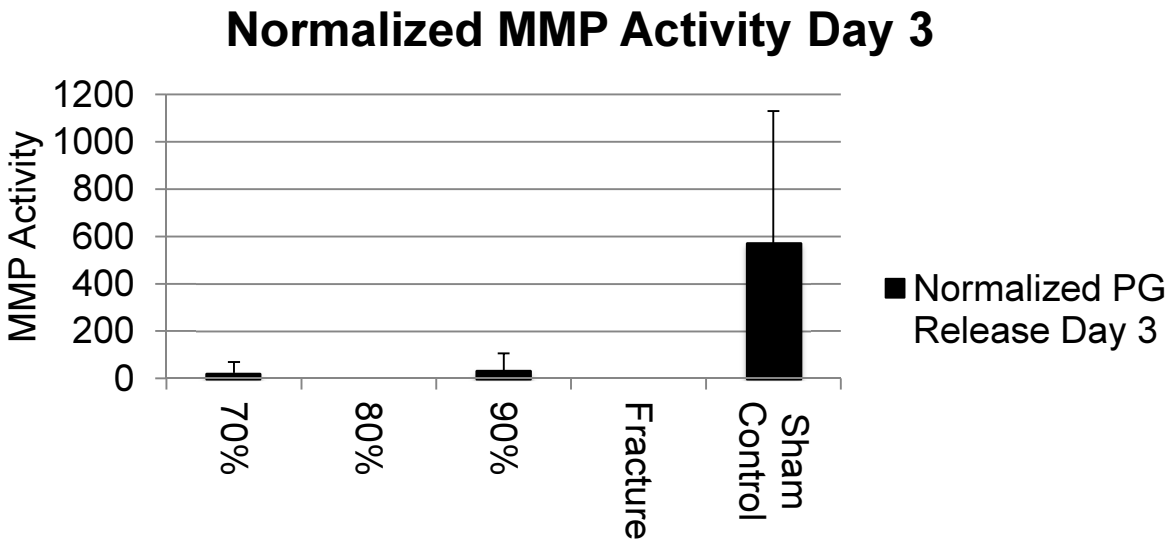

Fig. 97 MMP activity measured at day 3.

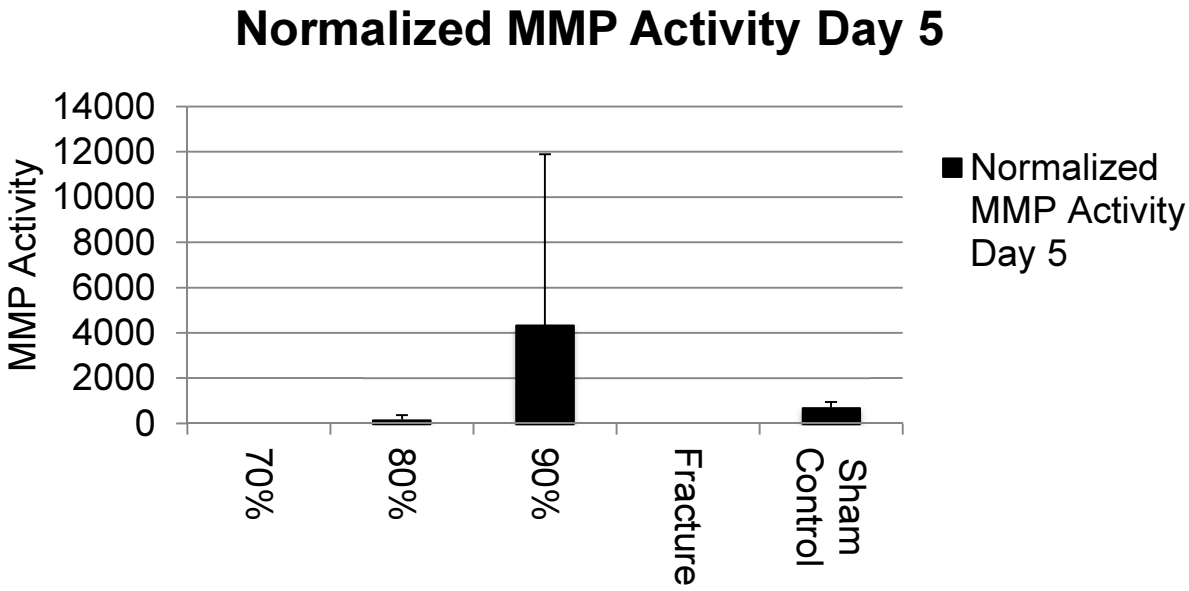

Fig. 98 MMP activity measured at day 5.

There are no meaningful and statistical differences in MMP activity between any group at day 3 (Fig. 97) or at day 5 (Fig. 98).

4.4.2.2 Aggrecanase Activity

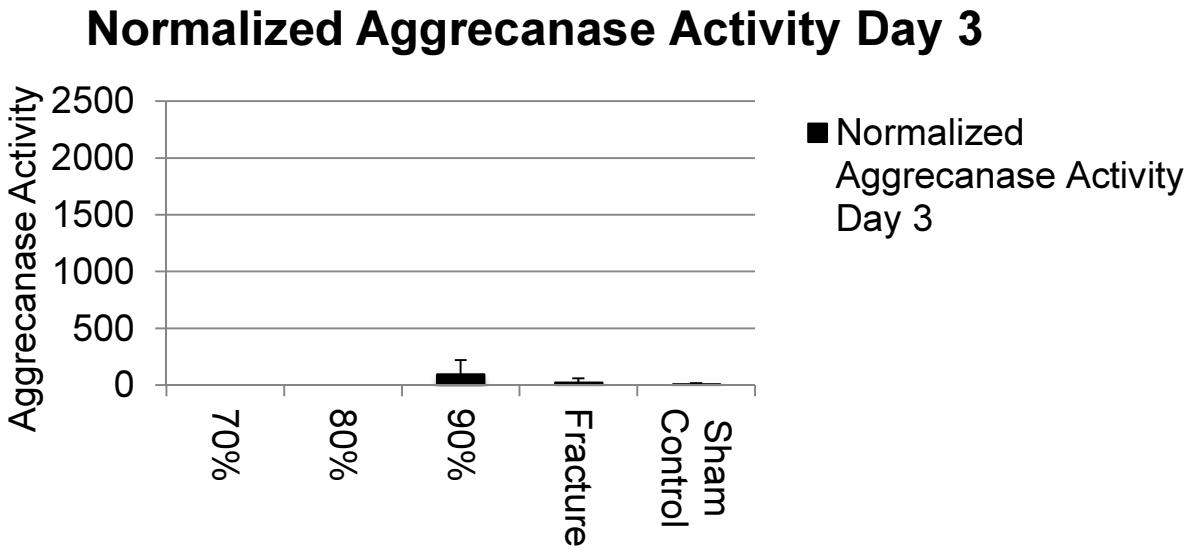

Fig. 99 Normalized aggrecanase activity at day 3.

Aggrecanase activity at day 3 did not show any statistical significant difference (Fig. 99).

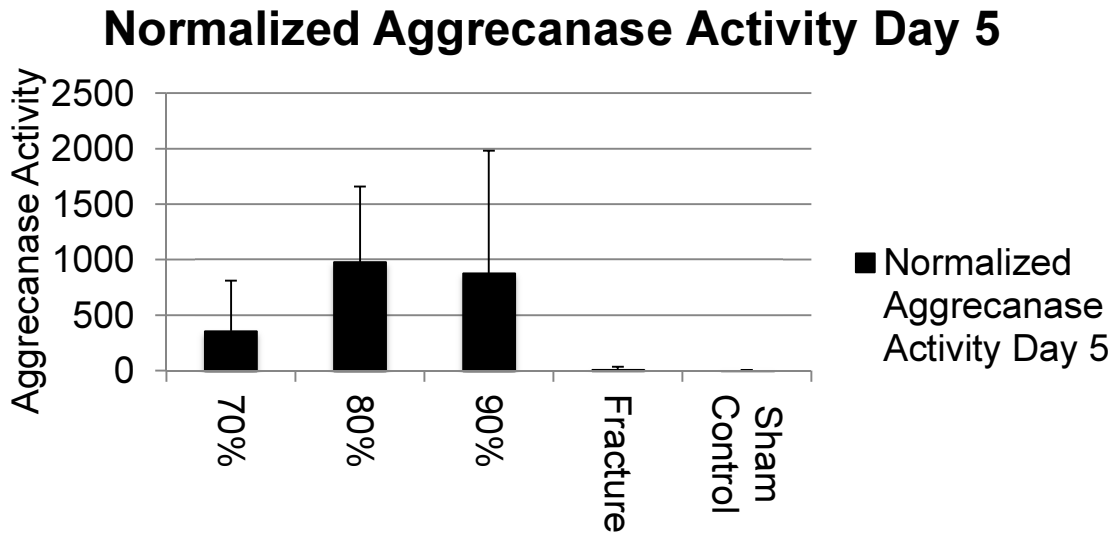

Fig. 100 Normalized aggrecanase activity at day 5.

Again, there was no statistical significant difference in aggrecanase activity at day 5 between any group (Fig. 100).

4.5 Characterization of Inflammatory Changes in PTA

4.5.1 Results Conditioned Media Experiment

4.5.1.1 Total S-GAG Release

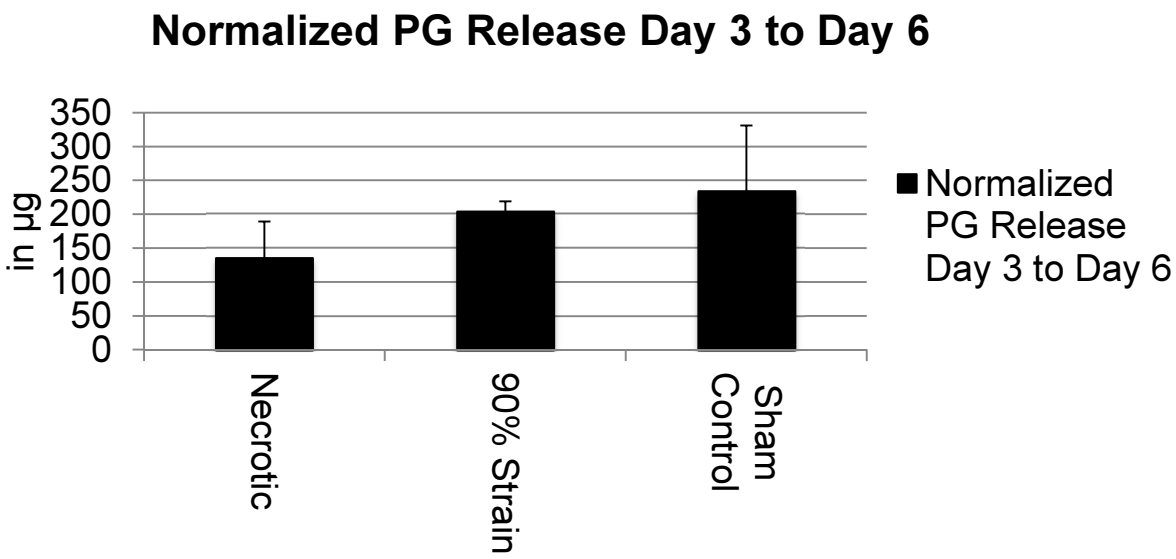

Fig. 101 Results normalized PG release between day 3 and 6.

4.5.1.2 Total NOX Release

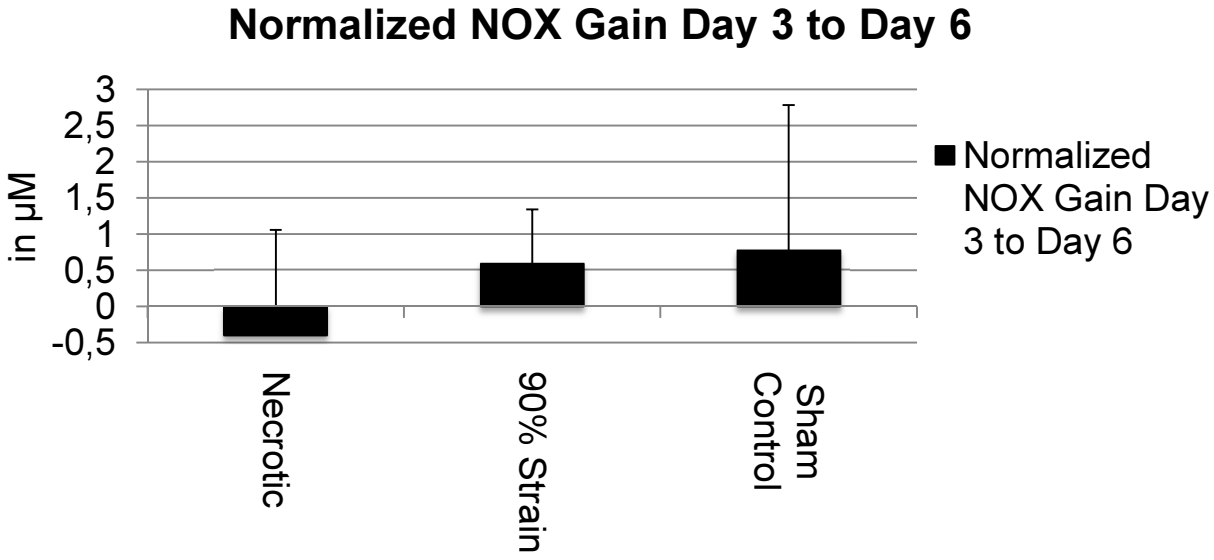

Fig. 102 Results of normalized NOX gain between day 3 and 6

Despite promising preliminary trail runs neither the total PG release (Fig. 101) nor the the NOX release (Fig. 102) showed significant and meaningful results. Based on this data no further testing was done.

4.5.2 Results PicoGreen Assay

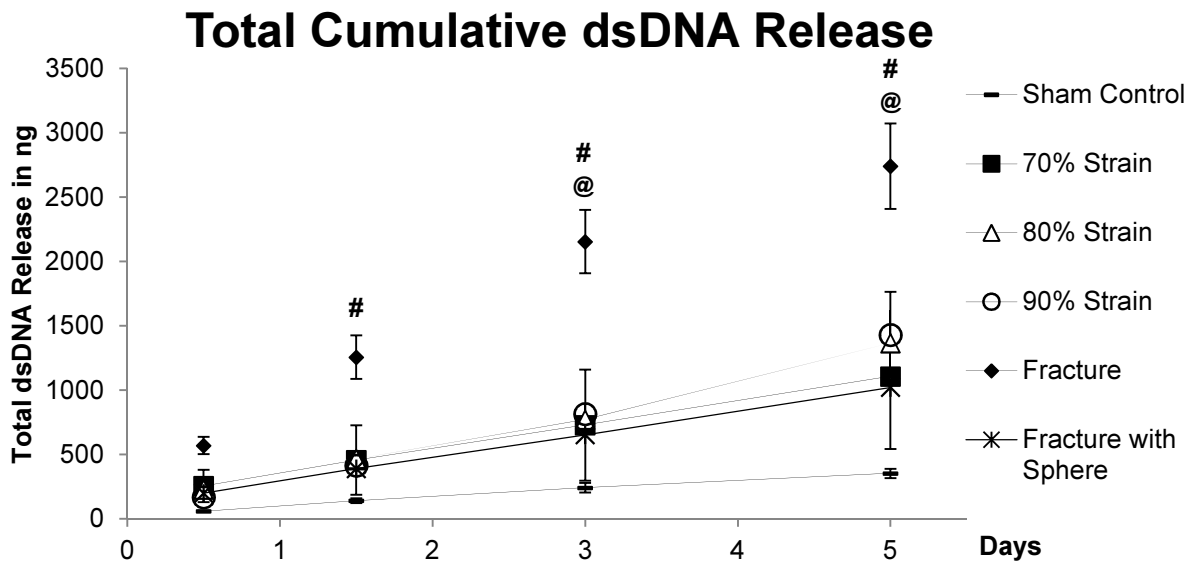

Fig. 103 Results normalized dsDNA release per 24 h (Stolberg-Stolberg 2013 [203]).

“Total release of dsDNA into the media increased with culture time for all groups. For the blunt impact loading conditions, 70% strain did not significantly increase the dsDNA release compared to sham controls at all time points. At 80% and 90% strain, again no statistically significant increases in dsDNA release were observed, although there was a trend in higher release at day 5 compared to sham controls ($p \geq 0.052$). For fractured cores, dsDNA release was significantly increased compared to sham controls at 1.5, 3 and 5 days ($p \leq 0.0447$). In comparing loading conditions, no statistically significant differences in dsDNA release were observed between 70%, 80% and 90% strain. However, fractured cores demonstrated greater release of dsDNA compared to the blunt loading conditions of 70%, 80% and 90% strain at days 3 and 5 ($p \leq 0.022$). Compared to samples that were bluntly fractured with the sphere, conventionally fractured cores released significantly mor dsDNA at days 3 and 5 ($p \leq 0.011$) (Fig. 103)” (Stolberg-Stolberg 2013 [203]).

4.5.3 Results HEK 293 Reporter Cells

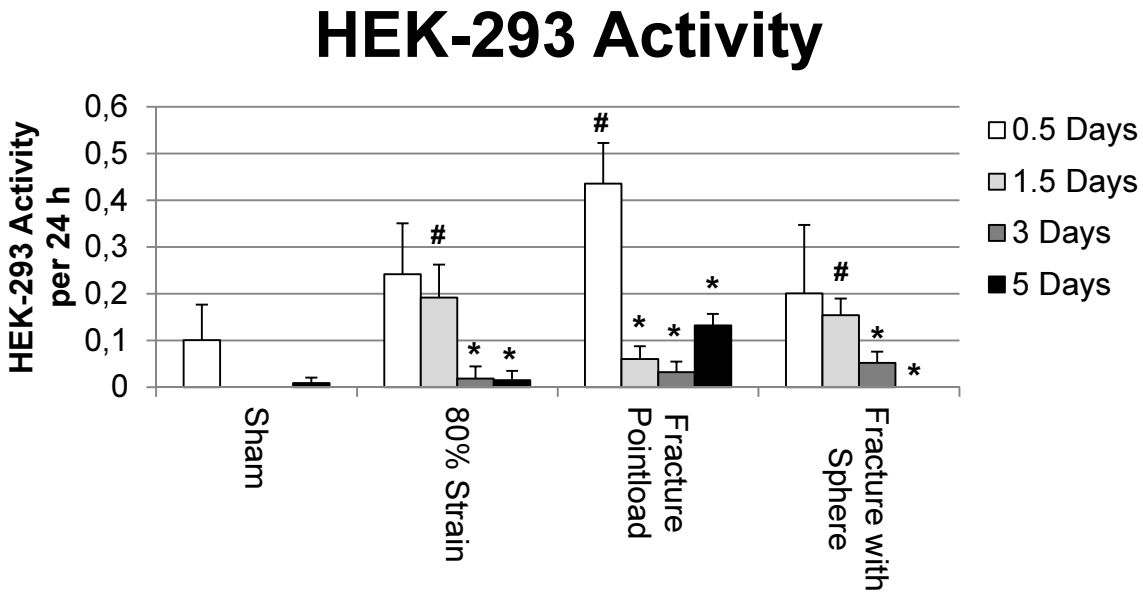

Fig. 104 Normalized HEK-293 cell activity per 24 h (* indicates significant difference to day 0, # indicates significant difference to sham control).

The background color change from blank media was subtracted from all samples and negative values were set to 0. Again, all data was converted to activity per 24 h.

With 80% strain, cores released significantly less TLR-4 ligand at days 3 ($p \leq 0.00133$) and 5 ($p \leq 0.00115$) than at day 0. Furthermore, there was significantly more release at 1.5 days than in the sham control ($p \leq 0.0155$).

Cores that were fractured with the point-load showed significantly more activity than sham controls at 0.5 days ($p \leq 0.00397$). Additionally, there was significantly less activity at days 1.5 ($p \leq 0.000187$), 3 ($p \leq 0.000089$) and 5 ($p \leq 0.0028$) than at day 0.5.

Cores that were fractured bluntly with the sphere showed significantly more activity than sham controls at day 3 ($p \leq 0.038$). At days 3 ($p \leq 0.0224$) and 4 ($p \leq 0.0033$) there was significantly less activity than at day 0 (Fig. 104).

4.5.4 Results Ramos Blue Reporter Cells

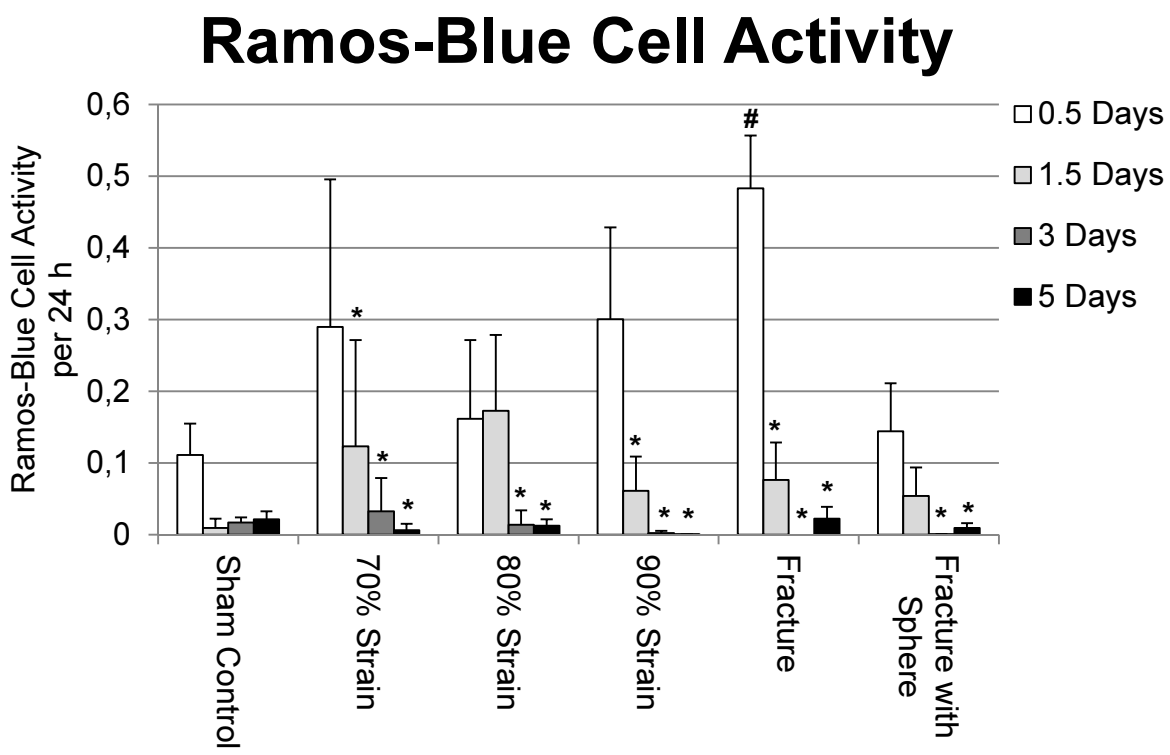

Fig. 105 Normalized Ramos Blue Activity per 24 h (# indicates significant difference to sham, * indicates significant difference to day 0) (Stolberg-Stolberg 2013 [203]).

The background color change from blank media was subtracted from all samples and negative values were set to 0. Again, all data was converted to Activity per 24 h. “The trends in Ramos-Blue cell activity were similar for blunt loading of 70%, 80% and 90% strain (Figure 8). With 70% strain, no significant differences were found in Ramos-Blue cell activity compared to sham controls or other loading conditions. However, there was significantly more activity at 0.5 days compared to all other time points ($p \leq 0.007$). With 80% strain, there was also no significant differences compared to sham controls, and Ramos-Blue cell activity was greater at 0.5 days compared to day 3 ($p \leq 0.016$) and day 5 ($p \leq 0.015$). Similarly, with 90% strain, again, no significant differences were found compared to sham controls or other loading conditions, and activity was significantly greater at 0.5 days compared to all other time points ($p \leq 0.00022$). With fracture, Ramos-Blue cell activity was significantly greater at 0.5 days than sham controls ($p \leq 0.0039$) and 80% strain ($p \leq 0.0095$). Similar to other loading conditions, at 90% strain activity was significantly greater at 0.5 days compared to all other time points ($p \leq 0.0000001$). As with 70%, 80% and 90% strain, cores that were fractured bluntly with the sphere, there was no significant difference to sham controls. At 0.5 days there was significantly more Ramos-Blue Cell activity than at day 3 ($p \leq 0.0183$) and at day 5 ($p \leq 0.027$)” (Stolberg-Stolberg 2013 [203]).

5 Discussion

5.1 Post-traumatic Arthritis

Post-traumatic arthritis (PTA) is frequently found after intra-articular fracture of weight-bearing joints (Furman 2006 [74]). The percentage of patients that will develop PTA varies depending on the site and severity of fracture. For hip, knee and ankle magnitudes of 24%, 31% and 24% (respectively) were reported (Day 2001 [60], Giannoudis 2005 [78], Matta 1996 [144], Rademakers 2007 [175], Stufkens 2010 [206]). It is estimated that around 5.6 million individuals suffer from PTA in US America alone. This accounts for 12% of all patients that suffer from osteoarthritis (OA). Additionally, 11.8 billion USD are lost due to direct and indirect costs from PTA. This is 0.156% of the total US health care costs. Furthermore, PTA is described as a very painful and debilitating disease that is commonly found in young patents (Brown 2006 [40]).

So far, open reduction and internal fixation is the prevailing treatment that can be offered to patients with intra-articular fracture. Accurate anatomical cartilage alignment is supposed to prevent fragment incongruity and instability and has been stated to be the most important factor in preventing PTA (Stufkens 2010 [206]). Despite all efforts made to improve surgical techniques the prevalence of PTA still remains high (Anderson 2011 [12]). This suggests that other factors must be crucial for the onset and progression of PTA.

Many factors that might contribute to PTA's pathogenesis have been put forward. Soft tissue injuries might lead to joint instability. For example, meniscal and ligamental damage in the knee might cause peak stresses at non-physiologic points and might initiate cartilage erosion (Roos 1995 [186], Setton 1994 [194]). Systemic comorbidities also affect the healing potential after intra-articular fracture. Diabetes, obesity and systemic inflammatory up-regulation after polytrauma can cause delayed healing (DeLong 2004 [62], Louer 2012 [134]). Certain genetic intervals are also associated with OA susceptibility. Genes coding for cytokine and enzyme regulation, PG and collagen expression are most likely involved (Furman 2006 [74], Loughlin 2005 [135], Spector 2004 [201]).

Most important for this study, however, are the fracture mechanism, chondrocyte viability and inflammation.

5.2 Impact Loading

Impact loading and intra-articular fractures represent complex injury patterns. The arcade-like collagen meshwork might be disrupted, proteoglycans are liberated, the subchondral layer might be fractured, bone marrow might enter the joint and joints function by its biomechanical integrity might be disturbed.

“Various *in vitro* models have been used to simulate supra-physiologic cartilage loading (Table 10). Closed joint fracture models showed a time dependent progression of chondrocyte death and an increase of MMP and AGG expression after intra-articular fracture (Backus 2010 [19], Tochigi 2011 [215]). Cartilage explants have mostly been loaded using drop towers. Surface fissuring and a stress dependent loss of chondrocyte viability have been reported (Jeffrey 1995 [108], Repo 1977 [181]). Cell death was described particularly along tissue cracks (Lewis 2003 [127]). Cartilage loading at different strain rates showed that high strain rates as present during cartilage injury cause cell death mainly in the superficial layer (Morel 2004 [151]). Low strain loading has been associated with a high percentage of apoptotic cell death (D'Lima 2001 [56]). The exact relation between loading condition and chondrocyte response, however, is not well understood ”(Stolberg-Stolberg 2013 [203]).

Our Model: As a recent report showed, our cartilage from 2-3 year old pigs can be considered as skeletally mature and sufficient differentiation in structure and mechanical properties can be expected between the superficial, middle and deep cartilage layer (Rieppo 2009 [183]). In order to reduce cartilage injury during explant extraction, subchondral bone was left attached to the cartilage. The cartilage-bone compound might have led to some inaccuracy during loading. To minimize this, bone thickness was kept constantly at 1 mm (Finlay 1978 [69]). Test loadings of bone confirmed that only around 10% of the total strain is absorbed by the bone. However, we also decided to use osteochondral explants for several other reasons: Firstly, our objective was to create an *in vitro* cartilage injury model which resembles as closely as possible a real trauma situation. Radial confinement by the bone is an important feature of cartilage trauma. Secondly, removing the bone would have created another injury zone. This potentially could have affected chondrocyte viability, apoptosis analysis, dsDNA release and release of DAMPs.

The blunt impact model provides a new experimental set-up which applies compression only. Many previous studies loaded the explants with a certain amounts of stress, whereas we chose total strain as this is a more functional parameter. In this way viability outcomes are less affected by explant specific mechanical

properties such as PG-content and collagen density.

“The fracture model proved to be a realistic intra-articular fracture simulation as we compared results to our previous closed joint injury study (Backus 2010 [19]). However, it is difficult to mechanically define the fracture as the indenter applied a very centered stress and some sample bending could be observed during loading. Additionally, it was not possible to determine the amount of strain applied as fractures occurred more than once and stepwise during each loading. For the blunt impact groups some inaccuracy in viability could also be caused by minor surface fissuring at 80% and 90% strain” (Stolberg-Stolberg 2013 [203]).

Future aspects of loading apparatus and clinical application: The blunt impact model is an exact simulation of purely compressive stress on articular cartilage. As osteochondral cylinders were used for this model cartilage was radially confined only by the bone. Depending on joint and site of injury cartilage during *in vivo* trauma might be more confined by the surrounding tissues. This might lead to higher interstitial pressure and chondrocytes might resist higher stresses (Soltz 2000 [199]). Thus, in order to improve understanding of blunt trauma-mechanisms and to design advanced *in vitro* models radial cartilage expansion particularly at edges of cartilage has to be defined *in vivo*.

Our fracture model reliably induced fractures with the application of 90% strain. The exact strain when fracture occurred varied throughout all samples. The fracture pattern also varied between samples. The reasons might be minor differences in bone height, differences in composition and structure of bone and cartilage between different animals including water, PG and collagen content and variation of sample positioning under the indenter. However, there seems to be little room to improve sample preparation. Additional knowledge of fracture mechanism can rather be achieved by application of indenters with different sphere-diameters or even angular devices. Personal observations showed that small diameter indenters lead to a more focused stress and thus sample bending with high tensional forces at the articular surface and early fracture. In this setting only the chondrocytes directly underneath the indenter might be subjected to high strains. Indenters with bigger diameters might induce injuries that resemble our blunt impact model with little sample bending, late fracture and more even distribution of compression throughout the sample. Additionally to numerous loading apparatus described in the appendix, altering the size of the indenter might be a novel approach to understand trauma mechanisms (Kruzic 2009 [118]). Conferred to real life situations this could explain different cartilage injury patterns e.g. after a dash-board injury and injury with a sharp object. This could potentially affect treatment of patients as depending on trauma mechanism different amounts of apoptotic and necrotic cell chondrocyte death can be expected.

5.3 Chondrocyte Viability

The exact role of chondrocyte death in the progression of PTA remains unclear. In articular cartilage chondrocytes are the only cells and are responsible for maintenance of the ECM. It would over simplify the pathogenesis of OA to state that loss of chondrocytes automatically causes OA. As a matter of fact many studies provide evidence for cell death at end stage OA but few dead chondrocytes are found in early OA (Carlo 2008 [45]).

In terms of PTA, “varying amounts of both chondrocyte necrosis and apoptosis have been detected in analysis of waste osteochondral fragments after surgical restoration (Hembree 2007 [97], Kim 2002 [112], Murray 2004 [157]). *In vivo* experiments showed a correlation between the level of impact stress and apoptosis. The absolute percentage of apoptotic chondrocytes varied greatly amongst different detection methods (Borrelli 2003 [38])“ (Stolberg-Stolberg 2013 [203]).

Viability: The fluorescence live/dead assay has been used in countless studies and has been confirmed to be a reliable method to assess viability (Backus 2010 [19], Guilak 1994 [82], Hembree 2007 [97]). The blunt impact model showed a decrease of viability with increasing strain. Furthermore, there was a gradient of cell death with high numbers of dead cells in the surface area and a decreasing number of dead cells in the middle and deep zone. This is consistent with previous studies and bulk modulus and deformation measurements of the different cartilage layers (Chahine 2007 [48], Guilak 1995 [83], Schinagl 1997 [191]).

Apoptosis: The live/dead assay used in this study marks cells green which exhibit an intact plasma membrane as it can be observed in live and early apoptotic cells. The red dye binds to nucleic acid of necrotic or late stage apoptotic cells. Bearing this in mind, a significant decrease of viability over time could only be detected in the superficial and middle zone of the 70% strain blunt impact group, indicating apoptosis. Apoptotic chondrocyte death was confirmed by ISOL in the superficial zone only at day 5. Our apoptotic and necrotic controls showed that ISOL is not able to detect apoptosis at earlier stages. Alternatively, the TUNEL assay is frequently used for apoptosis detection in cartilage. Test runs of the TUNEL assay on our control samples confirmed already reported problems such as high false positive detection of necrotic cells (Chen 2001 [51], Levin 2001 [126]). This study indicates that low strain blunt impact leads to chondrocyte apoptosis whereas high strain blunt impact leads to immediate cell death. Due to the inhomogeneity of cartilage it is not clear how much a chondrocyte must be strained to undergo apoptosis and where the threshold to necrosis is. Derived from our model we can state that 70% strain blunt impact induces apoptosis in the superficial layer and probably in the middle layer.

Strains ≥80% induce mainly necrosis. This is consistent with other studies (D'Lima 2001 [56], Rundell 2005 [187]). Our experiment, however, is the first study that confirms this in one model.

Future aspects of viability and clinical application: Physiologic cartilage strains may vary widely by location within the joint and activity. Previous studies have estimated strains ranging from 6% to 30% (Armstrong 1979 [16], Coleman [53], Van de Velde 2009 [222]). The strains utilized in our unconfined compression models are significantly higher than the reported levels of strain. Our data demonstrated that different loading scenarios induced different types of chondrocyte death. However, our loading model may not fully mimic loading occurring *in situ*. To utilize this knowledge strains occurring during real trauma situations have to be defined.

As stated previously, prevention of apoptotic chondrocyte death after mechanical trauma might be one way to delay or inhibit the onset of PTA (Anderson 2011 [12]). Various studies have been conducted to examine the potency of anti-apoptotic agents in articular cartilage (D'Lima 2001 [58], Hooiveld 2003 [101], Kim 2008 [113]). Positive effects of e.g. caspase-3 inhibitor and P 188 on cartilage structure after mechanical trauma haven been shown *ex vivo* (Garrido 2009 [75]). *In vivo* e.g. BMP-7 has cartilage protective properties (Hurtig 2009 [105]). Taking this data into account, in future it could be possible to apply anti-apoptotic drugs into the joint after mechanical trauma. Our data suggests that this could be particularly effective in low strain blunt impact ≤ 70% strain. Clinically it will be difficult to assess the strain cartilage has been exposed to. Thus, frequent injury mechanisms have to be better defined or a prophylactic application can be considered even after minor injuries.

“Mainly necrotic cell death along fracture edges has been shown in our model after intra-articular fracture. This stands in contrast to other studies (Hembree 2007 [97], Murray 2004 [157]). However, in these reports fracture mechanism has not been well defined although it might play a decisive role (also see future aspects of loading apparatus)” (Stolberg-Stolberg 2013 [203]).

Another barrier to clearly define role of apoptosis in PTA is the lack of reliable detection methods. Regarding cartilage, the TUNEL assay has broadly been used although apoptosis assessment can be subjective and false-high measurements of apoptosis have been reported (Chen 2001 [51], Levin 2001 [126]). Apoptosis is a time dependent process. Ultimately, enzymes break down cell organelles and nucleus content. The time point of apoptosis assessment varies greatly within the literature, and positive controls are not typically included. Some authors even state that 7-10 days after impact is the best time of apoptosis detection (Borrelli 2003 [38]). For our study we developed a new staining method using ApopTag® ISOL apoptosis detection kit together with a nuclear counterstain. The ISOL assay stains

dsDNA strand breaks that have been cut by DNAse I and II. A sufficient quantity of dsDNA strand breaks have to be present in order to obtain a strong visual signal. Due to this time dependence, few apoptotic cells were found at day 0. A gradual but not significant change took place until day 3 with significant changes at day 5. Personal observations and the use of necrotic and apoptotic controls confirmed its functionality. However, the same drawbacks of all immuno-stainings such as non-specific binding and manual cell counting also apply for this assay. Future work should scan for more accurate apoptosis detection methods or use more sensitive methods such as anti-caspase-3 antibodies or transmission electron microscopy (Borrelli 2006 [39]). Future work should also focus on factors that are released by apoptotic, necrotic cells or by brake down of the ECM. Understanding their origin will be crucial to inhibit inflammatory pathways.

5.4 Inflammation

Synovial inflammation is commonly found in early stage OA and is characterized by joint swelling, redness, heat and pain (Ayral 2005 [18], Benito 2005 [28]). The synovium is infiltrated by an increased number of synovial lining cells and immune cells such as macrophages, mast cells, T-, B-lymphocytes and plasma cells. Activated synovial cells, immune cells and chondrocytes produce large quantities of MMPs and ADAMTS (Sellam 2010 [193]). These proteolytic enzymes eventually degrade extracellular matrix macromolecules and cause a loss of cartilage's integrity and biomechanical strength (Cawston 2006 [47], Plaas 2007 [171], Rengel 2007 [180]). Pro-inflammatory cytokines act as soluble mediators and favor catabolic activities in articular cartilage (Goldring 2004 [79], Goldring 2004 [80]). Cytokine production is associated with immune cells. Their cellular source in OA, however, is still uncertain (de Lange-Brokaar 2012 [61]). The pro-inflammatory cytokines Il-1β and TNF-α are found in elevated concentration in synovial fluid and joint tissue of OA patients.

The acute response of chondrocytes to mechanical injury includes PG, MMP and AGG release (Backus 2010 [19]). Cartilage inflammation and degradation is perpetuated by cytokines such as IL-1, TNF-α, NOX and prostaglandin E_2 (Furman 2006 [74]). However, DAMPs such as endogenous DNA and other cartilage matrix breakdown products might also contribute to the inflammatory pathway (Bianchi 2007 [30]). TLRs are PRRs and allow cells to recognize various harmful stimuli, such as DAMPs. TLRs are constitutively expressed by immune cells and protect tissues from pathogens, but have also been identified in chondrocytes (Bobacz 2007 [37], Scanzello [190]). Activation of TLRs upon ligand binding results in signaling that

activates the transcription factors NF-κB and AP-1 and leads to the production of inflammatory cytokines and chemokines. Immune reporter cells express TLRs, are responsive to NF-κB inducers, and can be used to assess the immunogenic activity of the degradation products produced following injury to cartilage. The release of DAMPs from cartilage following injury and fracture provides a potential mechanism by which cartilage injury and chondrocyte death may promote a pro-inflammatory immunogenic response in the joint.

Several attempts were made to characterize the inflammatory and degradative potential of bluntly loaded and fractured cartilage. First of all, media from viability testing was analyzed for MMPs, AGGs and PGs. Only a significant increase of PG release from fractured cores on day 5 was consistent with our previous study (Backus 2010 [19]). An increase in MMP and AGG activity could not be confirmed. Secondly, sham cores were treated with conditioned media from mechanically treated explants. A similar effect as known from conditioned media of chondrogenic induction of mesenchymal stem cells could not be observed (Liu 2012 [130]). Conditioned media did not significantly change PG, NOX, MMP or AGG production of sham cores (*MMP and AGG Activity data not shown*). It is not clear whether the absence of inflammatory response was caused by a concentration of inflammatory inductors which was too low, or if the time points of media harvest were unfavorable, or if the presence of synovial lining and macrophages is indispensable for an increase of the above mentioned markers (Vieira-Sousa 2011 [225]). Consequently, the protocol was changed and samples were cultured in only 1 ml SFM and all media was removed and replaced at days 0.5, 1.5, 3 and 5. Analysis of media from fractured cores has been shown to consistently contain significantly more dsDNA and cause significantly more Ramos-Blue and HEK-293 cell activity compared to sham controls.

“Analysis of dsDNA release to assess the magnitude of cell death has been used in the past in a variety of studies (Bicknell 1995 [33], Tran 2008 [219]). In our experiments, quantification of total dsDNA release has been shown to be a reliable method of evaluating cartilage damage. Both apoptosis and necrosis result in dsDNA release (van der Vaart 2007 [223]). The amount of cell death might correlate with the dsDNA release. However, dsDNA data has to be interpreted carefully as apoptotic and necrotic cells may release dsDNA at different timepoints. Furthermore, it is not clear to what extent increased dsDNA, S-GAGs, and DAMP release is caused by cell lysis, a change in chondrocyte’s metabolism or by the augmented cartilage surface area after fracture. Comparing viability data and dsDNA release after fracture indicates that tissue and cells debris can diffuse far easier into the surrounding media. The increased cartilage surface area after fracture may enhance the release of cell debris and inflammatory molecules from the cartilage into the surrounding

media. Not only will fractured surfaces decrease the distance for molecules to diffuse to reach the media, it may also allow molecules to bypass the surface zone, which due to its anisotropic structure may slow down diffusion of molecules from cartilage into the media (Leddy 2006 [125]). This leads to an early peak of potential inflammatory mediators after intra-articular fracture and maybe to an onset of PTA. Additionally, media from fractured blunt impact cores did not contain significantly more dsDNA nor did it cause increased Ramos Blue Cell activity. This finding suggests that early fracture of the subchondral bone might also have a protective effect on the cartilage" (Stolberg-Stolberg 2013 [203]).

"Our model has successfully been used to examine the release of TLR ligands after intra-articular fracture. A wide array of TLRs is expressed on the outer membrane of Ramos-Blue Cells. A significant increase of activity from Ramos Blue reporter cells that have been cultured in media from fractured cores indicates the potential for an augmented immuno-induction through DAMPs and cartilage debris. As already confirmed for osteoarthritic cartilage, chondrocytes themselves can express complementary TLRs (Bobacz 2007 [37], Kim 2006 [111]). Furthermore, macrophages in the synovial lining can be activated by TLRs which might contribute to joint inflammation (Scanzello [190]). As one possible ligand we examined dsDNA release after loading (Takeda 2007 [209]). Again, significantly higher dsDNA release of fractured explants has been detected and might contribute to increased Ramos Blue Cell activity at 12 h. At 36 h, day 3 and day 5, however, dsDNA released remained high whereas Ramos Blue Cell activity returned to almost 0. This finding indicates that other ligands might play a decisive role or that another compound such as HMGB1 or immune complexes can alter the immunostimulatory activity of dsDNA. DNA and antiDNA, for example, can stimulate production of cytokines such as INF-γ. Other immune-complexes might allow the internalization of DNA and thus the interaction with endogenous receptors such as TLR-9. HMGB1 might also enhance other cytokines and act as DNA carrier into the cell (Pisetsky 2007 [170], Yanai 2011 [234]). However, in our experiment we were only able to show that loaded cartilage releases ligands that bind to one or more of the TLR-2, 3, 7, 8 and 9. It is not clear what effect they will have *in* vivo on the TLRs of chondrocytes, macrophages or other immune-stimulatory cells. Furthermore, it is still unclear to what extent inflammation contributes to the development of PTA (Furman 2006 [74])" (Stolberg-Stolberg 2013 [203]).

Only TLR-4 is expressed on the surface of HEK-293 cells. A similar pattern of activity as for Ramos-Blue cells has been found. This is of particular interest because proteins such as HA, fibronectin, HMGB1 and heat shock proteins act as ligands. Furthermore, TLR-4 is expressed in chondrocytes (Bobacz 2007 [37]). This suggests that no further immune-cell activation might be necessary to initiate inflammation in chondrocytes.

Future aspects of Toll-like receptors: Recently, the activation of Toll-like receptors in OA joints became a branch of intensive research (Scanzello [190]). Primary osteoarthritis is defined by fibrillation, fissuring and erosion of articular cartilage (Muehleman 1997 [156]). DAMPs and endogenous ligands are liberated during disease progress and as our experiment shows at a peak after intra-articular fracture in PTA. Understanding the inflammatory potency of TLR-activation, defining key-ligands and –receptors and research for TLR-inhibition will be crucial to evaluate importance and potential of OA treatment via TLRs. Our results show that our model is well suited to examine TLR-ligands that are released by cartilage.

5.5 Conclusion

The objective of this study was to develop *in vitro* model systems of cartilage impact with and without articular fracture. We hypothesized that impact loading would cause chondrocyte death whose mechanism depends on the magnitude of strain, and that the induction of an articular fracture would result in greater cell death. Using these model systems, we evaluated the effects of strain magnitude with and without articular fracture on chondrocyte viability, apoptosis, and the release of dsDNA. Media from these culture explants was examined post-impact for its ability to induce an immunostimulatory response via NF-κB activity using Ramos-Blue reporter cells.

This study provides novel *in vitro* models of chondrocyte response to impact loading with or without articular fracture in an osteochondral explant. Both models result in significantly reduced chondrocyte viability. However, distinct differences in temporal and zonal viability were found. The results from our study indicate that there is a threshold: blunt impact of 70% cartilage strain induced a loss in viability that increased with time whereas higher strain blunt impact above 80% strain caused immediate cell death. Our results were confirmed with the ISOL apoptosis staining and are consistent with previous studies that blunt impact at the lower strains caused mainly apoptosis (D'Lima 2001 [57]). Our fracture model induced low chondrocyte viability throughout all layers along fracture edges with minimal loss of viability away from the fracture, consistent with previous studies (Backus 2010 [19], Tochigi 2011

[215]). Because chondrocyte necrosis and apoptosis are observed clinically following trauma, both models will help in examining the role of decreased chondrocyte viability on the progression of PTA (Hembree 2007 [97]).

A variety of inflammation markers have been analyzed to explain possible induction of inflammation after intra-articular fracture. A significant increase in PG could be observed in media from fractured samples as also shown in our previous study (Backus 2010 [19]). Furthermore, there was significantly more Ramos-Blue and HEK-cell activity induced by media from fractured samples, indicating the presence of TLR-ligands. As one possible ligand dsDNA was analyzed. Throughout all time points, fractured cores released significantly more dsDNA than sham controls whereas Ramos-Blue and HEK-cells only showed a peak of activity at 0.5 days. This indicates that other ligands or immune-complexes that are only released *in vivo* play a crucial role for a continuous TLR-activity induction (Pisetsky 2007 [170]). Another explanation might be that only a high peak of immune activity as shown with fractured cores is able to start a general joint inflammation and the onset of PTA.

This study provides us with well-defined novel models of cartilage impact loading. Viability data and apoptosis staining indicate that low strain blunt impact leads to apoptosis whereas high strain blunt impact causes necrosis. Intra-articular fracture causes immediate chondrocyte death and leads to a peak release of inflammatory cell debris (Stolberg-Stolberg 2013 [203], Stolberg-Stolberg; Furman 2012 [204], Stolberg-Stolberg; Furman 2012 [205]).

6 Summary

Summary of the dissertation according to §6 Abs. 5 of the Promotionsordnung:

Post-traumatic arthritis (PTA) frequently develops after intra-articular fracture of weight bearing joints. Loss of cartilage viability and post-injury inflammation have both been implicated as possible contributing factors to PTA progression. In order to further investigate chondrocyte response to impact and fracture, we have developed a blunt impact model applying 70%, 80% or 90% surface-to-surface compressive strain with or without induction of an articular fracture in a cartilage explant model. Following mechanical loading, chondrocyte viability and apoptosis were assessed. Culture media were evaluated for the release of double-stranded DNA (dsDNA) and immunostimulatory activity via nuclear factor kappa B (NF-κB) activity in Toll-like receptor-expressing Ramos-Blue reporter cells. High compressive strains, with or without articular fracture, resulted in significantly reduced chondrocyte viability. Blunt impact at 70% strain induced a loss in viability over time through a combination of apoptosis and necrosis, whereas blunt impact above 80% strain caused predominantly necrosis. In the fracture model, a high level of primarily necrotic chondrocyte death occurred along the fracture edges. At sites away from the fracture, viability was not significantly different than controls. Interestingly, both dsDNA release and NF-κB activity in Ramos-Blue cells increased with blunt impact, but was only significantly increased in the media from fractured cores. This study indicates that the mechanism of trauma determines the type of chondrocyte death as well as the potential for post-injury inflammation.

7 Bibliography

1 Abramson, S. B. Osteoarthritis and nitric oxide. *Osteoarthritis Cartilage* **16 Suppl 2**, S15-20, doi:S1063-4584(08)60008-4 [pii]

10.1016/S1063-4584(08)60008-4 (2008).

2 Abramson, S. B. The role of COX-2 produced by cartilage in arthritis. *Osteoarthritis and Cartilage* **7**, 380-381 (1999).

3 Abramson, S. B., Attur, M. & Yazici, Y. Prospects for disease modification in osteoarthritis. *Nat Clin Pract Rheum* **2**, 304-312 (2006).

4 Adams, C. S. & Horton, W. E., Jr. Chondrocyte apoptosis increases with age in the articular cartilage of adult animals. *Anat Rec* **250**, 418-425, doi:10.1002/(SICI)1097-0185(199804)250:4<418::AID-AR4>3.0.CO;2-T [pii] (1998).

5 Agarwal, S., Deschner, J., Long, P., Verma, A., Hofman, C., Evans, C. H. & Piesc, N. Role of NF-kappa B transcription factors in antiinflammatory and proinflammatory actions of mechanical signals. *Arthritis Rheum.* **50**, 3541-3548, doi:10.1002/art.20601 (2004).

6 Ahmed, A. M., Burke, D. L. & Yu, A. INVITRO MEASUREMENT OF STATIC PRESSURE DISTRIBUTION IN SYNOVIAL JOINTS .2. RETROPATELLAR SURFACE. *J. Biomech. Eng.-Trans. ASME* **105**, 226-234 (1983).

7 Ahsan, T. & Sah, R. L. Biomechanics of integrative cartilage repair. *Osteoarthritis and Cartilage* **7**, 29-40 (1999).

8 Aizawa, T., Kon, T., Einhorn, T. A. & Gerstenfeld, L. C. Induction of apoptosis in chondrocytes by tumor necrosis factor-alpha. *Journal of Orthopaedic Research* **19**, 785-796 (2001).

9 Alaaeddine, N., Di Battista, J. A., Pelletier, J. P., Kiansa, K., Cloutier, J. M. & Martel-Pelletier, J. Inhibition of tumor necrosis factor alpha-induced prostaglandin E2 production by the antiinflammatory cytokines interleukin-4, interleukin-10, and interleukin-13 in osteoarthritic synovial fibroblasts: distinct targeting in the signaling pathways. *Arthritis Rheum* **42**, 710-718, doi:10.1002/1529-0131(199904)42:4<710::AID-ANR14>3.0.CO;2-4 (1999).

10 Amin, A. R., Di Cesare, P. E., Vyas, P., Attur, M., Tzeng, E., Billiar, T. R., Stuchin, S. A. & Abramson, S. B. The expression and regulation of nitric oxide synthase in human osteoarthritis-affected chondrocytes: evidence for up-regulated neuronal nitric oxide synthase. *J Exp Med* **182**, 2097-2102 (1995).

11 Amin, A. R., Marshall, P. J., Attur, M., Vyas, P., DiCesare, P. E., Stuchin, S. A., Rediske, J. & Abramson, S. B. Prostaglandin E(2) (PGE(2)) is an inflammatory component in osteoarthritis-affected cartilage: The yin-yang regulation of nitric oxide synthase and cyclooxygenase-2. *J Invest Med* **44**, A292-A292 (1996).

12 Anderson, D. D., Chubinskaya, S., Guilak, F., Martin, J. A., Oegema, T. R., Olson, S. A. & Buckwaltert, J. A. Post-Traumatic Osteoarthritis: Improved Understanding and Opportunities for Early Intervention. *Journal of Orthopaedic Research* **29**, 802-809, doi:10.1002/jor.21359 (2011).

13 Andersson, U. & Erlandsson-Harris, H. HMGB1 is a potent trigger of arthritis. *J Intern Med* **255**, 344-350, doi:1303 [pii] (2004).

14 Anghelina, M., Sjostrom, D., Perera, P., Nam, J., Knobloch, T. & Agarwal, S. Regulation of biomechanical signals by NF-kappaB transcription factors in chondrocytes. *Biorheology* **45**, 245-256 (2008).

15 Armstrong, C., Bahrani, A. & Gardner, D. In vitro measurement of articular cartilage deformations in the intact human hip joint under load. *J Bone Joint Surg Am* **61**, 744-755 (1979).

16 Armstrong, C. G., Bahrani, A. S. & Gardner, D. L. In vitro measurement of articular cartilage deformations in the intact human hip joint under load. *The Journal of bone and joint surgery. American volume* **61**, 744-755 (1979).

17 Ateshian, G. A. & Wang, H. A theoretical solution for the frictionless rolling contact of cylindrical biphasic articular cartilage layers - Reply. *Journal of Biomechanics* **30**, 99-99 (1997).
18 Ayral, X., Pickering, E. H., Woodworth, T. G., Mackillop, N. & Dougados, M. Synovitis: a potential predictive factor of structural progression of medial tibiofemoral knee osteoarthritis - results of a 1 year longitudinal arthroscopic study in 422 patients. *Osteoarthritis and Cartilage* **13**, 361-367, doi:10.1016/j.joca.2005.01.005 (2005).
19 Backus, J. D., Furman, B. D., Swimmer, T., Kent, C. L., McNulty, A. L., Defrate, L. E., Guilak, F. & Olson, S. A. Cartilage viability and catabolism in the intact porcine knee following transarticular impact loading with and without articular fracture. *J Orthop Res*, doi:10.1002/jor.21270 (2010).
20 Baeuerle, P. A. Pro-inflammatory signaling: last pieces in the NF-kappaB puzzle? *Curr Biol* **8**, R19-22, doi:S0960-9822(98)70010-7 [pii] (1998).
21 Baichwal, V. R. & Baeuerle, P. A. Activate NF-kappa B or die? *Curr Biol* **7**, R94-96, doi:S0960-9822(06)00046-7 [pii] (1997).
22 Baxevanis, A. D. & Landsman, D. The HMG-1 box protein family: classification and functional relationships. *Nucleic Acids Res* **23**, 1604-1613, doi:4s0775 [pii] (1995).
23 Bay-Jensen, A. C., Andersen, T. L., Tabassi, N. C. B., Kristensen, P. W., Kjaersgaard-Andersen, P., Sandell, L., Garnero, P. & Delaisse, J. M. Biochemical markers of type II collagen breakdown and synthesis are positioned at specific sites in human osteoarthritic knee cartilage. *Osteoarthritis and Cartilage* **16**, 615-623, doi:10.1016/j.joca.2007.09.006 (2008).
24 Beer, F. P. J., E. Russell JR. Mechanics of Materials. **Second Edition** (1992).
25 Beg, A. A. Endogenous ligands of Toll-like receptors: implications for regulating inflammatory and immune responses. *Trends in Immunology* **23**, 509-512, doi:Pii s1471-4906(02)02317-7

10.1016/s1471-4906(02)02317-7 (2002).
26 Bell, C. G., Walley, A. J. & Froguel, P. The genetics of human obesity. *Nature Reviews Genetics* **6**, 221-234, doi:10.1038/nrg1556 (2005).
27 Belmokhtar, C. A., Hillion, J. & Segal-Bendirdjian, E. Staurosporine induces apoptosis through both caspase-dependent and caspase-independent mechanisms. *Oncogene* **20**, 3354-3362, doi:10.1038/sj.onc.1204436 (2001).
28 Benito, M. J., Veale, D. J., Fitzgerald, O., van den Berg, W. B. & Bresnihan, B. Synovial tissue inflammation in early and late osteoarthritis. *Annals of the Rheumatic Diseases* **64**, 1263-1267, doi:10.1136/ard.2004.025270 (2005).
29 Bian, L., Lima, E. G., Angione, S. L., Ng, K. W., Williams, D. Y., Xu, D., Stoker, A. M., Cook, J. L., Ateshian, G. A. & Hung, C. T. Mechanical and biochemical characterization of cartilage explants in serum-free culture. *Journal of Biomechanics* **41**, 1153-1159 (2008).
30 Bianchi, M. E. DAMPs, PAMPs and alarmins: all we need to know about danger. *J Leukocyte Biol* **81**, 1-5, doi:10.1189/jlb.0306164 (2007).
31 Bianchi, M. E. & Agresti, A. HMG proteins: dynamic players in gene regulation and differentiation. *Curr Opin Genet Dev* **15**, 496-506, doi:S0959-437X(05)00137-1 [pii]

10.1016/j.gde.2005.08.007 (2005).
32 Bianchi, M. E., Beltrame, M. & Paonessa, G. Specific recognition of cruciform DNA by nuclear protein HMG1. *Science* **243**, 1056-1059 (1989).
33 Bicknell, G. R. & Cohen, G. M. CLEAVAGE OF DNA TO LARGE KILOBASE PAIR FRAGMENTS OCCURS IN SOME FORMS OF NECROSIS AS WELL AS APOPTOSIS. *Biochem Bioph Res Co* **207**, 40-47, doi:10.1006/bbrc.1995.1150 (1995).
34 Blanco, F. J., Guitian, R., Vazquez-Martul, E., de Toro, F. J. & Galdo, F. Osteoarthritis chondrocytes die by apoptosis - A possible pathway for osteoarthritis pathology. *Arthritis Rheum.* **41**, 284-289 (1998).
35 Blanco, F. J., Guitian, R., Vazquez-Martul, E., de Toro, F. J. & Galdo, F. Osteoarthritis chondrocytes die by apoptosis. A possible pathway for osteoarthritis pathology. *Arthritis Rheum* **41**, 284-289, doi:10.1002/1529-0131(199802)41:2<284::AID-ART12>3.0.CO;2-T (1998).

36 Blanco, F. J., Ochs, R. L., Schwarz, H. & Lotz, M. CHONDROCYTE APOPTOSIS INDUCED BY NITRIC-OXIDE. *Am. J. Pathol.* **146**, 75-85 (1995).
37 Bobacz, K., Sunk, I. G., Hofstaetter, J. G., Amoyo, L., Toma, C. D., Akira, S., Weichhart, T., Saemann, M. & Smolen, J. S. Toll-like receptors and chondrocytes - The lipopolysaccharide-induced decrease in cartilage matrix synthesis is dependent on the presence of Toll-like receptor 4 and antagonized by bone morphogenetic protein 7. *Arthritis Rheum.* **56**, 1880-1893, doi:10.1002/art.22637 (2007).
38 Borrelli, J., Tinsley, K., Ricci, W. M., Burns, M., Karl, I. E. & Hotchkiss, R. Induction of chondrocyte apoptosis following impact load. *Journal of Orthopaedic Trauma* **17**, 635-641 (2003).
39 Borrelli, J. J. Chondrocyte Apoptosis and Posttraumatic Arthrosis. *Journal of Orthopaedic Trauma* **20**, 726-731 710.1097/1001.bot.0000249882.0000277629.0000249885c (2006).
40 Brown, T. D., Johnston, R. C., Saltzman, C. L., Marsh, J. L. & Buckwalter, J. A. Posttraumatic osteoarthritis: a first estimate of incidence, prevalence, and burden of disease. *J Orthop Trauma* **20**, 739-744, doi:10.1097/01.bot.0000246468.80635.ef

00005131-200611000-00015 [pii] (2006).
41 Bucholz, R. W. H., James D. Fractures in Adults. **Volume 1**, 264 to 268 (2001).
42 Bullough, P. Orthopaedic Pathology. **4th Edition**, 239 to 362 (2004).
43 Camosso, M. E. & Marotti, G. The Mechanical Behavior of Articular Cartilage Under Compressive Stress. *J Bone Joint Surg Am* **44**, 699-709 (1962).
44 Campo, G. M., Avenoso, A., Campo, S., D'Ascola, A., Nastasi, G. & Calatroni, A. Molecular size hyaluronan differently modulates toll-like receptor-4 in LPS-induced inflammation in mouse chondrocytes. *Biochimie* **92**, 204-215, doi:10.1016/j.biochi.2009.10.006 (2010).
45 Carlo, M., Jr. & Loeser, R. Cell death in osteoarthritis. *Curr Rheumatol Rep* **10**, 37-42, doi:10.1007/s11926-008-0007-8 (2008).
46 Caron, J. P., Fernandes, J. C., MartellPelletier, J., Tardif, G., Mineau, F., Geng, C. S. & Pelletier, J. P. Chondroprotective effect of intraarticular injections of interleukin-1 receptor antagonist in experimental osteoarthritis - Suppression of collagenase-1 expression. *Arthritis Rheum.* **39**, 1535-1544 (1996).
47 Cawston, T. E. & Wilson, A. J. Understanding the role of tissue degrading enzymes and their inhibitors in development and disease. *Best Practice & Research in Clinical Rheumatology* **20**, 983-1002, doi:10.1016/j.berh.2006.06.007 (2006).
48 Chahine, N. O., Ateshian, G. A. & Hung, C. T. The effect of finite compressive strain on chondrocyte viability in statically loaded bovine articular cartilage. *Biomechanics and Modeling in Mechanobiology* **6**, 103-111, doi:10.1007/s10237-006-0041-2 (2007).
49 Chahine, N. O., Ateshian, G. A. & Hung, C. T. The effect of finite compressive strain on chondrocyte viability in statically loaded bovine articular cartilage. *Biomech Model Mechanobiol* **6**, 103-111, doi:10.1007/s10237-006-0041-2 (2007).
50 Chang, K., Lee, S. J., Cheong, I., Billiar, T. R., Chung, H. T., Han, J. A., Kwon, Y. G., Ha, K. S. & Kim, Y. M. Nitric oxide suppresses inducible nitric oxide synthase expression by inhibiting post-translational modification of IkappaB. *Exp Mol Med* **36**, 311-324, doi:200406301 [pii] (2004).
51 Chen, C. T., Burton-Wurster, N., Borden, C., Hueffer, K., Bloom, S. E. & Lust, G. Chondrocyte necrosis and apoptosis in impact damaged articular cartilage. *Journal of Orthopaedic Research* **19**, 703-711, doi:10.1016/s0736-0266(00)00066-8 (2001).
52 Clancy, R. M., Gomez, P. F. & Abramson, S. B. Nitric oxide sustains nuclear factor kappaB activation in cytokine-stimulated chondrocytes. *Osteoarthritis Cartilage* **12**, 552-558, doi:10.1016/j.joca.2004.04.003

S1063458404000640 [pii] (2004).
53 Coleman, J. L., Widmyer, M. R., Leddy, H. A., Utturkar, G. M., Spritzer, C. E., Moorman, C. T., 3rd, Guilak, F. & Defrate, L. E. Diurnal variations in articular cartilage thickness and strain in the human knee. *J Biomech*, doi:10.1016/j.jbiomech.2012.09.013 (2012).
54 Cotran, K., Collins. Pathologic Basis of Disease. **Sixth Edition**, 18 to 25 (1999).
55 Cox, D. L. N. a. M. M. Principles of Biochemistry. **Third Edition**, 476 f (2000).

56 D'Lima, D. D., Hashimoto, S., Chen, P. C., Colwell, C. W. & Lotz, M. K. Human chondrocyte apoptosis in response to mechanical injury. *Osteoarthritis and Cartilage* **9**, 712-719, doi:10.1053/joca.2001.0468 (2001).
57 D'Lima, D. D., Hashimoto, S., Chen, P. C., Lotz, M. K. & Colwell, C. W. Cartilage injury induces chondrocyte apoptosis. *Journal of Bone and Joint Surgery-American Volume* **83A**, 19-21 (2001).
58 D'Lima, D. D., Hashimoto, S., Chen, P. C., Lotz, M. K. & Colwell, C. W. Prevention of chondrocyte apoptosis. *Journal of Bone and Joint Surgery-American Volume* **83A**, 25-26 (2001).
59 Darling, E. M., Zauscher, S. & Guilak, F. Viscoelastic properties of zonal articular chondrocytes measured by atomic force microscopy. *Osteoarthritis and Cartilage* **14**, 571-579, doi:10.1016/j.joca.2005.12.003 (2006).
60 Day, G. A., Swanson, C. E. & Hulcombe, B. G. Operative treatment of ankle fractures: A minimum ten-year follow-up. *Foot & Ankle International* **22**, 102-106 (2001).
61 de Lange-Brokaar, B. J. E., Ioan-Facsinay, A., van Osch, G. J. V. M., Zuurmond, A. M., Schoones, J., Toes, R. E. M., Huizinga, T. W. J. & Kloppenburg, M. Synovial inflammation, immune cells and their cytokines in osteoarthritis: a review. *Osteoarthritis and cartilage / OARS, Osteoarthritis Research Society* **20**, 1484-1499, doi:10.1016/j.joca.2012.08.027 (2012).
62 DeLong, W. G. & Born, C. T. Cytokines in patients with polytrauma. *Clin Orthop Relat R*, 57-65, doi:10.1097/01.blo.0000130840.64528.1e (2004).
63 Donald Voet, J. G. V., Charlotte W. Pratt. Fundamentals of Biochemistry. **Second Edition**, 1061f (2006).
64 Dossumbekova, A., Anghelina, M., Madhavan, S., He, L. L., Quan, N., Knobloch, T. & Agarwal, S. Biomechanical signals inhibit IKK activity to attenuate NF-kappa B transcription activity in inflamed Chondrocytes. *Arthritis Rheum.* **56**, 3284-3294, doi:10.1002/art.22933 (2007).
65 Erenpreisa, J. & Roach, H. I. Aberrant death in dark chondrocytes of the avian growth plate. *Cell Death and Differentiation* **5**, 60-66 (1998).
66 Eroschenko, V. P. Atlas of Histology with Functional Correlations. *Lippincott Willams & Wilkins* **10th Edition**, 65 to 72 (2005).
67 Farndale, R. W., Buttle, D. J. & Barrett, A. J. Improved quantitation and discrimination of sulphated glycosaminoglycans by use of dimethylmethylene blue. *Biochimica et Biophysica Acta (BBA) - General Subjects* **883**, 173-177, doi:Doi: 10.1016/0304-4165(86)90306-5 (1986).
68 Fermor, B., Weinberg, J. B., Pisetsky, D. S., Misukonis, M. A., Fink, C. & Guilak, F. Induction of cyclooxygenase-2 by mechanical stress through a nitric oxide-regulated pathway. *Osteoarthritis and Cartilage* **10**, 792-798, doi:10.1053/joca.2002.0832 (2002).
69 Finlay, J. B. & Repo, R. U. CARTILAGE IMPACT IN-VITRO EFFECT OF BONE AND CEMENT. *Journal of Biomechanics* **11**, 379-388, doi:10.1016/0021-9290(78)90072-6 (1978).
70 Fischer, B. A., Mundle, S. & Cole, A. A. Tumor necrosis factor-alpha induced DNA cleavage in human articular chondrocytes may involve multiple endonucleolytic activities during apoptosis. *Microscopy Research and Technique* **50**, 236-242 (2000).
71 Frankel, M. N. a. V. H. Basic Biomechanics of the Musculoskeletal System. **Third Edition**, 60 to 101 (2001).
72 Fulda, S. & Debatin, K. M. Extrinsic versus intrinsic apoptosis pathways in anticancer chemotherapy. *Oncogene* **25**, 4798-4811, doi:1209608 [pii]

10.1038/sj.onc.1209608 (2006).
73 Fung, Y. C. Biomechanics. **Second Edition**, 500 to 538 (1993).
74 Furman, B. D., Olson, S. A. & Guilak, F. The development of posttraumatic arthritis after articular fracture. *Journal of Orthopaedic Trauma* **20**, 719-725 (2006).
75 Garrido, C. P., Hakimiyan, A. A., Rappoport, L., Oegema, T. R., Wimmer, M. A. & Chubinskaya, S. Anti-apoptotic treatments prevent cartilage degradation after acute trauma to human ankle cartilage. *Osteoarthritis and Cartilage* **17**, 1244-1251, doi:10.1016/j.joca.2009.03.007 (2009).
76 Gartner, L. P. H., James L. Color Atlas of Histology. **Third Edition**, 72 to 78 (2000).

77 Ghosh, S., May, M. J. & Kopp, E. B. NF-kappa B and Rel proteins: evolutionarily conserved mediators of immune responses. *Annu Rev Immunol* **16**, 225-260, doi:10.1146/annurev.immunol.16.1.225 (1998).
78 Giannoudis, P. V., Grotz, M. R. W., Papakostidis, C. & Dinopoulos, H. Operative treatment of displaced fractures of the acetabulum - A meta-analysis. *Journal of Bone and Joint Surgery-British Volume* **87B**, 2-9 (2005).
79 Goldring, M. B. & Berenbaum, F. The regulation of chondrocyte function by proinflammatory mediators - Prostaglandins and nitric oxide. *Clin Orthop Relat R*, S37-S46, doi:10.1097/01.blo.0000144484.69656.e4 (2004).
80 Goldring, S. R. & Goldring, M. B. The role of cytokines in cartilage matrix degeneration in osteoarthritis. *Clin Orthop Relat R*, S27-S36, doi:10.1097/01.blo.0000144854.66565.8f (2004).
81 Granger, D. L., Anstey, N. M., Miller, W. C. & Weinberg, J. B. in *Methods in Enzymology* Vol. Volume 301 (ed Packer Lester) 49-61 (Academic Press, 1999).
82 Guilak, F. Volume and surface area measurement of viable chondrocytes in situ using geometric modelling of serial confocal sections. *Journal of Microscopy (Oxford)* **173**, 245-256 (1994).
83 Guilak, F., Ratcliffe, A. & Mow, V. C. CHONDROCYTE DEFORMATION AND LOCAL TISSUE STRAIN IN ARTICULAR-CARTILAGE - A CONFOCAL MICROSCOPY STUDY. *Journal of Orthopaedic Research* **13**, 410-421, doi:10.1002/jor.1100130315 (1995).
84 Guilak, F., Sah, R. & Setton, L. A. Physical regulation of cartilage metabolism. *Basic orthopaedic biomechanics, Second edition*, 179-207 (1997).
85 Guilak, F. B., David L.; Goldstein, Steven A.; Mooney, David J. Functional Tissue Engineering. 227 to 242, 277 to 290 (2003).
86 Guilak, F. B., David L.; Goldstein, Steven A.; Mooney, David J. Functional Tissue Engineering. 46 to 69 (2003).
87 Hak, D. J., Hamel, A. J., Bay, B. K., Sharkey, N. A. & Olson, S. A. Consequences of transverse acetabular fracture malreduction on load transmission across the hip joint. *Journal of Orthopaedic Trauma* **12**, 90-100 (1998).
88 Hall, B. K. Cartilage, Biomedical Aspects. 49 to 80 (1983).
89 Hall, B. N., Stuart. Cartilage: Molecular Aspects. 213 to 242 (1991).
90 Hansson, G. K. & Edfeldt, K. Toll To Be Paid at the Gateway to the Vessel Wall. *Arterioscler Thromb Vasc Biol* **25**, 1085-1087, doi:10.1161/01.atv.0000168894.43759.47 (2005).
91 Hasbold, J. & Klaus, G. G. Anti-immunoglobulin antibodies induce apoptosis in immature B cell lymphomas. *Eur J Immunol* **20**, 1685-1690, doi:10.1002/eji.1830200810 (1990).
92 Hashimoto, S., Ochs, R. L., Rosen, F., Quach, J., McCabe, G., Solan, J., Seegmiller, J. E., Terkeltaub, R. & Lotz, M. Chondrocyte-derived apoptotic bodies and calcification of articular cartilage. *P Natl Acad Sci USA* **95**, 3094-3099 (1998).
93 Hashimoto, S., Setareh, M., Ochs, R. L. & Lotz, M. Fas/Fas ligand expression and induction of apoptosis in chondrocytes. *Arthritis Rheum.* **40**, 1749-1755 (1997).
94 Hashimoto, S., Takahashi, K., Amiel, D., Coutts, R. D. & Lotz, M. Chondrocyte apoptosis and nitric oxide production during experimentally induced osteoarthritis. *Arthritis Rheum.* **41**, 51 (1998).
95 Hayes, V. C. M. a. W. Basic Orthopaeic Biomechanics

Second Edition, 113 to 178 (1997).
96 Helminen, H. J. K., I; Tammi, M; Säämänen, A-M; Paukkonen, K; Jurvelin, J. Joint Loading. 64 to 88 (1986).
97 Hembree, W. C., Ward, B. D., Furman, B. D., Zura, R. D., Nichols, L. A., Guilak, F. & Olson, S. A. Viability and apoptosis of human chondrocytes in osteochondral fragments following joint trauma. *Journal of Bone and Joint Surgery-British Volume* **89B**, 1388-1395, doi:10.1302/0301-620x.89b10.18907 (2007).
98 Heraud, F., Heraud, A. & Harmand, M. F. Apoptosis in normal and osteoarthritic human articular cartilage. *Ann Rheum Dis* **59**, 959-965 (2000).

99 Hills, B. A. Boundary lubrication in vivo. *Proceedings of the Institution of Mechanical Engineers Part H-Journal of Engineering in Medicine* **214**, 83-94, doi:10.1243/0954411001535264 (2000).
100 Hodge, W. A., Carlson, K. L., Fijan, R. S., Burgess, R. G., Riley, P. O., Harris, W. H. & Mann, R. W. CONTACT PRESSURES FROM AN INSTRUMENTED HIP ENDOPROSTHESIS. *Journal of Bone and Joint Surgery-American Volume* **71A**, 1378-1386 (1989).
101 Hooiveld, M., Roosendaal, G., Wenting, M., van den Berg, M., Bijlsma, J. & Lafeber, F. Short-term exposure of cartilage to blood results in chondrocyte apoptosis. *Am. J. Pathol.* **162**, 943-951, doi:10.1016/s0002-9440(10)63889-8 (2003).
102 Huberbetzer, H., Brown, T. D. & Mattheck, C. SOME EFFECTS OF GLOBAL JOINT MORPHOLOGY ON LOCAL STRESS ABERRATIONS NEAR IMPRECISELY REDUCED INTRAARTICULAR FRACTURES. *Journal of Biomechanics* **23**, 811-822 (1990).
103 Huiskes, V. C. M. a. R. Basic Orthopaedic Biomechanics and Mechano- Biology. **Third Edition**, 259 to 300 (2005).
104 Huiskes, V. C. M. a. R. Basic Orthopaedics and Mechano- Biology. **Third Edition**, 181 to 258 (2005).
105 Hurtig, M., Chubinskaya, S., Dickey, J. & Rueger, D. BMP-7 Protects against Progression of Cartilage Degeneration after Impact Injury. *Journal of Orthopaedic Research* **27**, 602-611, doi:10.1002/jor.20787 (2009).
106 Irie, K., Uchiyama, E. & Iwaso, H. Intraarticular inflammatory cytokines in acute anterior cruciate ligament injured knee. *Knee* **10**, 93-96 (2003).
107 Islam, N., Haqqi, T. M., Jepsen, K. J., Kraay, M., Welter, J. F., Goldberg, V. M. & Malemud, C. J. Hydrostatic pressure induces apoptosis in human chondrocytes from osteoarthritic cartilage through up-regulation of tumor necrosis factor-alpha, inducible nitric oxide synthase, p53, c-myc, and bax-alpha, and suppression of bcl-2. *Journal of Cellular Biochemistry* **87**, 266-278, doi:10.1002/jcb.10317 (2002).
108 Jeffrey, J. E., Gregory, D. W. & Aspden, R. M. Matrix damage and chondrocyte viability following a single impact load on articular cartilage. *Arch Biochem Biophys* **322**, 87-96, doi:S0003-9861(85)71439-7 [pii]

10.1006/abbi.1995.1439 (1995).
109 Johnson, G. B., Brunn, G. J., Kodaira, Y. & Platt, J. L. Receptor-mediated monitoring of tissue well-being via detection of soluble heparan sulfate by toll-like receptor 4. *Journal of Immunology* **168**, 5233-5239 (2002).
110 Kariko, K., Ni, H. P., Capodici, J., Lamphier, M. & Weissman, D. mRNA is an endogenous ligand for Toll-like receptor 3. *J Biol Chem* **279**, 12542-12550, doi:10.1074/jbc.M310175200 (2004).
111 Kim, H. A., Cho, M. L., Choi, H. Y., Yoon, C. S., Jhun, J. Y., Oh, H. J. & Kim, H. Y. The catabolic pathway mediated by Toll-like receptors in human osteoarthritic chondrocytes. *Arthritis Rheum.* **54**, 2152-2163, doi:10.1002/art.21951 (2006).
112 Kim, H. T., Lo, M. Y. & Pillarisetty, R. Chondrocyte apoptosis following intraarticular fracture in humans. *Osteoarthritis and Cartilage* **10**, 747-749, doi:10.1053/joca.2002.0828 (2002).
113 Kim, H. T., Teng, M. S. & Dang, A. C. Chondrocyte apoptosis: Implications for osteochondral allograft transplantation. *Clin Orthop Relat R* **466**, 1819-1825, doi:10.1007/s11999-008-0304-6 (2008).
114 Kim, S. J., Hwang, S. G., Shin, D. Y., Kang, S. S. & Chun, J. S. p38 kinase regulates nitric oxide-induced apoptosis of articular chondrocytes by accumulating p53 via NF kappa B-dependent transcription and stabilization by serine 15 phosphorylation. *J Biol Chem* **277**, 33501-33508, doi:10.1074/jbc.M202862200 (2002).
115 Kokkola, R., Li, J., Sundberg, E., Aveberger, A. C., Palmblad, K., Yang, H., Tracey, K. J., Andersson, U. & Harris, H. E. Successful treatment of collagen-induced arthritis in mice and rats by targeting extracellular high mobility group box chromosomal protein 1 activity. *Arthritis Rheum* **48**, 2052-2058, doi:10.1002/art.11161 (2003).
116 Kokkola, R., Sundberg, E., Ulfgren, A. K., Palmblad, K., Li, J., Wang, H., Ulloa, L., Yang, H., Yan, X. J., Furie, R., Chiorazzi, N., Tracey, K. J., Andersson, U. & Harris, H. E. High mobility

group box chromosomal protein 1: a novel proinflammatory mediator in synovitis. *Arthritis Rheum* **46**, 2598-2603, doi:10.1002/art.10540 (2002).

117 Kon, T., Cho, T. J., Aizawa, T., Yamazaki, M., Nooh, N., Graves, D., Gerstenfeld, L. C. & Einhorn, T. A. Expression of osteoprotegerin, receptor activator of NF-kappa B ligand (osteoprotegerin ligand) and related proinflammatory cytokines during fracture healing. *Journal of Bone and Mineral Research* **16**, 1004-1014 (2001).

118 Kruzic, J. J., Kim, D. K., Koester, K. J. & Ritchie, R. O. Indentation techniques for evaluating the fracture toughness of biomaterials and hard tissues. *Journal of the Mechanical Behavior of Biomedical Materials* **2**, 384-395, doi:10.1016/j.jmbbm.2008.10.008 (2009).

119 Kuettner, K. E. P., Jacques G.; Schleyerbach, Rudolf; Hascall, Vincent C. Articular Cartilage and Osteoarthritis. 291 to 350 (1991).

120 Kuhn, K., D'Lima, D. D., Hashimoto, S. & Lotz, M. Cell death in cartilage. *Osteoarthritis and Cartilage* **12**, 1-16 (2004).

121 Kuhn, K., Hashimoto, S. & Lotz, M. IL-1 beta protects human chondrocytes from CD95-induced apoptosis. *Journal of Immunology* **164**, 2233-2239 (2000).

122 Kuhn, K. & Lotz, M. Regulation of CD95 (Fas/APO-1)-induced apoptosis in human chondrocytes. *Arthritis Rheum.* **44**, 1644-1653 (2001).

123 Kumar, A., Fausto. Pathologic Basis of Disease. **Seventh Edition**, 11 to 32 (2005).

124 Leadbetter, E. A., Rifkin, I. R., Hohlbaum, A. M., Beaudette, B. C., Shlomchik, M. J. & Marshak-Rothstein, A. Chromatin-IgG complexes activate B cells by dual engagement of IgM and Toll-like receptors. *Nature* **416**, 603-607, doi:10.1038/416603a (2002).

125 Leddy, H. A., Haider, M. A. & Guilak, F. Diffusional anisotropy in collagenous tissues: Fluorescence imaging of continuous point photobleaching. *Biophysical Journal* **91**, 311-316, doi:10.1529/biophysj.105.075283 (2006).

126 Levin, A., Burton-Wurster, N., Chen, C. T. & Lust, G. Intercellular signaling as a cause of cell death in cyclically impacted cartilage explants. *Osteoarthritis and Cartilage* **9**, 702-711, doi:10.1053/joca.2001.0467 (2001).

127 Lewis, J. L., Deloria, L. B., Oyen-Tiesma, M., Thompson, R. C., Ericson, M. & Oegema, T. R. Cell death after cartilage impact occurs around matrix cracks. *Journal of Orthopaedic Research* **21**, 881-887, doi:10.1016/s0736-0266(03)00039-1 (2003).

128 Lisignoli, G., Grassi, F., Zini, N., Toneguzzi, S., Piacentini, A., Guidolin, D., Bevilacqua, C. & Facchini, A. Anti-Fas-induced apoptosis in chondrocytes reduced by hyaluronan - Evidence for CD44 and CD54 (intercellular adhesion molecule 1) involvement. *Arthritis Rheum.* **44**, 1800-1807 (2001).

129 Liu-Bryan, R. & Terkeltaub, R. Chondrocyte Innate Immune Myeloid Differentiation Factor 88-Dependent Signaling Drives Procatabolic Effects of the Endogenous Toll-like Receptor 2/Toll-like Receptor 4 Ligands Low Molecular Weight Hyaluronan and High Mobility Group Box Chromosomal Protein 1 in Mice. *Arthritis Rheum.* **62**, 2004-2012, doi:10.1002/art.27475 (2010).

130 Liu, J. C., Liu, X., Zhou, G. D., Xiao, R. & Cao, Y. L. Conditioned Medium from Chondrocyte/Scaffold Constructs Induced Chondrogenic Differentiation of Bone Marrow Stromal Cells. *Anatomical Record-Advances in Integrative Anatomy and Evolutionary Biology* **295**, 1109-1116, doi:10.1002/ar.22500 (2012).

131 Loeser, R. F., Carlson, C. S., Del Carlo, M. & Cole, A. Detection of nitrotyrosine in aging and osteoarthritic cartilage: Correlation of oxidative damage with the presence of interleukin-1beta and with chondrocyte resistance to insulin-like growth factor 1. *Arthritis Rheum* **46**, 2349-2357, doi:10.1002/art.10496 (2002).

132 Lotz, M. K. Posttraumatic osteoarthritis: pathogenesis and pharmacological treatment options. *Arthritis Res. Ther.* **12**, doi:211

10.1186/ar3046 (2010).

133 Lotze, M. T. & Tracey, K. J. High-mobility group box 1 protein (HMGB1): nuclear weapon in the immune arsenal. *Nat Rev Immunol* **5**, 331-342, doi:nri1594 [pii]

10.1038/nri1594 (2005).

134 Louer, C. R., Furman, B. D., Huebner, J. L., Kraus, V. B., Olson, S. A. & Guilak, F. Diet-induced obesity significantly increases the severity of posttraumatic arthritis in mice. *Arthritis Rheum.* **64**, 3220-3230, doi:10.1002/art.34533 (2012).
135 Loughlin, J. The genetic epidemiology of human primary osteoarthritis: current status. *Expert Reviews in Molecular Medicine* **7**, 1-12, doi:doi:10.1017/S1462399405009257 (2005).
136 Loughlin, J. The genetic epidemiology of human primary osteoarthritis: current status. *Expert Reviews in Molecular Medicine* **7**, 1-12, doi::10.1017/s1462399405009257 (2005).
137 Lucchinetti, E., Adams, C. S., Horton, W. E., Jr. & Torzilli, P. A. Cartilage viability after repetitive loading: a preliminary report. *Osteoarthritis Cartilage* **10**, 71-81, doi:10.1053/joca.2001.0483

S1063458401904832 [pii] (2002).
138 Maneiro, E., Martin, M. A., de Andres, M. C., Lopez-Armada, M. J., Fernandez-Sueiro, J. L., del Hoyo, P., Galdo, F., Arenas, J. & Blanco, F. J. Mitochondrial respiratory activity is altered in osteoarthritic human articular chondrocytes. *Arthritis Rheum.* **48**, 700-708, doi:10.1002/art.10837 (2003).
139 Mankin, K. P. & Zaleske, D. J. Response of physeal cartilage to low-level compression and tension in organ culture. *Journal of Pediatric Orthopaedics* **18**, 145-148 (1998).
140 Mansour, J. M. Biomechanics of Cartilage. Chapter 5 (2003).
141 Margareta Nordin, V. H. F. Basic Biomechanics of the Musculoskeletal System. **Third Edition**, 60 to 69 (2001).
142 Martel-Pelletier, J., Alaaeddine, N. & Pelletier, J.-P. Cytokines and their role in the pathophysiology of osteoarthritis. *Frontiers in Bioscience* **4**, d694-703 (1999).
143 Martin, J. A., McCabe, D., Walter, M., Buckwalter, J. A. & McKinley, T. O. N-acetylcysteine inhibits post-impact chondrocyte death in osteochondral explants. *J Bone Joint Surg Am* **91**, 1890-1897, doi:91/8/1890 [pii]

10.2106/JBJS.H.00545 (2009).
144 Matta, J. M. Fractures of the acetabulum: Accuracy of reduction and clinical results in patients managed operatively within three weeks after the injury. *Journal of Bone and Joint Surgery-American Volume* **78A**, 1632-1645 (1996).
145 Matthews, L. S. S., D.A., and Hanke, J.A. Load bearing characteristics of the patellofemoral joint. *Acta Orthop. Scand.* **48**, 511- 516 (1977).
146 Mistry, D., Oue, Y., Chambers, M. G., Kayser, M. V. & Mason, R. M. Chondrocyte death during murine osteoarthritis. *Osteoarthritis Cartilage* **12**, 131-141, doi:S1063458403002711 [pii] (2004).
147 Miwa, M., Saura, R., Hirata, S., Hayashi, Y., Mizuno, K. & Itoh, H. Induction of apoptosis in bovine articular chondrocyte by prostaglandin E-2 through cAMP-dependent pathway. *Osteoarthritis and Cartilage* **8**, 17-24 (2000).
148 Molecular Probes, P. I. LIVE/DEAD ® Viability/Cytotoxicity Kit *for mammalian cells. (2005).
149 Mollica, L., De Marchis, F., Spitaleri, A., Dallacosta, C., Pennacchini, D., Zamai, M., Agresti, A., Trisciuoglio, L., Musco, G. & Bianchi, M. E. Glycyrrhizin binds to high-mobility group box 1 protein and inhibits its cytokine activities. *Chem Biol* **14**, 431-441, doi:S1074-5521(07)00104-4 [pii]

10.1016/j.chembiol.2007.03.007 (2007).
150 Mooney, F. G. a. D. L. B. a. S. A. G. a. D. J. Functional Tissue Engineering. **First Edition**, 227 to 242 (2003).
151 Morel, V. & Quinn, T. M. Short-term changes in cell and matrix damage following mechanical injury of articular cartilage explants and modelling of microphysical mediators. *Biorheology* **41**, 509-519 (2004).
152 Morisset, S., Patry, C., Lora, M. & de Brum-Fernandes, A. J. Regulation of cyclooxygenase-2 expression in bovine chondrocytes in culture by interleukin 1 alpha, tumor necrosis factor-alpha, glucocorticoids, and 17 beta-estradiol. *Journal of Rheumatology* **25**, 1146-1153 (1998).

153 Mow, V. C. & Mansour, J. M. The nonlinear interaction between cartilage deformation and interstitial fluid flow. *Journal of Biomechanics* **10**, 31-39, doi:Doi: 10.1016/0021-9290(77)90027-6 (1977).
154 Mow, V. C. H., Rik. Basic Orthopaedic Biomechanics and Mechano- Biology. **Third Edition**, 185 to 198 (2005).
155 Mow, V. C. H., Rik. Basic Orthopaedic Biomechanics and Mechano- Biology. **Third Edition**, 181 to 300 (2005).
156 Muehleman, C., Bareither, D., Huch, K., Cole, A. A. & Kuettner, K. E. Prevalence of degenerative morphological changes in the joints of the lower extremity. *Osteoarthritis and Cartilage* **5**, 23-37 (1997).
157 Murray, M. M., Zurakowski, D. & Vrahas, M. S. The death of articular chondrocytes after intra-articular fracture in humans. *J. Trauma-Injury Infect. Crit. Care* **56**, 128-131, doi:10.1097/01.ta.0000051934.96670.37 (2004).
158 Murray, R. K. G., Darly K.; Mayes, Peter A.; Rodwell, Victor W. Harper´s Illustrated Biochemistry

26th Edition, 535 to 539 (2003).
159 Okamura, Y., Watari, M., Jerud, E. S., Young, D. W., Ishizaka, S. T., Rose, J., Chow, J. C. & Strauss, J. F. The extra domain A of fibronectin activates toll-like receptor 4. *J Biol Chem* **276**, 10229-10233, doi:10.1074/jbc.M100099200 (2001).
160 Okazaki, R., Sakai, A., Ootsuyama, A., Sakata, T., Nakamura, T. & Norimura, T. Apoptosis and p53 expression in chondrocytes relate to degeneration in articular cartilage of immobilized knee joints. *Journal of Rheumatology* **30**, 559-566 (2003).
161 Okeefe, R. J., Crabb, I. D., Puzas, J. E. & Rosier, R. N. INFLUENCE OF PROSTAGLANDINS ON DNA AND MATRIX SYNTHESIS IN GROWTH PLATE CHONDROCYTES. *Journal of Bone and Mineral Research* **7**, 397-404 (1992).
162 Pahl, H. L. Activators and target genes of Rel/NF-kappaB transcription factors. *Oncogene* **18**, 6853-6866, doi:10.1038/sj.onc.1203239 (1999).
163 Park, J. S., Svetkauskaite, D., He, Q. B., Kim, J. Y., Strassheim, D., Ishizaka, A. & Abraham, E. Involvement of toll-like receptors 2 and 4 in cellular activation by high mobility group box 1 protein. *J Biol Chem* **279**, 7370-7377, doi:10.1074/jbc.M306793200 (2004).
164 Paul, J. P. Force Actions Transmitted by Joints in the Human Body. *Proceedings of the Royal Society of London. Series B, Biological Sciences* **192**, 163-172 (1976).
165 Pelletier, J. P., Jovanovic, D., Fernandes, J. C., Manning, P., Connor, J. R., Currie, M. G. & Martel-Pelletier, J. Reduction in the structural changes of experimental osteoarthritis by a nitric oxide inhibitor. *Osteoarthritis and Cartilage* **7**, 416-418 (1999).
166 Pelletier, J. P., Jovanovic, D. V., Lascau-Coman, V., Fernandes, J. C., Manning, P. T., Connor, J. R., Currie, M. G. & Martel-Pelletier, J. Selective inhibition of inducible nitric oxide synthase reduces progression of experimental osteoarthritis in vivo - Possible link with the reduction in chondrocyte apoptosis and caspase 3 level. *Arthritis Rheum.* **43**, 1290-1299 (2000).
167 Pelletier, J. P., Lascau-Coman, V., Jovanovic, D., Fernandes, J. C., Manning, P., Connor, J. R., Currie, M. G. & Martel-Pelletier, J. Selective inhibition of inducible nitric oxide synthase in experimental osteoarthritis is associated with reduction in tissue levels of catabolic factors. *Journal of Rheumatology* **26**, 2002-2014 (1999).
168 Pelletier, J. P., Martel-Pelletier, J. & Abramson, S. B. Osteoarthritis, an inflammatory disease: potential implication for the selection of new therapeutic targets. *Arthritis Rheum* **44**, 1237-1247, doi:10.1002/1529-0131(200106)44:6<1237::AID-ART214>3.0.CO;2-F (2001).
169 Pickvance, E. A., Oegema, T. R. & Thompson, R. C. IMMUNOLOCALIZATION OF SELECTED CYTOKINES AND PROTEASES IN CANINE ARTICULAR-CARTILAGE AFTER TRANSARTICULAR LOADING. *Journal of Orthopaedic Research* **11**, 313-323 (1993).
170 Pisetsky, D. S. The role of nuclear macromolecules in innate immunity. *Proceedings of the American Thoracic Society* **4**, 258-262, doi:10.1513/pats.200701-027AW (2007).
171 Plaas, A., Osborn, B., Yoshihara, Y., Bai, Y., Bloom, T., Nelson, F., Mikecz, K. & Sandy, J. D. Aggrecanolysis in human osteoarthritis: confocal localization and biochemical characterization

of ADAMTS5 - hyaluronan complexes in articular cartilages. *Osteoarthritis and Cartilage* **15**, 719-734, doi:10.1016/j.joca.2006.12.008 (2007).
172 Poppen, N. K. & Walker, P. S. FORCES AT GLENOHUMERAL JOINT IN ABDUCTION. *Clin Orthop Relat R*, 165-170 (1978).
173 Quinn, T. M., Allen, R. G., Schalet, B. J., Perumbuli, P. & Hunziker, E. B. Matrix and cell injury due to sub-impact loading of adult bovine articular cartilage explants: effects of strain rate and peak stress. *Journal of Orthopaedic Research* **19**, 242-249 (2001).
174 Quinn, T. M., Kocian, P. & Meister, J. J. Static compression is associated with decreased diffusivity of dextrans in cartilage explants. *Arch Biochem Biophys* **384**, 327-334, doi:S0003-9861(00)92077-0 [pii]

10.1006/abbi.2000.2077 (2000).
175 Rademakers, M. V., Kerkhoffs, G., Sierevelt, I. N., Raaymakers, E. & Marti, R. K. Operative treatment of 109 tibial plateau fractures: Five- to 27-year follow-up results. *Journal of Orthopaedic Trauma* **21**, 5-10 (2007).
176 Rakoff-Nahoum, S. & Medzhitov, R. Toll-like receptors and cancer. *Nat Rev Cancer* **9**, 57-63 (2009).
177 Rasmussen, F. H., Yeung, N., Kiefer, L., Murphy, G., Lopez-Otin, C., Vitek, M. P. & Moss, M. L. Use of a multiple-enzyme/multiple-reagent assay system to quantify activity levels in samples containing mixtures of matrix metalloproteinases. *Biochemistry* **43**, 2987-2995, doi:10.1021/bi036063m (2004).
178 Reginster, J.-Y. P., J.-P.; Martel- Pelletier, J.; Henrotin, Y. Osteoarthritis. **First**, 156 to 175 (1999).
179 Renard, P. & Raes, M. The proinflammatory transcription factor NF kappa B: a potential target for novel therapeutical strategies. *Cell Biology and Toxicology* **15**, 341-344 (1999).
180 Rengel, Y., Ospelt, C. & Gay, S. Proteinases in the joint: clinical relevance of proteinases in joint destruction. *Arthritis Res. Ther.* **9**, doi:221

10.1186/ar2304 (2007).
181 Repo, R. U. & Finlay, J. B. SURVIVAL OF ARTICULAR-CARTILAGE AFTER CONTROLLED IMPACT. *Journal of Bone and Joint Surgery-American Volume* **59**, 1068-1076 (1977).
182 Ridnour, L. A., Windhausen, A. N., Isenberg, J. S., Yeung, N., Thomas, D. D., Vitek, M. P., Roberts, D. D. & Wink, D. A. Nitric oxide regulates matrix metalloproteinase-9 activity by guanylyl-cyclase-dependent and -independent pathways. *Proc Natl Acad Sci U S A* **104**, 16898-16903, doi:0702761104 [pii]

10.1073/pnas.0702761104 (2007).
183 Rieppo, J., Hyttinen, M. M., Halmesmaki, E., Ruotsalainen, H., Vasara, A., Kiviranta, I., Jurvelin, J. S. & Helminen, H. J. Changes in spatial collagen content and collagen network architecture in porcine articular cartilage during growth and maturation. *Osteoarthritis and Cartilage* **17**, 448-455, doi:10.1016/j.joca.2008.09.004 (2009).
184 Rifkin, I. R., Leadbetter, E. A., Busconi, L., Viglianti, G. & Marshak-Rothstein, A. Toll-like receptors, endogenous ligands, and systemic autoimmune disease. *Immunological Reviews* **204**, 27-42, doi:10.1111/j.0105-2896.2005.00239.x (2005).
185 Roach, H. I. & Clarke, N. M. P. “Cell Paralysis” as an Intermediate Stage in the Programmed Cell Death of Epiphyseal Chondrocytes During Development. *Journal of Bone and Mineral Research* **14**, 1367-1378, doi:10.1359/jbmr.1999.14.8.1367 (1999).
186 Roos, H., Adalberth, T., Dahlberg, L. & Lohmander, L. S. Osteoarthritis of the knee after injury to the anterior cruciate ligament or meniscus: The influence of time and age. *Osteoarthritis and Cartilage* **3**, 261-267, doi:10.1016/s1063-4584(05)80017-2 (1995).
187 Rundell, S. A., Baars, D. C., Phillips, D. M. & Haut, R. C. The limitation of acute necrosis in retro-patellar cartilage after a severe blunt impact to the in vivo rabbit patello-femoral joint. *Journal of Orthopaedic Research* **23**, 1363-1369, doi:10.1016/j.orthres.2005.06.001 (2005).
188 Sadler, T. W. Medical Embryology. **seventh edition**, 147 to 165 (1995).
189 Sahap Atik, O. Leukotriene B4 and prostaglandin E2-like activity in synovial fluid in osteoarthritis. *Prostaglandins Leukot Essent Fatty Acids* **39**, 253-254 (1990).

190 Scanzello, C. R. & Goldring, S. R. The role of synovitis in osteoarthritis pathogenesis. *Bone*, doi:10.1016/j.bone.2012.02.012.
191 Schinagl, R. M., Gurskis, D., Chen, A. C. & Sah, R. L. Depth-dependent confined compression modulus of full-thickness bovine articular cartilage. *J Orthop Res* **15**, 499-506, doi:10.1002/jor.1100150404 (1997).
192 Seibel, M. J. R., Simon P.; Blezikian, John P. Dynamics of Bone and Cartilage Metabolism. 301 to 318 (1999).
193 Sellam, J. & Berenbaum, F. The role of synovitis in pathophysiology and clinical symptoms of osteoarthritis. *Nature Reviews Rheumatology* **6**, 625-635, doi:10.1038/nrrheum.2010.159 (2010).
194 Setton, L. A., Mow, V. C., Muller, F. J., Pita, J. C. & Howell, D. S. MECHANICAL-PROPERTIES OF CANINE ARTICULAR-CARTILAGE ARE SIGNIFICANTLY ALTERED FOLLOWING TRANSECTION OF THE ANTERIOR CRUCIATE LIGAMENT. *Journal of Orthopaedic Research* **12**, 451-463, doi:10.1002/jor.1100120402 (1994).
195 Setton, L. A., Mow, V. C., Muller, F. J., Pita, J. C. & Howell, D. S. Mechanical behavior and biochemical composition of canine knee cartilage following periods of joint disuse and disuse with remobilization. *Osteoarthritis and Cartilage* **5**, 1-16 (1997).
196 Shingu, M., Miyauchi, S., Nagai, Y., Yasutake, C. & Horie, K. The role of IL-4 and IL-6 in IL-1-dependent cartilage matrix degradation. *Br J Rheumatol* **34**, 101-106 (1995).
197 Sloane, J. A., Blitz, D., Margolin, Z. & Vartanian, T. A Clear and Present Danger: Endogenous Ligands of Toll-like Receptors. *Neuromolecular Medicine* **12**, 149-163, doi:10.1007/s12017-009-8094-x (2010).
198 Smiley, S. T., King, J. A. & Hancock, W. W. Fibrinogen stimulates macrophage chemokine secretion through toll-like receptor 4. *Journal of Immunology* **167**, 2887-2894 (2001).
199 Soltz, M. A. & Ateshian, G. A. Interstitial fluid pressurization during confined compression cyclical loading of articular cartilage. *Annals of Biomedical Engineering* **28**, 150-159, doi:10.1114/1.239 (2000).
200 Spector, T. D. & MacGregor, A. J. Risk factors for osteoarthritis: genetics. *Osteoarthritis Cartilage* **12 Suppl A**, S39-44 (2004).
201 Spector, T. D. & MacGregor, A. J. Risk factors for osteoarthritis: genetics. *Osteoarthritis and Cartilage* **12, Supplement**, 39-44, doi:http://dx.doi.org/10.1016/j.joca.2003.09.005 (2004).
202 Sternberg, S. S., M.D. Histology for Pathologists. **Second Edition**, 107 to126 (1997).
203 Stolberg-Stolberg, J. A., Furman, B. D., Garrigues, N. W., Lee, J., Pisetsky, D. S., Stearns, N. A., DeFrate, L. E., Guilak, F. & Olson, S. A. Effects of cartilage impact with and without fracture on chondrocyte viability and the release of inflammatory markers. *Journal of Orthopaedic Research* **31**, 1283-1292, doi:10.1002/jor.22348 (2013).
204 Stolberg-Stolberg; Furman, B. S. G., Ph.D.; Lee, Ph.D.; Pisetsky, M.D., Ph.D.; Stearns; DeFrate, Ph.D.; Guilak, Ph.D.; Olson, M.D. A Novel In Vitro Model of Chondrocyte Response to Impact with or without Articular Fracture. *Orthopaedic Research Society Annual Meeting 2012* **Posterpresentation** (2012).
205 Stolberg-Stolberg; Furman, B. S. G., Ph.D.; Lee, Ph.D.; Pisetsky, M.D., Ph.D.; Stearns; DeFrate, Ph.D.; Burgkart, PD; Guilak, Ph.D.; Olson, M.D. Ein inVitro Modell Degenerativer und Entzündlicher Veränderungen im Hyalinem Knorpel nach Stumpfen Trauma und Fraktur. *DKOU 2012* **Posterpresentation** (2012).
206 Stufkens, S. A., van den Bekerom, M. P., Kerkhoffs, G. M., Hintermann, B. & van Dijk, C. N. Long-term outcome after 1822 operatively treated ankle fractures: A systematic review of the literature. *Injury*, doi:S0020-1383(10)00258-5 [pii]

10.1016/j.injury.2010.04.006 (2010).
207 Su, S. L., Tsai, C. D., Lee, C. H., Salter, D. M. & Lee, H. S. Expression and regulation of toll-like receptor 2 by IL-1 beta and fibronectin fragments in human articular chondrocytes. *Osteoarthritis and Cartilage* **13**, 879-886, doi:10.1016/j.joca.2005.04.017 (2005).
208 Swiontkowski, M. F., Agel, J., McAndrew, M. P., Burgess, A. R. & MacKenzie, E. J. Outcome validation of the AO/OTA fracture classification system. *Journal of Orthopaedic Trauma* **14**, 534-541 (2000).

209 Takeda, K. & Akira, S. Toll-like receptors. *Curr Protoc Immunol* **Chapter 14**, Unit 14 12, doi:10.1002/0471142735.im1412s77 (2007).
210 Takeda, K. & Akira, S. Toll-like receptors in innate immunity. *Int Immunol* **17**, 1-14, doi:17/1/1 [pii]

10.1093/intimm/dxh186 (2005).
211 Taskiran, D., Stefanovic-Racic, M., Georgescu, H. & Evans, C. Nitric oxide mediates suppression of cartilage proteoglycan synthesis by interleukin-1. *Biochem Biophys Res Commun* **200**, 142-148, doi:S0006291X84714264 [pii] (1994).
212 Taylor, K. B. & Jeffree, G. M. A NEW BASIC META CHROMATIC DYE I.9 DI METHYL METHYLENE BLUE RAT. *Histochemical Journal* **1**, 199-204 (1969).
213 Termeer, C., Benedix, F., Sleeman, J., Fieber, C., Voith, U., Ahrens, T., Miyake, K., Freudenberg, M., Galanos, C. & Simon, J. C. Oligosaccharides of hyaluronan activate dendritic cells via toll-like receptor 4. *Journal of Experimental Medicine* **195**, 99-111, doi:10.1084/jem.20001858 (2002).
214 Tew, S. R., Kwan, A. P. L., Hann, A., Thomson, B. M. & Archer, C. W. The reactions of articular cartilage to experimental wounding - Role of apoptosis. *Arthritis Rheum.* **43**, 215-225 (2000).
215 Tochigi, Y., Buckwalter, J. A., Martin, J. A., Hillis, S. L., Zhang, P., Vaseenon, T., Lehman, A. D. & Brown, T. D. Distribution and Progression of Chondrocyte Damage in a Whole-Organ Model of Human Ankle Intra-Articular Fracture. *Journal of Bone and Joint Surgery-American Volume* **93A**, 533-539, doi:10.2106/jbjs.j.01777 (2011).
216 Tomita, M., Sato, E. F., Nishikawa, M., Yamano, Y. & Inoue, M. Nitric oxide regulates mitochondrial respiration and functions of articular chondrocytes. *Arthritis Rheum.* **44**, 96-104 (2001).
217 Torzilli, P. A., Deng, X. H. & Ramcharan, M. Effect of compressive strain on cell viability in statically loaded articular cartilage. *Biomech Model Mechanobiol* **5**, 123-132, doi:10.1007/s10237-006-0030-5 (2006).
218 Torzilli, P. A., Grigiene, R., Borrelli, J. & Helfet, D. L. Effect of impact load on articular cartilage: Cell metabolism and viability, and matrix water content. *J. Biomech. Eng.-Trans. ASME* **121**, 433-441 (1999).
219 Tran, T. T., Groben, P. & Pisetsky, D. S. The release of DNA into the plasma of mice following hepatic cell death by apoptosis and necrosis. *Biomarkers* **13**, 184-200, doi:10.1080/13547500701791719 (2008).
220 Tsan, M. F. & Gao, B. C. Endogenous ligands of toll-like receptors. *J Leukocyte Biol* **76**, 514-519, doi:10.1189/jlb.0304127 (2004).
221 Tsung, A., Klune, J. R., Zhang, X., Jeyabalan, G., Cao, Z., Peng, X., Stolz, D. B., Geller, D. A., Rosengart, M. R. & Billiar, T. R. HMGB1 release induced by liver ischemia involves Toll-like receptor 4-dependent reactive oxygen species production and calcium-mediated signaling. *Journal of Experimental Medicine* **204**, 2913-2923, doi:10.1084/jem.20070247 (2007).
222 Van de Velde, S. K., Bingham, J. T., Gill, T. J. & Li, G. Analysis of tibiofemoral cartilage deformation in the posterior cruciate ligament-deficient knee. *The Journal of bone and joint surgery. American volume* **91**, 167-175, doi:10.2106/JBJS.H.00177 (2009).
223 van der Vaart, M. & Pretorius, P. J. The origin of circulating free DNA. *Clinical Chemistry* **53**, 2215-2215, doi:10.1373/clinchem.2007.092734 (2007).
224 Vandeloo, F. A. J., Joosten, L. A. B., Vanlent, P., Arntz, O. J. & Vandenberg, W. B. ROLE OF INTERLEUKIN-1, TUMOR-NECROSIS-FACTOR-ALPHA, AND INTERLEUKIN-6 IN CARTILAGE PROTEOGLYCAN METABOLISM AND DESTRUCTION - EFFECT OF IN-SITU BLOCKING IN MURINE ANTIGEN-INDUCED AND ZYMOSAN-INDUCED ARTHRITIS. *Arthritis Rheum.* **38**, 164-172 (1995).
225 Vieira-Sousa, E., Gerlag, D. M. & Tak, P. P. Synovial tissue response to treatment in rheumatoid arthritis. *The open rheumatology journal* **5**, 115-122 (2011).
226 Vigorita, V. J. Orthopaedic Pathology. **Second Edition**, 50 to 100 (2008).
227 Vigorita, V. J. Orthopaedic Pathology. **Second Edition**, 90 to 99 (2008).
228 Vigorita, V. J. Orthopaedic Pathology. **second edition**, 626 to 676 (2008).

229 Wang, P., Zhu, F., Tong, Z. & Konstantopoulos, K. Response of chondrocytes to shear stress: antagonistic effects of the binding partners Toll-like receptor 4 and caveolin-1. *Faseb J* **25**, 3401-3415, doi:10.1096/fj.11-184861 (2011).
230 Warner, M. D., Taylor, W. R. & Clift, S. E. Cyclic loading moves the peak stress to the cartilage surface in a biphasic model with isotropic solid phase properties. *Med Eng Phys* **26**, 247-249, doi:10.1016/j.medengphy.2003.10.010

S1350453303001644 [pii] (2004).
231 Woo, V. C. M. a. A. R. a. S. L.-Y. Biomechanics of Diarthrodial Joints. **Volume 1**, 215 to 437 (1990).
232 Wright, R., Barrett, K., Christie, M. J. & Johnson, K. D. ACETABULAR FRACTURES - LONG-TERM FOLLOW-UP OF OPEN REDUCTION AND INTERNAL-FIXATION. *Journal of Orthopaedic Trauma* **8**, 397-403 (1994).
233 Yamada, S. & Maruyama, I. HMGB1, a novel inflammatory cytokine. *Clin Chim Acta* **375**, 36-42, doi:DOI 10.1016/j.cca.2006.07.019 (2007).
234 Yanai, H., Chiba, S., Ban, T., Nakaima, Y., Onoe, T., Honda, K., Ohdan, H. & Taniguchi, T. Suppression of immune responses by nonimmunogenic oligodeoxynucleotides with high affinity for high-mobility group box proteins (HMGBs). *P Natl Acad Sci USA* **108**, 11542-11547, doi:10.1073/pnas.1108535108 (2011).
235 Yang, C. L., Li, S. W., Helminen, H. J., Khillan, J. S., Bao, Y. H. & Prockop, D. J. Apoptosis of chondrocytes in transgenic mice lacking collagen II. *Experimental Cell Research* **235**, 370-373 (1997).
236 Yu, M., Wang, H., Ding, A., Golenbock, D. T., Latz, E., Czura, C. J., Fenton, M. J., Tracey, K. J. & Yang, H. HMGB1 signals through toll-like receptor (TLR) 4 and TLR2. *Shock* **26**, 174-179, doi:10.1097/01.shk.0000225404.51320.82 (2006).
237 Zemmyo, M., Meharra, E. J., Kuhn, K., Creighton-Achermann, L. & Lotz, M. Accelerated, aging-dependent development of osteoarthritis in alpha 1 integrin-deficient mice. *Arthritis Rheum.* **48**, 2873-2880, doi:10.1002/art.11246 (2003).
238 Zhang, Q., Hui, W., Litherland, G. J., Barter, M. J., Davidson, R., Darrah, C., Donell, S. T., Clark, I. M., Cawston, T. E., Robinson, J. H., Rowan, A. D. & Young, D. A. Differential Toll-like receptor-dependent collagenase expression in chondrocytes. *Annals of the Rheumatic Diseases* **67**, 1633-1641, doi:10.1136/ard.2007.079574 (2008).
239 Zhang, Y., Xu, J., Levin, J., Hegen, M., Li, G., Robertshaw, H., Brennan, F., Cummons, T., Clarke, D., Vansell, N., Nickerson-Nutter, C., Barone, D., Mohler, K., Black, R., Skotnicki, J., Gibbons, J., Feldmann, M., Frost, P., Larsen, G. & Lin, L.-L. Identification and Characterization of 4-[[4-(2-Butynyloxy)phenyl]sulfonyl]-N-hydroxy-2,2-dimethyl-(3S)thiomorpholinecarboxamide (TMI-1), a Novel Dual Tumor Necrosis Factor-α-Converting Enzyme/Matrix Metalloprotease Inhibitor for the Treatment of Rheumatoid Arthritis. *Journal of Pharmacology and Experimental Therapeutics* **309**, 348-355, doi:10.1124/jpet.103.059675 (2004).
240 Zimmerman, N. B., Smith, D. G., Pottenger, L. A. & Cooperman, D. R. MECHANICAL DISRUPTION OF HUMAN PATELLAR CARTILAGE BY REPETITIVE LOADING INVITRO. *Clin Orthop Relat R*, 302-307 (1988).

8 Appendix

8.1 Loading Apparatus Used in the Past

In the past 70 years a large variety of loading apparatus and models have been used to characterize the mechanical properties of articular cartilage. They mainly concentrated on topics such as elasticity, viscoelasticity, microstructural theories, porous media theories and physical chemistry theories. Most commonly, indentation with a flat, spherical or porous indenter, uniaxial tensile testing, (un-)confined compression, shearing of blocks, failure under impact loading and closed joint models have been used (Frankel 2001 [71], Fung 1993 [73], Hayes 1997 [95], Huiskes 2005 [104], Mansour 2003 [140], Mooney 2003 [150], Woo 1990 [231]).

The following table (Table 10) provides an overview of 10 of the existing papers that cover areas closely related to this project. The table outlines the various experimental setups and results of experiments using osteochondral cores and various types of impact loading:

Paper	Type of Explant	Loading Device	Load/ Impact Energy	Result
Camosso et al., 1962(Camosso 1962 [43])	10 x 10 mm explants, articular cartilage of proximal epiphysis of metacarpal bone of cattle, osteochondral core with upper 250µm cartilage removed and bone only were tested	Universal Baldwin materials-testing machine (not further specified)	Compression, starting from an initial load of 20 kg/cm^2 which was increased gradually until fracture of the specimen occurred. For each sample the following parameters were recorded: 1. Total deformation for each 20 kg/cm^2 2. Permanent deformation for each 100 kg/cm^2 3. Deformation under constant load for each 100 kg/cm^2	Deformation rate is higher in younger than in older animals. The degree of deformability is much higher for the samples of bone + cartilage than for those of bone proper. The rate of deformation decreases under increasing load in the samples of bone + cartilage and increases under the same conditions in the samples of bone alone. Fracturing occurs sooner in bone samples than in samples of bone + cartilage.
Repo and Finlay, 1977(Repo 1977 [181])	Human tibial-plateau articular cartilage + bone, 9 mm in diameter were prepared by removing all but a 1mm layer of the subchondral bone	Impactor of 51 mm in diameter, flat surface	Drop tower, 6.5 Kg and 15.5 Kg, velocities up to 3.37m/s, strain rate 500 s^{-1} and 1000s^{-1}	Strain rates of 500 s^{-1} and 1000 s^{-1} suggest that impact loads sufficient to fracture a femoral shaft of an automobile occupant are nearly sufficient to cause chondrocyte death and fissuring in the articular cartilage of either the knee or the hip of the loadbearing areas.
Jeffrey et al., 1995(Jeffrey 1995 [108])	Osteochondral and chondral cores 5mm in diameter from carpometacarpal joints of calves	Indenter with flat surface	drop tower, weights of 1 kg and 500 g, heights of 5 cm, 10 cm and 20 cm	100% viablity in 500 g, 5 cm down to 40% viability in 500 g and 20 cm: Visible damage more severe in samples without bone attachment. The higher the impact the more cracking in the cartilage surface.

Quinn et al., 2000(Quinn 2001 [173])	Osteochondral cores 6 mm in diameter from bovine shoulder	Loading in axial direction, with impermeable loading post of 10 mm in diameter and without radial confinement	Each explant was individually subjected to a single ramp compression characterized by a strain rate (3x 10^{-5}, 0.3, 0.5, or 0. 7 s^{-1}) and a peak stress (3.5, 7, or 14 MPa), compression was applied at specified strain rate until the predetermined peak stress was obtained, after a two minute period during which samples were held at the attained peak strain, explants were removed	Tissue cracks and cell deactivation were most severe near the cartilage superficial zone at high strain rates, associated with increased release of proteoglycan: Cell activity and proteoglycan synthesis were suppressed throughout the cartilage depth at low strain rates.
Lucchinetti et al., 2002(Lucchinetti 2002 [137])	Full-thickness cartilage explants 7 mm in diameter, from the occipital joint of 18-24-month-old cows	Uniaxial confined compressive load to the explants through a 7 mm diameter, plane ended, porous load platen	Static stress of 0.5 MPa for 1, 1.5, 2, 2.5, and 3 h or a continuous cyclic stress of 1 MPa (peak stress) for 3, 6, 14, 24, and 72 h	Repetitive loading at physiological levels of stress was found to be harmful to only the chondrocytes in the superficial tangential zone. Static loads caused cell death at an early time. Death peaked at 6 h of cyclic loading.
Warner et al., 2003(Warner 2004 [230])	Axisymmetric model of an articular cartilage plug with a thickness of 3 mm and radius of 20 mm, constructed within the ABAQUS finite-element package	Indenter: stiff and impermeable hemispherical surface	Monophasic and cyclic (1 Hz, peak force 10 N, max. cartilage displacement 10%) unconfined loading	Under monotonic loading high pore pressure at surface and base of sample moves to cartilage-bone- interface by cyclic loading, Radial tensile stress moves from the middle zone to the surface by cyclic loading.

Morel and Quinn, 2004(Morel 2004 [151])	Osteochondral explants 4 mm in diameter were drilled from adult bovine humeral heads, the full-thickness cartilage layer was trimmed to 2.7 mm diameter and the bone to 1 mm thickness	Flat indenter	Single ramp compression to 14 MPa peak stress at one of three strain rates: 7×10^{-1}, 7×10^{-3} or 7×10^{-5} s^{-1}	Loading at the highest strain rate resulted in acute cell death near the superficial zone in association with cracks, followed over the 11 days after compression by a gradual increase in cell death and loss of demarcation between matrix zones containing viable versus nonviable cells. In contrast, loading at the lowest strain rate resulted in more severe, nearly full-depth cell death acutely, but with no apparent worsening over the 11 days following compression.
Torzilli et al., 2005(Torzilli 2006 [217])	Mature and immature 5 mm diameter bovine cartilage cylinders from knee	Confined compression, 5mm diameter plane-ended, porous stainless-steel indenter	Immature specimens 0.5MPa (ε=10%), 1.0 MPa (20–40%) or 3.0 MPa (50–70%), mature specimens loaded with a stress of 0.25–2.0 MPa (10–40%) or 2.5 MPa (50–70%). For the 10% strain the creep times for the immature and mature specimens were very fast (7 ± 4 and 21 ± 17 s, respectively) while for the 70% strain the times were significantly longer (2,343 ± 913 and 1,606 ± 628 s, respectively)	Cell death was always initiated at the articular surface and increased linearly in depth with increasing strain magnitude.

Chahine et al., 2007(Chahine 2007 [49])	Osteochondral plugs (4 and 5 mm in diameter), carpometacarpal joints of calves	Custom static compression device, flat surface of indenter	50% or 80% strain, static loading (6 or 12 h), axial or transverse loading, unconfined compression	Axial loading: strain 77% in superficial zone, 55% in deep zone. Transverse loading: strain at 65% evenly distributed. In both groups similar patterns of cell death distribution with most cell death in superficial zone.
Martin et al., 2009(Martin 2009 [143])	Bovine osteochondral explants, 25 by 25 mm square from the lateral tibial plateau, subchondral bone was cut from the underside of each specimen to a thickness of 4 to 8 mm	Single impact load with use of a drop-tower. The indenter was a flat-faced brass rod 5.0mm in diameter with rounded edges	Impact energy was modulated by dropping a 2 kg mass from a height of 14 or 7 cm, which resulted in impact energy densities of 14 J/cm^2 and 7 J/ cm^2	Treatment with N-acetylcysteine soon after a blunt impact injury can reduce chondrocyte death and proteoglycan loss.

Table 10: Loading Apparatus used in the past.